Study on beach profile change of gravel beach and countermeasure against beach erosion

VU THI LAN HUONG

Supervised by

Prof. MIZUTANI Norimi

Coastal & Ocean Engineering Laboratory
Department of Civil Engineering
Nagoya University
JAPAN

ACKNOWLEDGEMENT

I would like to thank the Department of Civil Engineering in Nagoya University for giving me the permission to implement this thesis and do necessary research works.

I am very grateful to my supervisor, Prof. Norimi Mizutani. With his enthusiasm and great efforts to explain things clearly and simply, he inspired me to do the research. During my thesis-writing period, he encouraged and gave me lots of valuable advices. It is very difficult to accomplish this thesis without his supports.

I also would like to express my gratitude to Prof. Tsujimoto, Prof. Kobayashi, Assoc. Prof. Toda, Assoc. Prof. Nakamura, since they spent their precious time to review the thesis and give critical comments.

I would like to thank Assoc. Prof. Koji Kawasaki, Dr. Kiku for their willingness to share their knowledge and experience with me, which are helpful for my research.

I would like to thank Dr. Cho, Dr. Ren, Dr. Chathura Manawasekara, Mr Suzuki Mr. Nishiura, Mr.Watanabe for their help and co-operation in doing research, and my colleagues who emotional support me when I study oversea, as well as the secretaries of the Civil Engineering Department, the secretaries in GCOE for their assistance in many ways.

Meanwhile, I particularly thank to Nitori International scholarship, Yokoyama International scholarship, Hirose International scholarship for financial support in my study.

Lastly and most importantly, I wish to thank my family. They teach me, support me and love me. To them I dedicate this thesis.

TABLE OF CONTENTS

Chapter 1

INTRODUCTION

1.1 Background and motivation

From the past, human have gained their livelihood directly or indirectly from the coastal area with many kind of economic activities such as fishing, tourism, aquaculture, etc. which result in negative impacts on the natural coastal system. Among those impacts, destroying the balance of nature is one of the worst impacts to the future earth development. And the popular case is destroying the natural balance of sediment system, which leads to coastal erosion. Naturally, beach face has been continuously formed through long-shore and cross-shore sediment transport processes, and it needs a very long time to reach the natural dynamic equilibrium, in which input sediment amount is equal to output sediment amount. However, today many kinds of near-shore structures, such as port facilities, coastal resorts, are constructed to meet the rapidly growth of human demands. The natural sediment transports in near shore hereby are interrupted, then the natural dynamic equilibrium of sediment is destroyed and coastal erosion occurred as a consequence. Along with the rapid increase of economy, the exploitation of coastal areas, and the negative impact on natural coastal system are inevitable. Therefore, it is very important to find out a mode of exploitation which has less impact to natural coastal system, then it leads to the requirement of better understanding about coastal processes. For that reason, from the past, many kind of anti-erosion method have been constructed as an additive constructer to reduce negative impact of near-shore facilities, such as artificial reef in Shichirimihama Beach to reduce beach erosion caused by break water construction at Udono port, breakwaters

for reducing the effect of dam construction in Nangoku Beach Coast, Kochi (Wada, 2007). Among those kinds of anti-erosion methods, artificial reefs are popular countermeasure for its environmental friendly effect. The formation of new aquaculture community around artificial reef plays an important role in conservation of marine environment. In the future, artificial reef will become the most popular coastal defense alternative in terms of integrated coastal zone management. On the other hand, artificial reef is still a new measure on coastal defense, and it requires more study to understand the effective of this measure on coastal process. From many studies, it can be found that investigated behavior of coastal zone due to the construction of reef is an impossible task without numerical simulation. Hence, today investigation of coastal process through analyzing the mechanic of shoreline change, beach geomorphologic change combined with analyzing the behavior of near-shore flow field is the most effective method to evaluate the coastal process. This approach requires the need of shoreline data and topography data as well as the development of numerical simulation

1.2. Literature review

1.2.1 Shoreline observation

A shoreline is defined as a physical interface of land and water (Dolan et al., 1980). Many researchers consider shoreline position as a visually shoreline which is visible to the human eye, for example: high-water line (Mcbeth, 1956; Gorman, Morang and Larson, 1998), high mean water line (List and Farris, 1999; Parker, 2001). These kinds of shoreline are considered as long term changes of shoreline. However the shoreline position changes continually associate with various tide level and wave condition, which result in different on-shore and off-shore sediment transport processes. So it need to be considered carefully when determining an average shoreline. Recently, there is another category of shoreline called “instantaneous shoreline” which is collected through WEB camera system, such as ARGUS camera system. By this method, the shoreline data can be collected continuously, and it contributes to understand the shoreline behavior from very short period (in minute) to long period (in years), from small area (m) to large area (km). Moreover, after installing, the camera can be worked safely under bad weather condition, even in a storm, when the shoreline change cannot be observed by field survey or satellite image. Therefore, Web camera is

a very useful tool to research the mechanics of shoreline change.

1.2.2. Topography change observation

Beside shoreline position, topography data plays an importance role on investigating near-shore process, especially sediment transport processes. Along with the development of recently science and technology, topography data mapping technique has shown a signnificant development from traditional methods such as beach profiling by ground survey (Birkemeier, 1985; Morton, 1993; Larson, 1994) to remote sensing such as aerial photogrammetry (Adam, 2002; Erik, 2007; David, 2010). Ground survey provides a good performance in low cost (Gorman et al. 1998) but it has limitation in observation area. Aerial photogrammetry can achieve better technical performance, with wider area than ground survey. However, this method can work only in good weather and good light condition. Recently, the improvement of laser technology leads to the development of a new topography mapping method, called topography mapping by laser scanner system. The popular methods are Airborne Laser Scanning System (ALSS) (Kraus, 1998; David, 2001; Woolard, 2002; Oude, 2011) and Terrestrial Laser Scanning System (TLSS) (David, 2008; Shi, 2009; Dimitri, 2013). ALSS is based on flight measurement, while TLSS is ground based measurement system. Both methods show a good performance on reproduction nature topography. However, ALSS requires higher cost than TLSS and it is the most expensive technique among all topography data mapping methods. Moreover, due to the limitation of flight high, the small size objects morphology cannot be captured correctly. Hence, TLSS is more effective for mapping small size objects

1.2.3. Near-shore gravel beach hydrodynamic

Near-shore hydrodynamic is a very complicated process with many driven forces, such as tide level change, incoming waves with different conditions, and so on. Many researchers have done a huge effort to investigate the near-shore hydrodynamic in order to gain more knowledge of near-shore dynamic behavior. However, most of researchers focus on sand beach hydrodynamic. The knowledge about gravel beach hydrodynamic is still lagging behind that of sand beach. There are two main approaches on research related to gravel beach, including long-term approach and

short-term approach (Edward, 2009). Long-term approach focuses on investigating the gravel shore dynamic through field survey morphology and hydrodynamic observation. However, this approach may not reflect correctly the main driving force of gravel shore process. On the other hand, shore-term process aims to analyze the hydrodynamic of gravel beach by doing short period ground based hydrological field survey and doing numerical simulation. But gravel beach is very dynamic even under low-to-medium wave energy conditions, and therefore it is very difficult to conduct a field survey in gravel beach. Consequently, numerical simulation is the most cost-effect method for evaluating the existing coastal defense measurement, as well as developing a new coastal defense measure on gravel beach. And the most important phenomena of hydrodynamic in gravel shore have been investigated by numerical modeling study. Jenning and Shulmeister (2002) showed that gravel is reflective beach type which has steeper beach face, then sediment on gravel beach is more movable compared with sand beach. Turner and Masselink (2001) indicated that the high permeability of gravel beach results in strong asymmetry on up-wash and back-wash cycle. This swash cycle asymmetry enhances onshore sediment flow and reduces offshore sediment flow that contributes to maintain beach face steepness and increase erosion trend on gravel beach. Ma et.al (2004) found that there is an upward flow inside gravel under the wave breaking point, and it may play an important role in swash zone sediment transport process. However, because of the complexity of the interaction among solid, liquid and gas inside gravel beach and the sensible change of hydrological process varies with sediment size as well as permeability, a fully developed model which can well reproduce

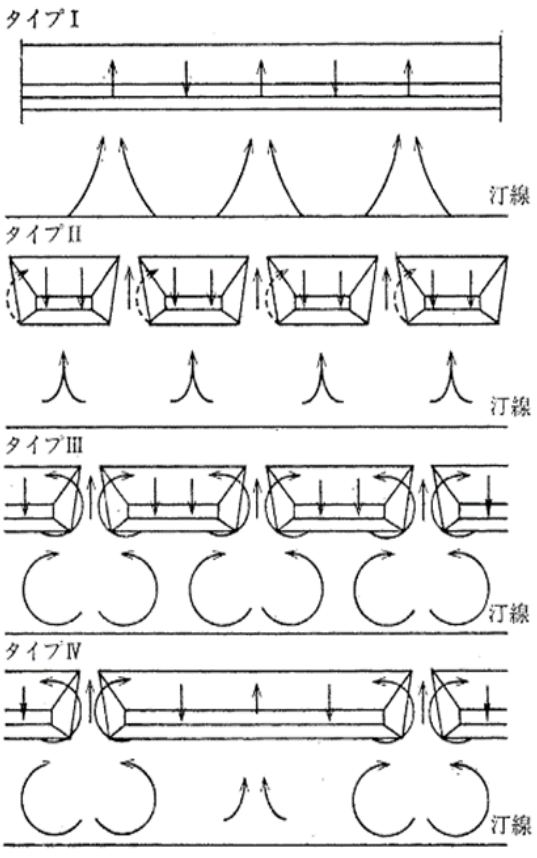

Figure 1.1. Flow pattern around artificial reef.
Source: Kawashima, 1992

the hydrodynamic process of gravel beach is still a big challenge for many researchers.

1.2.4. Flow field around artificial reef

As mentioned above, an artificial reef has become the most popular coastal defense measure in recent. Artificial reef has been functioned well on reducing the wave energy off to the coast, hence it reduces negative impact of erosion on coastal zone. On the other hand, there are many cases in which beach erosion is still increasing after the installation of artificial reefs (Ranasinghe and Turner, 2006). This fact indicated that the hydrodynamic behavior around artificial reef is not fully understood yet. Some studies about flow field inside permeable submerged structure showed that wave energy was dissipated over artificial reef due to wave breaking, which results in a decrease of coastal erosion (Izumiya, 1989; Kichida, 2000). However most of studies have been researched for impermeable seabed, and the relationship between the flow inside seabed and flow inside artificial reef has not been investigated. Also, the effects of artificial hydrodynamic conductivity as well as bed permeability to flow field have not been investigated yet. The flow field type around artificial reef was investigated by Kawashima (1992) through 3D experiment (See Figure 1.1). He indicated that there is a planar offshore flow on the gap between two adjacent artificial reefs. It is said to be the main reason leading to the erosion of artificial reef lee (Red circle in Figure 1.2) which reduces the function of artificial reef (Shimizu, 1993). In order to understand such kind of phenomena, a three dimensional simulation which can investigate the behavior flow field not only in planar but also in depth direction is required.

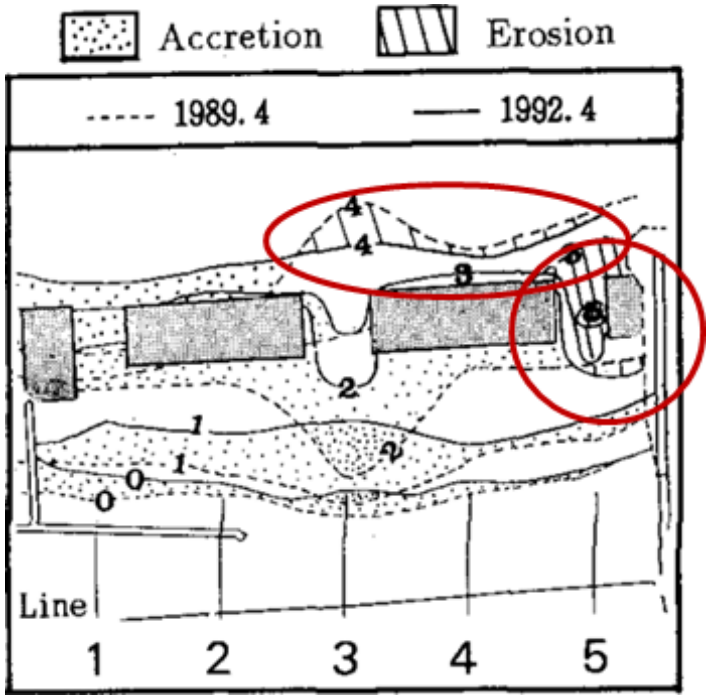

Figure 1.2. Erosion at artificial reef lee
Source: Shimizu, 1993

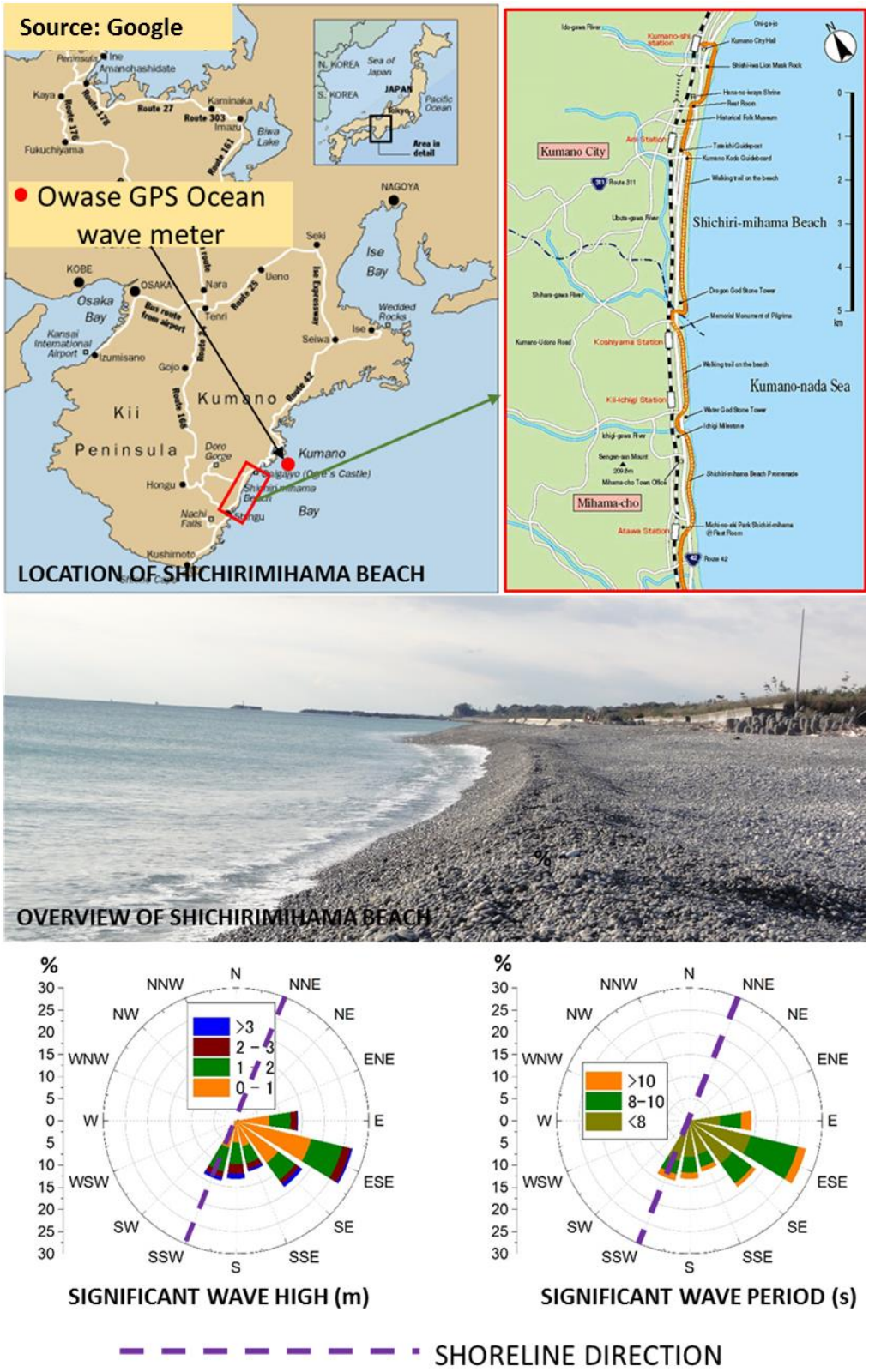

Figure 1.3. General of Shichirimihama Beach

1.3. Study area

The object of this study is to discuss the Shichirimihama beach profile change. Shichirimihama Beach is a gravel beach about 20 km long, extending southern part of Mie Prefecture, located in front of national highway (Route 42) and belong to Kumano-Yoshino national park. As showed in Figure 1.3, wave approaches to the coast almost from the E, ESE and SE directions, which causes northward longshore current. Kumano River located on the south of Shichirimihama beach is considered to be the major source of beach material. During the period of rapid economic

(a) Artificial reef

(b) Wave-dissipating block

(c) Beach nourishment

Figure 1.4 Anti-erosion method Shichirimihama Beach

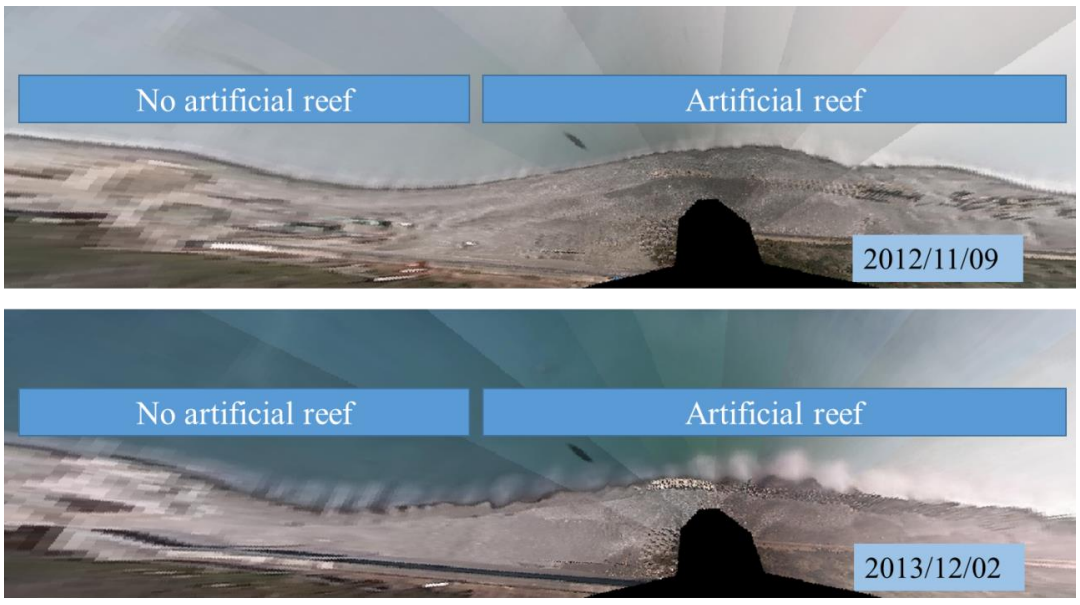

Figure 1.5 Beach profile in 2012 and 2013

growth in Japan, many dams have been constructed in Kumano River, and also large amounts of bed material had been dredged from this river, therefore the supply of materials to beaches had been reduced and the shoreline retreated as a result. Recently, because of the restrictions on the collection of material from Kumano River, Ojigahama Beach, located on the right side of Kumano River, has gradually recovered. In contrast, the erosion in Ida coast, which is the southern end of Shichirimihama beach located in the left side of Kumano River, is still suffering from severe beach erosion due to the breakwaters in Udono Port. In order to reduce the effects of erosion, variety of measures such as artificial reef, beach nourishment, have been done in recent years (See Figure 1.4). However, beach is still suffering from beach erosion, especially in storm season. Figure 1.5 shows the beach state in 2012 and 2013. It can be said that the area without artificial reef is more eroded than the area with artificial reef. So artificial reef play an importance role on reducing shoreline retreat. However, recent continuous shoreline retreat indicates that artificial reef did not function well as expected because the hydrodynamic behavior around artificial reef is not fully understood yet. In order to find out a more effective measure and create more stable beach, the behavior of flow field around the present artificial reef should be reassessed considering the permeability of gravel sea bed.

1.4. Scope of study

This study aims to investigate the function of artificial reef on Shichirimihama beach through analyzing the change of shoreline position and beach topography. After that, the flow field of coast, in which artificial reef has been installed as countermeasure against beach erosion, will be investigated by conducting numerical simulation in order to clarify the mechanism of hydrodynamic change on the swash zone as well as around artificial reef. In numerical simulation model, the permeability of sea bed is considered to clarify the mechanism of hydrodynamic change on gravel beach which has high permeability as Shichirimihama beach. In summary, this study aims to:

(1) To investigate the shoreline change based on image obtained from coast based WEB camera system as well as to propose new method of shoreline detection from image.

(2) To collect and analyze the change of topography in Shichirimihama beach using 3D terrestrial laser scanning system.

(3) To investigate mechanism of flow field around artificial reef in considering the effect of seabed permeability using numerical simulation.

(4) To validate the present artificial reef in Shichirimihama Beach and investigate a more effective method to increase the function of present artificial reef.

1.5. Content of dissertation

The contents of dissertation are as follows:

In Chapter 1, the background and objective of the present study has been clarified considering the existing research.

In Chapter 2, shoreline data observation method using WEB camera system will be presented. Firstly, the validation of exiting CCD method will be examined. Then a new method of extracting shoreline from RGB image will be discussed. Final part of this chapter describes the analysis of shoreline change considering wave conditions.

Chapter 3 aims to discuss the topography change in Shichirimihama beach. The early part of this chapter introduces the berm development in Shichirimihama Beach. The last part of the chapter is the method of mapping topography data using 3D Terrestrial Laser Scanning.

Chapter 4 investigates the mechanism of flow field around artificial reef over a permeable seabed through numerical simulations. Firstly, the effect of seabed permeability on the behavior of hydrodynamic field around artificial reef will be discussed. Then, the relationship between permeability of artificial reef and hydrodynamic change will be investigated. Later, the validation the function of present artificial reef in Shichirimihama beach by comparing the hydrodynamic behavior of two scenarios: with and without artificial reef. Lastly, the change of hydrodynamic varies with offshore distance of artificial reef will be investigated to research for a

more effect arrangement method for future artificial reef construction.

Chapter 5 summarizes the conclusions of this study and discuss about the future works.

The references will be collected in the final part of this dissertation.

Chapter 2

CHARACTERISTIC OF SHORELINE CHANGE

2.1 Overview

Since, wave plays as an external force on shoreline movement, mechanism of shoreline change should be analyzed with wave condition, which changing continuously over time. In addition, due to continuously data collection, potential Web camera is one of the most effective techniques for regularly collecting shoreline data over long period. In this case, a method of detecting shoreline from image is required. Some techniques for extracting shoreline from RGB image have been adopted. These techniques depend on the difference between color component of land and sea, or between wetland and dry land. All of these methods were proposed for sand beach. However, due to high sunlight reflection ratio of gravel beach, the color component of image of gravel beach showed a different manner in compared with image of gravel beach. Figure 2.1a, Figure 2.1b show two different kinds of image, one is gravel beach, and other is sand beach. Figure 2.1c, Figure 2.1 d show the average color composition of cross-shore transects of gravel beach image and sand beach image, respectively. Comparing two figures, it can be said that the intensity along cross-shore transect of gravel beach is higher than sand beach, due to light reflection of the gravel beach.

In this study, in addition to the existing CCD method (Suzuki et al, 2008) which has been applied for many sandy beaches, a new method of extracting shoreline from image will be proposed. At first, RGB image data collected by Web camera system in Ida Coast were used as an input data to examine the applicability of the CCD method. As a result, there still have room for improvement images that was taken ịn bad

weather such as rain. In consideration the features of the image in such a case, we have proposed a new image processing method.

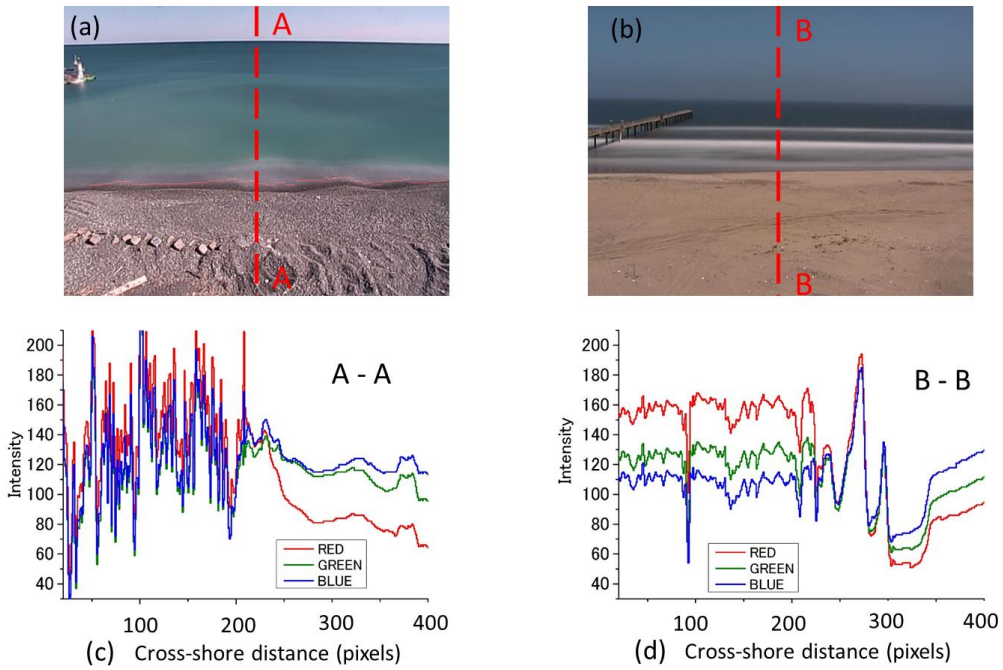

Figure 2.1 Different between color component of sand beach and gravel beach

2.2 WEB camera system on Shichirimihama Beach:

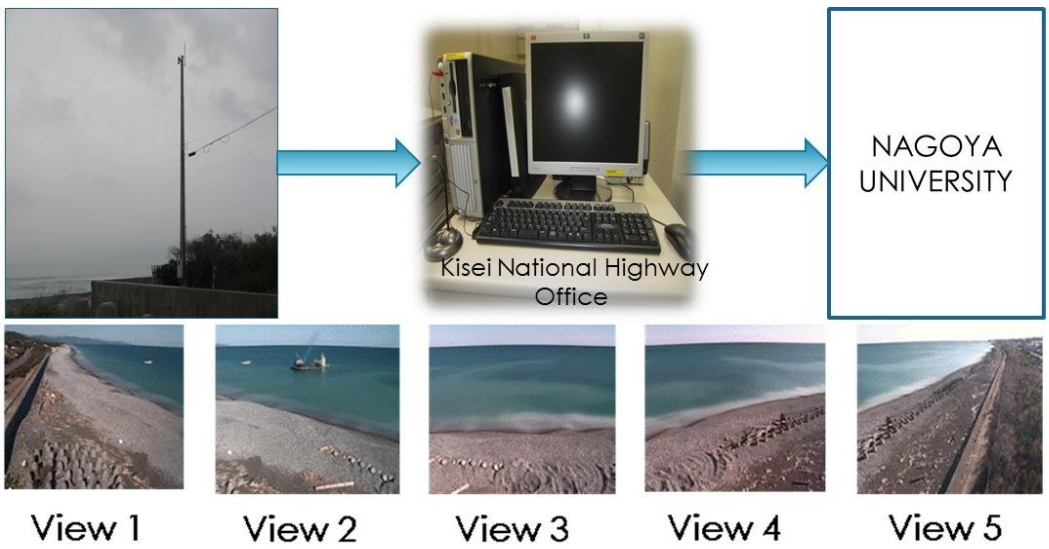

Figure 2.2 WEB camera system at Shichirimihama Beach

The Web camera is installed on the seawall behind the Shichirimihama Ida coast, and the images are saved in the PC installed at the Ministry of Land, Infrastructure and Transport, Kisei National Highway Office Kumano maintain branch by optical cable. Then the data is transferred to Nagoya University by the private Internet cable. Working status of camera can be checked regularly at Nagoya University, Coastal and Ocean Laboratory through internet. Both snapshot image data and average image data can be directly downloaded from the computer through internet. The camera operates seven days a week, from 6:00 to 18:00 every day. The operating angle of camera is 180 degree, and the study area extends 3km on long shore direction. During working time, camera captures the view of 180 degree by 5 frames. Image is recorded continuously for 5 minutes at each frame with the interval of one second (See Figure. 2.2). After 5 minutes, the camera will stop in 5 minutes, then move to the next frame automatically. Approximate 300 snapshots at one frame are used as one input data of image processing (Figure 2.3).

2.3. Procedure of image processing

Image processing is any form of signal processing, in which the input is an image, such as photograph or frame of video; the output can be either an image or a set of characteristics or parameters related to the image. In this study, output of image processing is the physical shoreline, i.e. the interaction point of dry land and wet land.

In general, the image processing in this study can be done through 3 steps (See Figure 2.3). In the first step, each 300 images, which were taken in 5 minutes, will be gathered to create one 5 minute-exposure average image. The next step is coordinated calibration, in which, five views of image will be combined to create one continuous object image. Finally, the shoreline can be detected from image.

2.3.1 Making average image from snapshot image

Wave moves toward the coast and breaks in a wide range of sizes and shapes, as shown in snapshot image (See Figure 2.4 a-f). Breaking position is also various, depend on many different kinds of wave. In Shichirimihama Beach, under low wave condition, wave will break near from the coast. Under server weather condition, when

wave energy become higher, wave will break very far from coast. However, basically the wave will break only in shallow water, so it can be adjusted that the position where wave breaking occur (white color in image) is shallow water. Taking average images will reveal a smooth pattern of bright image intensities (Figure 2.4 h). In addition, by taking average images, moving objects from the camera's field of view, such as ships, vehicles and people, are also "removed".

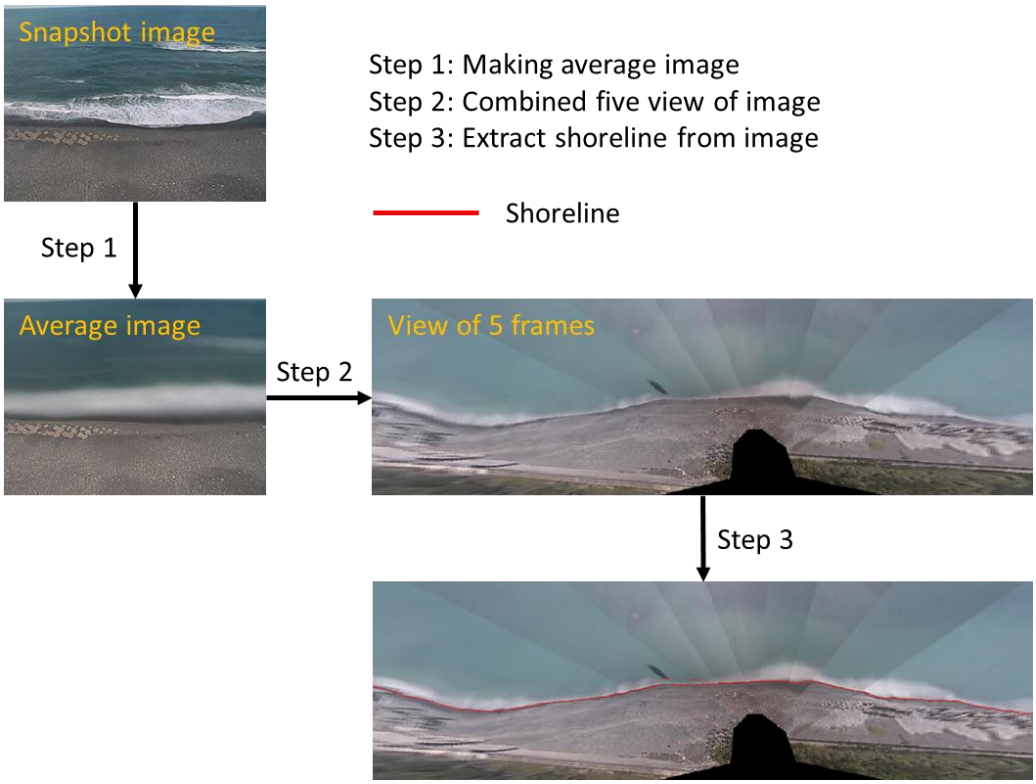

Figure 2.3. Image processing step by step

2.3.2 Coordinate calibration

Images taken from five frames have different views of angle and scale. Hence coordinate calibration has done in order to produce one continuously image, in which all objects are presented in same scale. Coordinate calibration has two steps. First step was done through field survey to collection the ground control points. The second step was conducted on the lab.

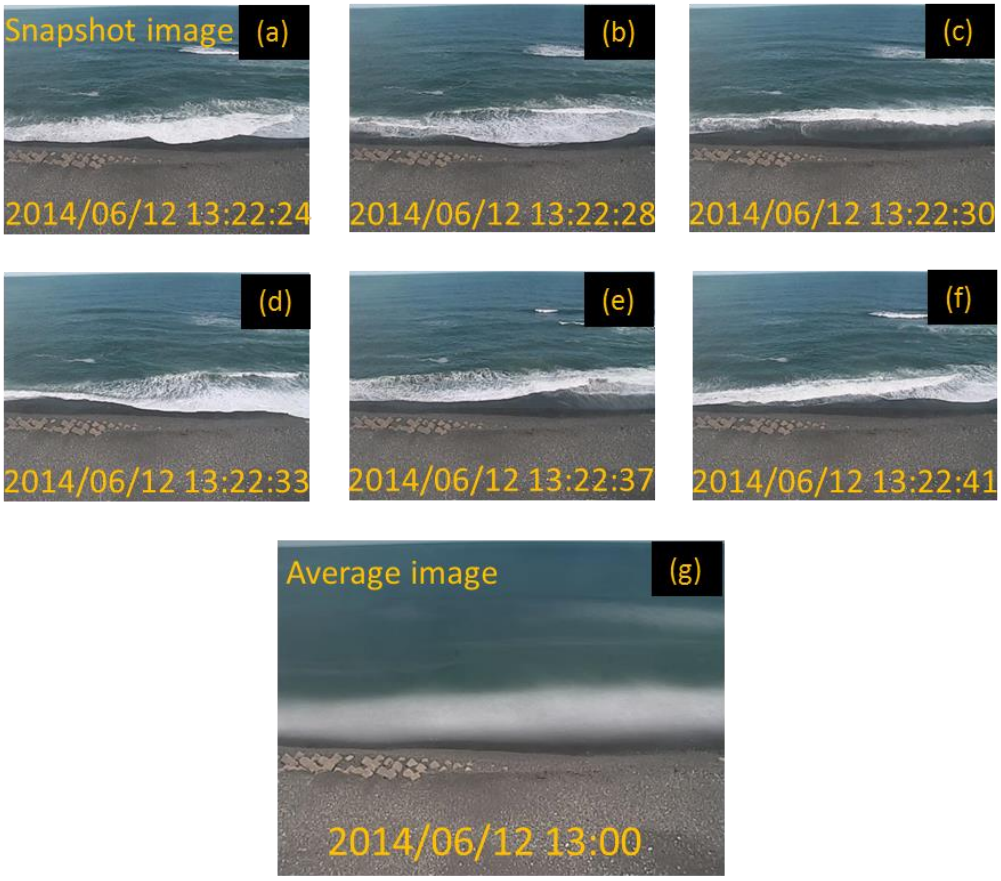

Figure 2.4. Snapshot image and average image

Figure 2.5. Snapshot image and average image

Link	X Source	Y Source	X Map	Y Map	Residual_x	Residual_y	Residual
1	136.027605	33.764466	136.027598	33.764452	0	4.28839e-007	4.28839e-007
2	136.027230	33.764212	136.027229	33.764181	0	0	0
3	136.027242	33.764164	136.027246	33.764137	0	0	0
4	136.027519	33.764208	136.027522	33.764201	-2.4909e-006	-1.20197e-006	2.76574e-006
5	136.027231	33.764243	136.027227	33.764209	-2.02404e-006	-7.68777e-007	2.16513e-006

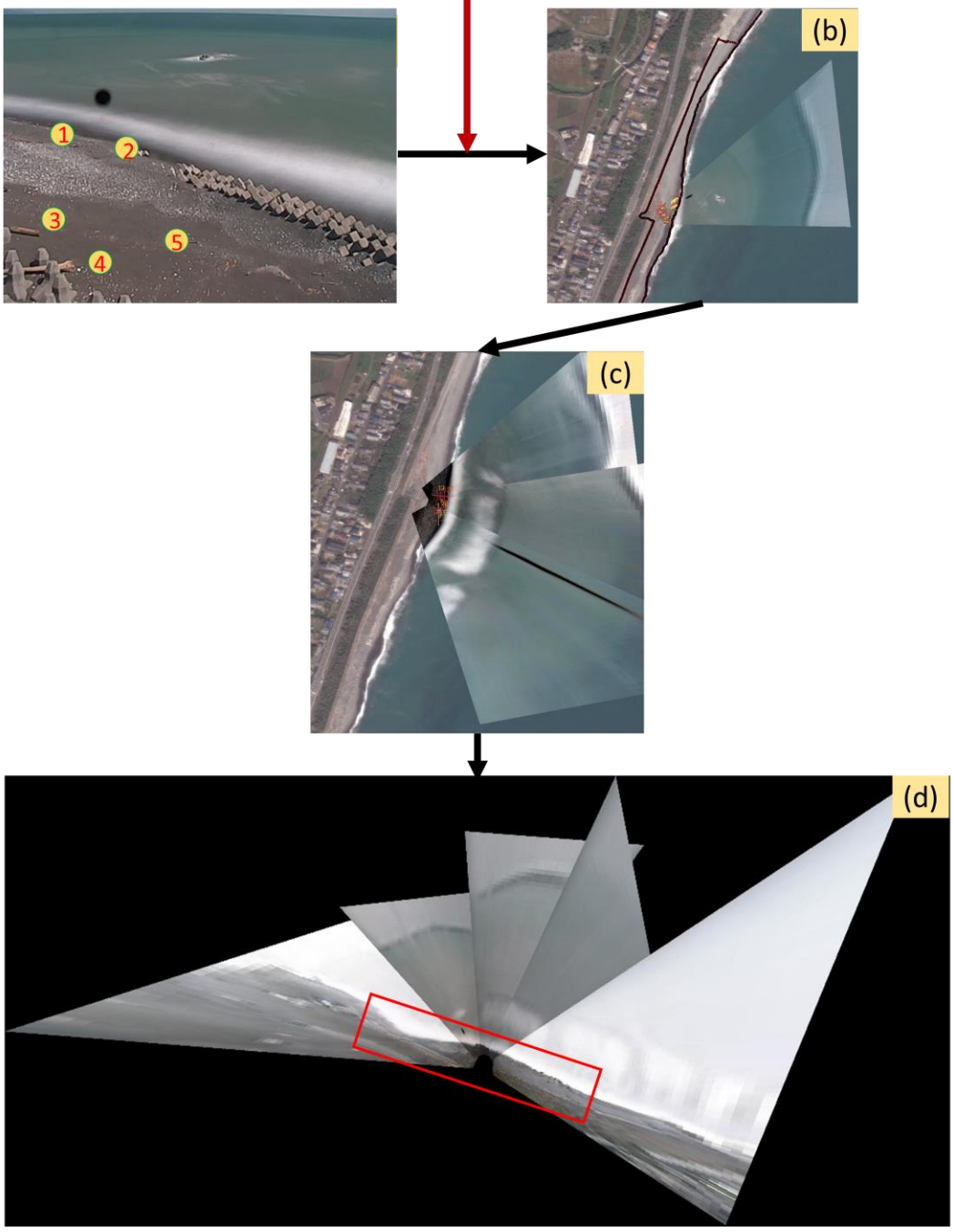

Figure 2.6 Coordinate calibration process

2.3.2.1 Ground control point data collection

Data ground control was collected by handy GPS on 27th July, 2012. There are about 20 points collected for each camera view. Because the wave in Shichirimihama is usually high and it is very dangerous to work in the water, so the ground control point collection work was done on land. The total number control points and the position of control points are showed in Figure 2.5.

2.3.2.2 Coordinate calibration using ArcGIS software

Coordinate calibration was operated using ArcGIS software. The main task of this step is converting image coordinate to world coordinate based on data collection on field survey. The target world coordinate is Bing map coordinate system. Results of coordinate calibration process were validated by comparing the shoreline of the image with the shoreline data collected by handy GPS on the same day (purple line on Figure 2.6c). The area covered by red rectangle in Figure 2.6d will be used for shoreline extraction on the step 3.

2.3.3 Extract shoreline from image

2.3.3.1 Evaluate CCD method

CCD model (Turner et al., 2000; Turner & Leyden, 2000) is based on the physical principal that ambient light from the sky is reflected by the ocean surface in a manner that is different to distinguish it from land features. More particularly, to the naked eye the ocean usually appears blue under a wide range of light conditions, and it is this high reflectivity of light at wave lengths corresponding to the blue color that is used within the CCD model to distinguish the shoreline. The first step to apply this model is separating color images into their individual red, green and blue components. The color of each pixel is thus defined as the triplet corresponding to the intensity of each of the three fundamental colors. The initial estimate shoreline at any location alongshore can then be found by locating the point where the individual RGB color

components of the image diverge, with 'ocean' pixels exhibiting higher intensity in the blue color band. Figure 2.7 shows the intensity of each separated color band (normalized in the range of 0 - 255) of a typical time-exposure color image obtained from Web camera system. Moving seawards, initially the intensity of each of the individual RGB color components are similar, resulting from the 'white' color of the beach. At a critical point all three separate color bands can be seen to dip, then rapidly diverge. The physical interpretation of this characteristic initial estimate shoreline signal is that the coincident decrease in all three color bands corresponds to the upper swash limit, with color divergence occurring at a point in the mid swash zone where the beach face is usually covered by swash during the ten-minute period during which the time-exposure image is created. Moving further seawards along these transect, the coincident maxima in all three (now diverged) color bands corresponds to the intensity

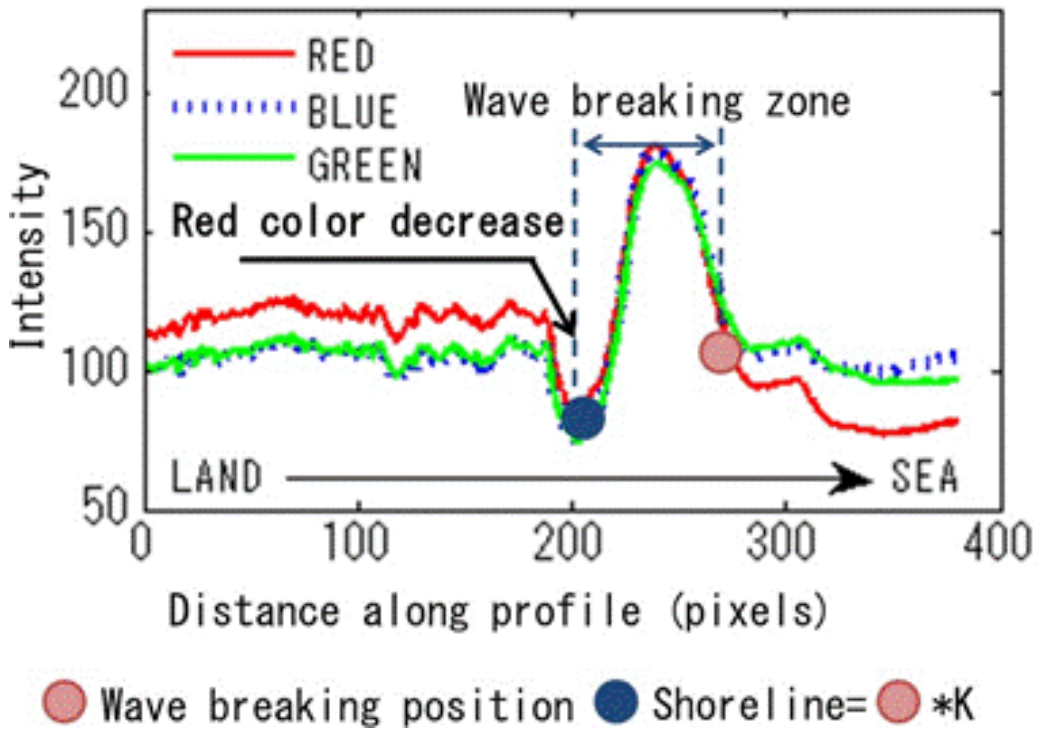

Figure 2.7. Principle of CCD method and new method

maximum resulting from wave breaking in the near-shore can be seen. The detection of the initial estimate shoreline by the CCD model utilizes the divergence of color bands in the swash zone to define the cross-shore position of the shoreline at regular increments alongshore. This procedure is repeated at multiple shore-normal transects alongshore, to define the initial shoreline along the entire region of interest. The final

shoreline is the product of initial estimate shoreline and particular threshold divergence value K. The value K to define the shoreline can be selected by calibration with available survey data; or alternatively, any value can be chosen for a particular site, which as long as this remains constant, can be used to assess the relative landward and seawards translation of the waterline. For Shichirimihama beach K=0.81. After image processing, two drawbacks can be identified. The first issue is that the results of CCD model depend strongly on weather. In bad weather condition, the blue band of the sea and the different between red band and blue band is not significant apparent, so it is hard to find out the critical point (the point at which three color rapidly diverge) (Figure 2.8a). The second issue is that it is hard to find a constant threshold divergence value for the particular site. Due to high effective wave energy dissipation of beach slope, or permeability of the gavel beach, waves off to the beach almost break near the shoreline. On the other hand, as illustrated in Figure 2.8 (b), in typhoon and cyclones weathers, wave breaking occurs very far from the coast, hence finding a constant K value for specific coast is a tough task. Moreover, Shichirihama Ida coast faces to the east direction and it made more difficulties for extracting shoreline by CCD method with images taken in the early morning because of sun light. Therefore, in the present study, a new shoreline detection method is proposed considering all mentioned factors.

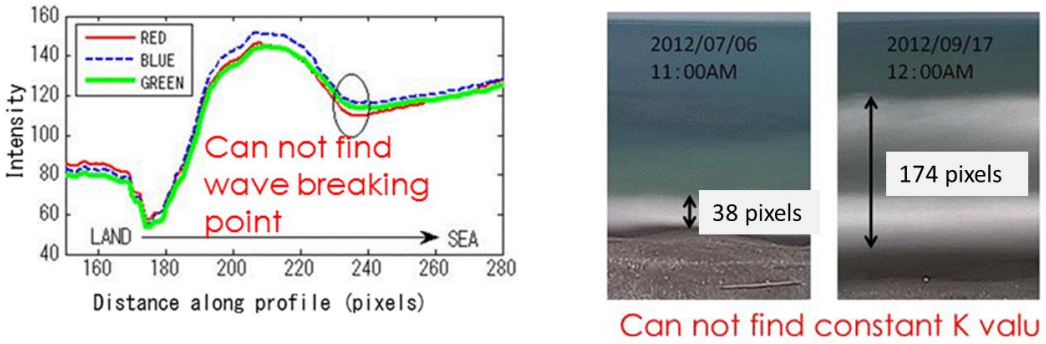

(a) Color component of land and sea are same (b) Different wave breaking width

Figure 2.8. Limitation of CCD method

2.3.3.2 Proposal image processing method

In this study, the shoreline rather than the surf zone was detected with paying attention to change in color tone of the beach itself. As shown in Figure 2.7, on land

side of the surf zone, intensity of the red decreases approaching to the sea and it drops suddenly near the shoreline. This trend has been confirmed as a common characteristic for all images, despite of weather condition. So shoreline can be detected by finding the position at which the intensity of red color drops abruptly. An example of an output shoreline detected by this method is shown in Figure 2.9 by a blue dot line. The red line in the same figure shows the result of the shoreline detected by the CCD method. Figure 4a shows an image taken under cloudy weather condition. Under this condition, white color spreads over sea surface, thus the wave breaking point could not be detected,

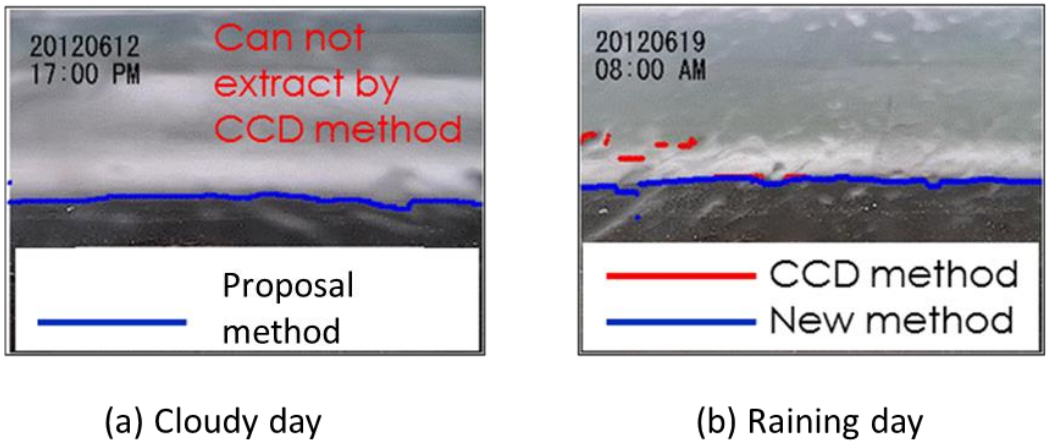

Figure 2.9 Comparison of CCD method and new method

then shoreline could not be extracted by the CCD method. However, there is a clear difference in the color tone between the sea surface and beach, and the change in intensity of red color can be clearly identified, so it is possible to detect shoreline by the new method. Figure 2.9b illustrates an image under rainy weather. Rain drops on camera screen reflect as white color on output image, results locally change of wave breaking zone width, hence a constant K value over image cannot be found for the CCD method. However, similarly to the case of cloudy weather in Figure 2.9a, shoreline can be extracted stably by the present method.

2.4 Characteristic of shoreline change

In this section the behavior of shoreline change will be analyzed with the income wave condition, in order to understand whether the shoreline forward or backward under different wave condition. Wave data at Owase, located northern offshore at the study area, analyzed from data recorded by a GPS buoy system, NOWPHAS, are available. Short-term change was investigated by comparing the shoreline position before and after special even or special income wave condition. The seasonal change will be clarified through analyzing shoreline data in the year of 2013. After that, the shoreline change during the period of 2012 and 2 014 will be studied in order to investigate the behavior of long-term shoreline change. In the last part of this section, the shoreline change of some arbitrary points will be shown to understand the effect of artificial reefs on reducing the beach erosion.

2.4.1 Raw shoreline data and effect of wave run up, tide level

By using the new method, the output shoreline position includes the shoreline fluctuation due to changes of tide level and run up length. In order to remove tide effect, the shoreline used in analyzing process was chosen at the same tide level. Meanwhile, the run up length is varied with wave height. However, Figure 2.10 shows an image taken when incoming height less than 1m. From Figure it can be said that when the wave height is smaller than 1m, the run up length is nearly zero, (there is no white part in average image). This is the common characteristic for all waves which have difference value of wave period and direction. Therefore, only the shoreline results under 1m wave high were used in analyzing process. And one pixel equal to 40 cm.

Figure 2.10 Small wave run-up under 1m wave height

2.4.2 Short term shoreline change

As mentioned before, beach erosion has become a common problem in many countries. And many researchers has tried to investigate the behavior of the shoreline during a period of days, weeks, or years in order to understand the mechanism of beach erosion. However, shoreline is changing gradually under every income wave. In other word, wave play as an external force of shoreline movement. In addition, the relationship between income wave conditions and beach erosion is still not clearly due to the lack of data set. In this study, by using continuously data set from WEB image, this problem can be solved. In this section, in order to understand the shoreline behavior under different income wave condition, income wave were divided into 6 categories: under 1.3m wave high, from 1m to 2m wave high, from 2m to 3m wave high, from 3m-4m wave high, from 4m-6m wave, and over 6m wave high. In each category, the relationship of shoreline change and wave period as well as wave direction will be discussed.

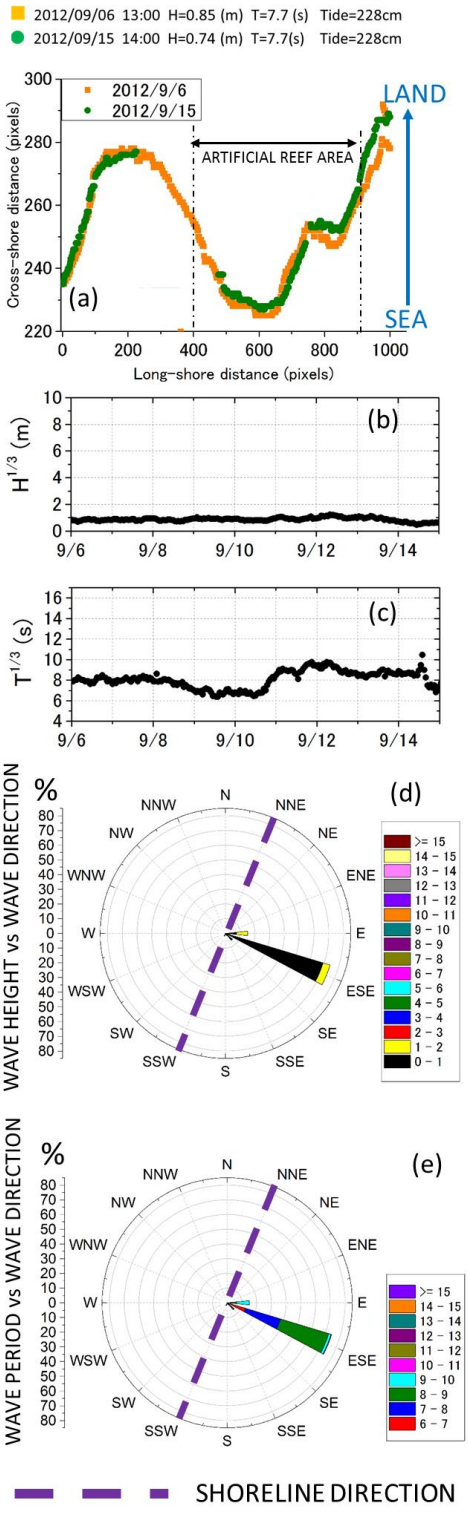

Figure 2.11 Shoreline change during 2012/09/06~2012/09/15

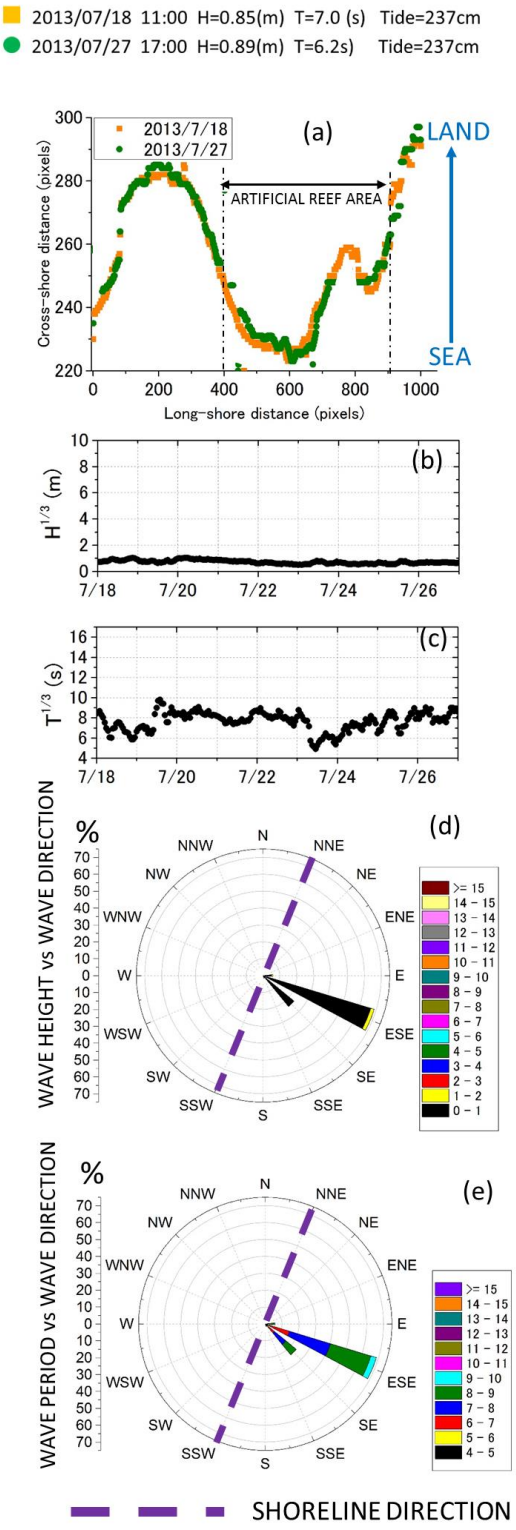

Figure 2.12 Shoreline change during 2013/7/18~2013/07/27

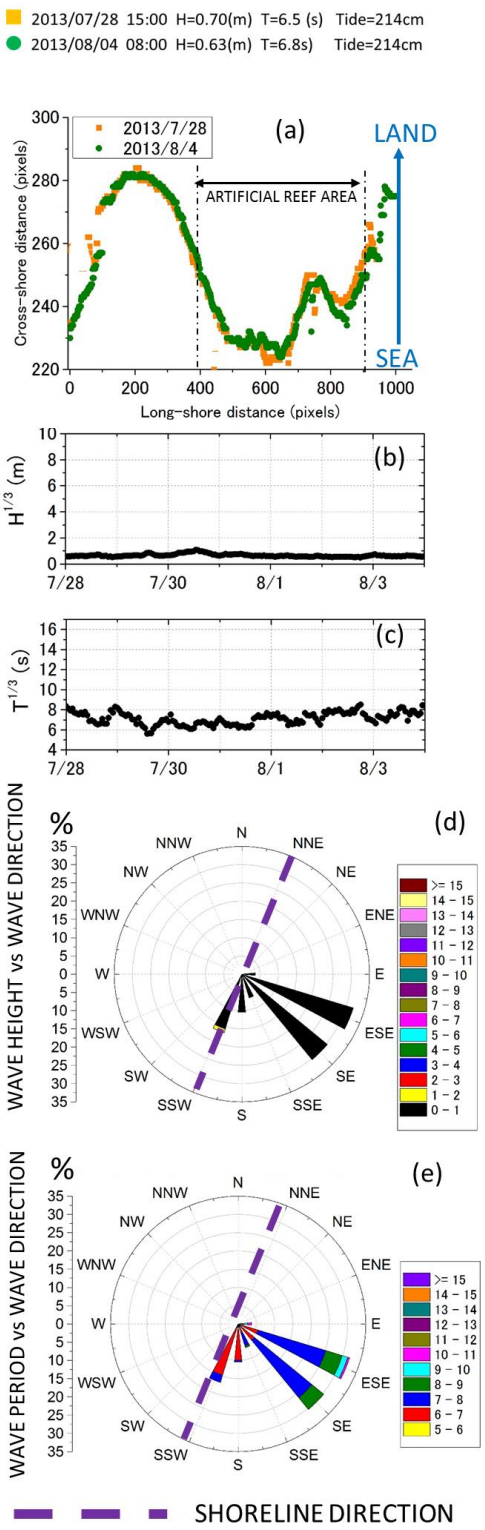

Figure 2.13 Shoreline change during 2013/7/28~2013/8/04

2.4.2.1 Shoreline change due to wave less than 1.3m high

During the period from 2012/09/06 to 2012/09/15, and from 2013/07/18 to 2013/07/27, wave approached to the coast from ESE direction with wave period range from 5s to 11s. Figure 2.11b shows an increase of wave high from the begining to the end of the period, while Figure 2.12b shows a contrast trend. However, the shoreline changes during these two periods have same behavior. From Figure 2.11a and Figure 2.12a, there is a slightly shoreline retreat in the right side and left side in compared with slightly shoreline forward in the middle part of area behind artificial reef. While the shoreline in the area without artificial reef stand stable during entire period. In the period from 2013/07/28 to 2013/08/04 wave approached to the coast from ESE and SE direction (Figure 2.13d) with 6s-8s wave periods (Figure 2.13c). Figure show that wave high is less than 0.8m in the begining and the end of period. This wave condition caused shoreline forwards in the entire area behind artificial reef and stands stable in the area without artificial reef (Figure 2.13a).

2.4.2.2 Shoreline change due to 1m-2m wave high

In the period from 2012/06/30~2012/07/08 the highest wave is 1.68m and the longest wave period is 9.1s, both of two waves come from SSW direction (See Figure 2.14d, Figure 2.14e). This wave condition caused the shoreline forward in the area behind the artificial reef and retreat in the area without artificial reef.

During the period from 2013/06/18~2013/06/23 wave's height with the longest period is wave approached to the coast from SSW (Figure 2.15d). From 18th June, 2013 to 21st June, 2013, the wave's height is larger than 1.5m (Figure 2.15b), and from 21st June, 2013 to 23rd June, 2013 wave period more than 8s (Figure 2.15c). Under this wave condition, shoreline retreat in the area without artificial reef and in the middle part of area behind artificial reef (Figure 2.15a).

In the period from 2013/08/17~2013/08/27 and from 2013/8/26~2013/09/03, there was a similar income wave condition. In this time, wave approached to the coast from SSW (Figure 2.16e, Figure 2.17e) with wave period 5s-11s ((Figure 2.16c, Figure 2.17c)).

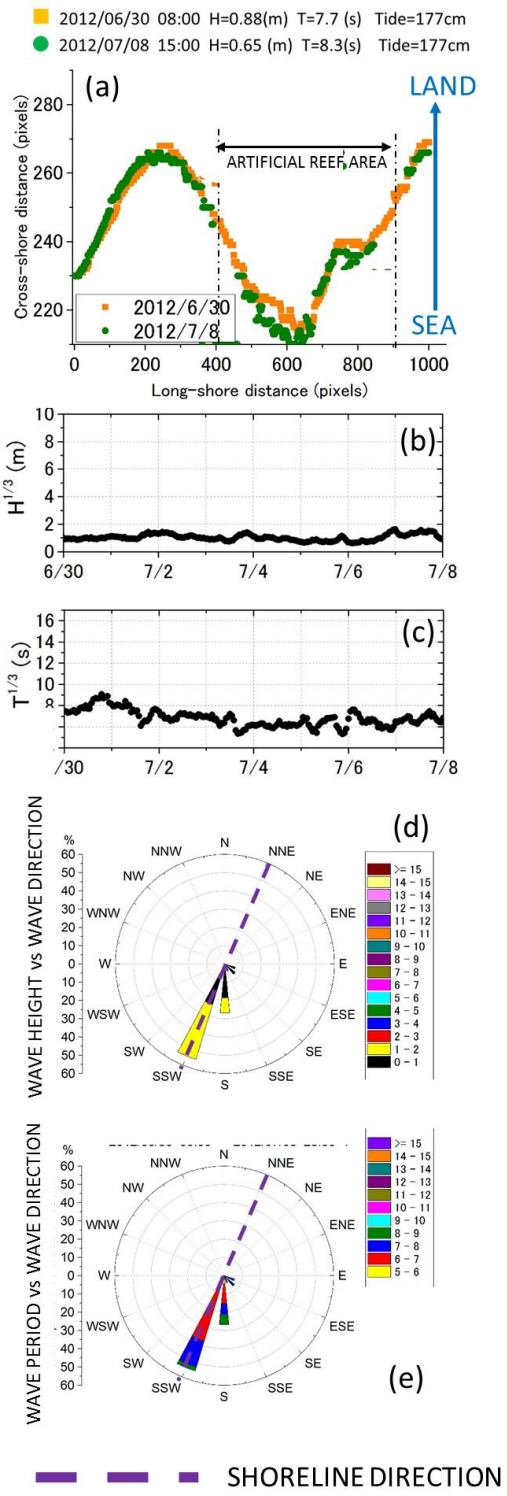

Figure 2.14 Shoreline change during 2012/06/30~2012/07/08

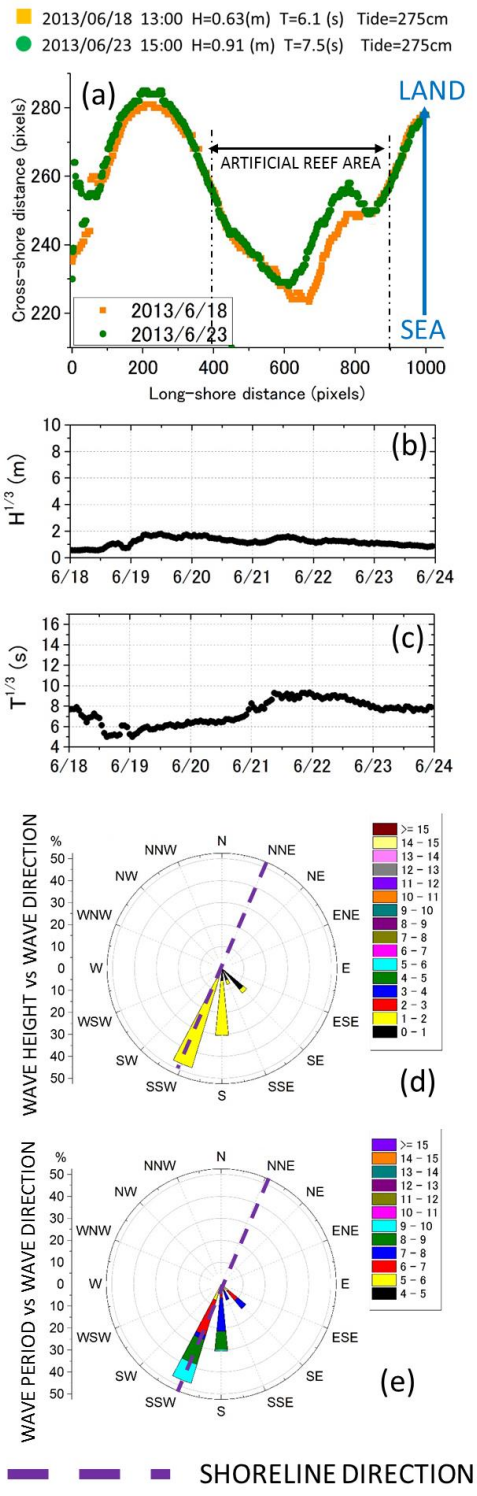

Figure 2.15 Shoreline change during 2013/06/18~2013/06/23

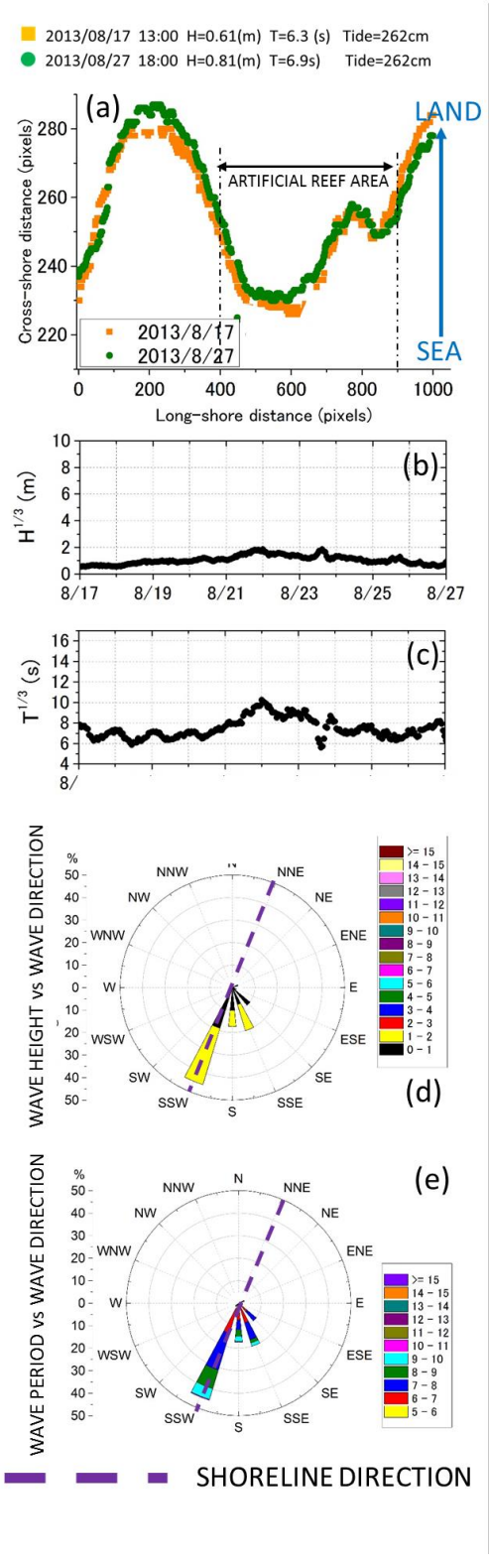

Figure 2.16 Shoreline change during 2013/08/17~2013/08/27

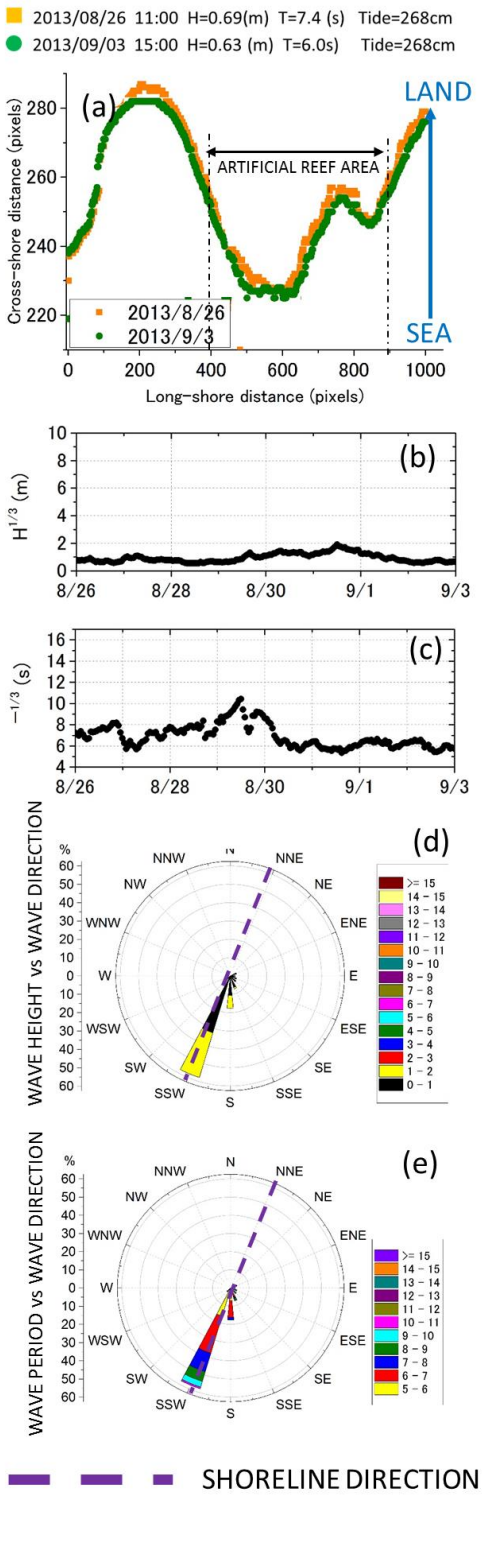

Figure 2.17 Shoreline change during 2013/8/26~2013/09/03

However, during 2013/08/17~2013/08/27, there was a short period (about 3 day from 21st August, 2013 to 23rd August, 2013) wave's height were continuously higher than 1.9m (Figure 2.16b) with the wave period more than 10s (Figure 2.16c). While in the period from 2013/8/26~2013/09/03, there is only one day that wave's height reach to 1.9m (Figure 2.17b) with wave period 9s (Figure 2.17c). From Figure 2.16a and Figure 2.17a, it can be seen that shoreline change in different way in these two periods. In 2013/08/17~2013/08/27, shoreline retreat on the entire study area, while in 2013/8/26~2013/09/03 shoreline forward on the entire study area. From this result, it can be understand that the duration of wave attack is also play an important role on beach erosion.

2.4.2.3 Shoreline change due to 2m-3m wave high

Figure 2.18 to Figure 2.21 shows the shoreline change under 2m-3m income wave high. Figure 2.18 indicate that, during 2013/01/12~2013/01/20, except a single wave exceed 2.4m on 14th January, 2013, wave's height through this period is small compared with other cases. And the shoreline forward on entire the study area. Figure 2.19a shows that, in 2013/05/09~2013/05/15 shoreline also forward even there is a group wave with the wave high about 2m off to the coast during 3days (Figure 2.19b). This period shows the different trend with the shoreline change during 2013/05/23~2013/06/05 although these two periods had similar wave condition. In 2013/05/09~2013/05/15, high wave approach to the coast from SSW direction, and in 2013/05/23~2013/06/05 high wave approach to coast from SSE, SE, ESE. This difference of wave direction might be the reason leading to the contrast shoreline change of these two periods. From Figure 2.21, it can be understood that 2m-3m wave approached to the coast from SSW, S will result the shoreline retreat on both side of study area, and shoreline forward in the middle part of study area.

2.4.2.3 Shoreline change due to 3m-4m wave high

Figure 2.22 shows the shoreline change from 25th, April, 2014 to 04th May, 2014. During this time, wave approached to the coast from SE direction (Figure 2.22d). Wave periods increase from 7s at the beginning of period to nearly 10s at the end of period (Figure 2.22c). Wave's height is smaller than 1m at the beginning of period,

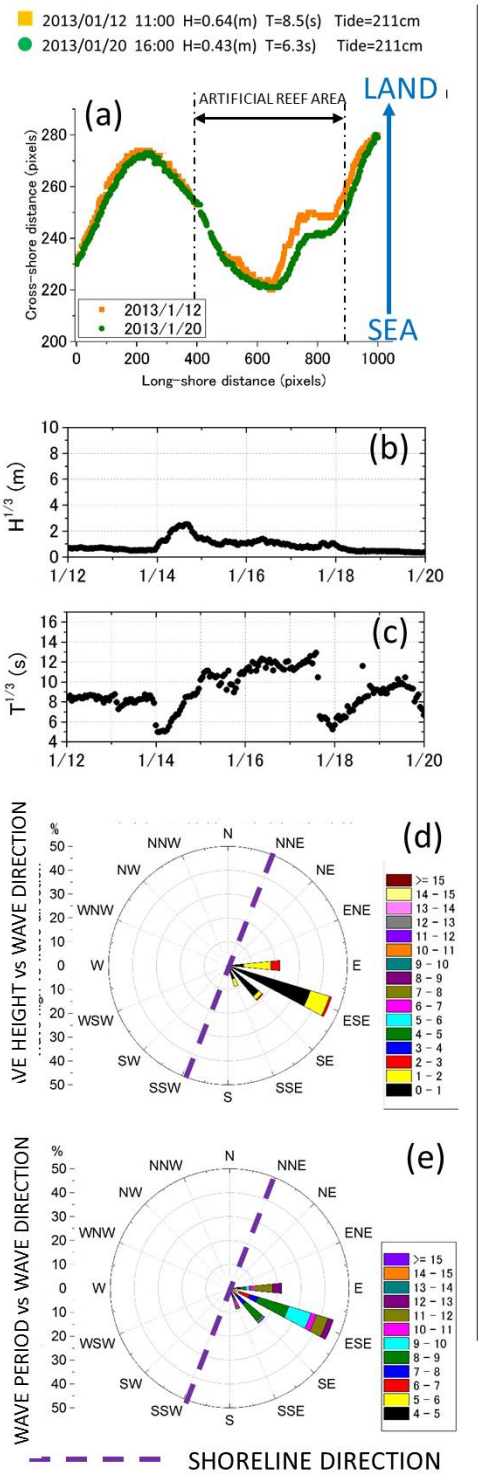

Figure 2.18 Shoreline change during 2013/01/12~2013/01/20

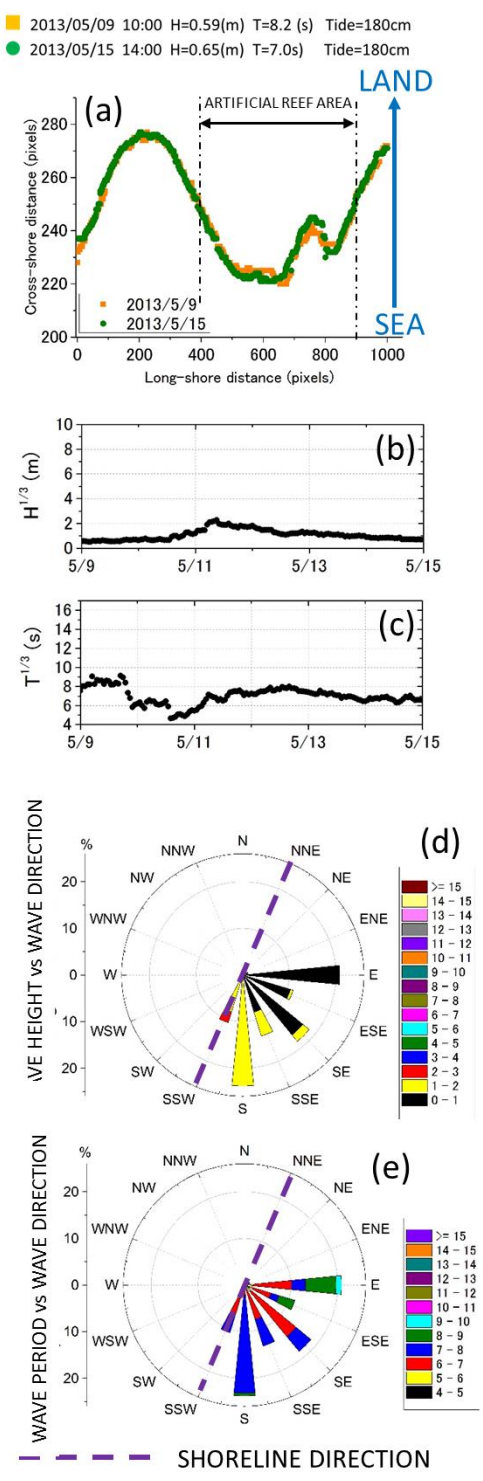

Figure 2.19 Shoreline change during 2013/05/09~2013/05/15

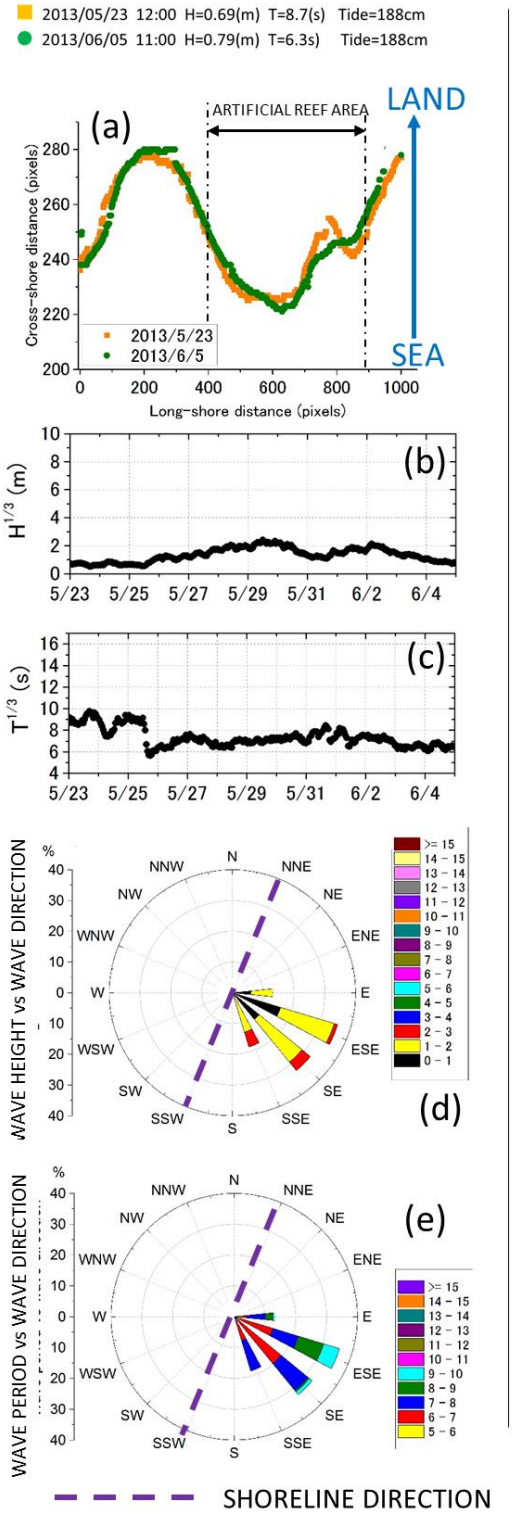

Figure 2.20 Shoreline change during 2013/05/23~2013/06/05

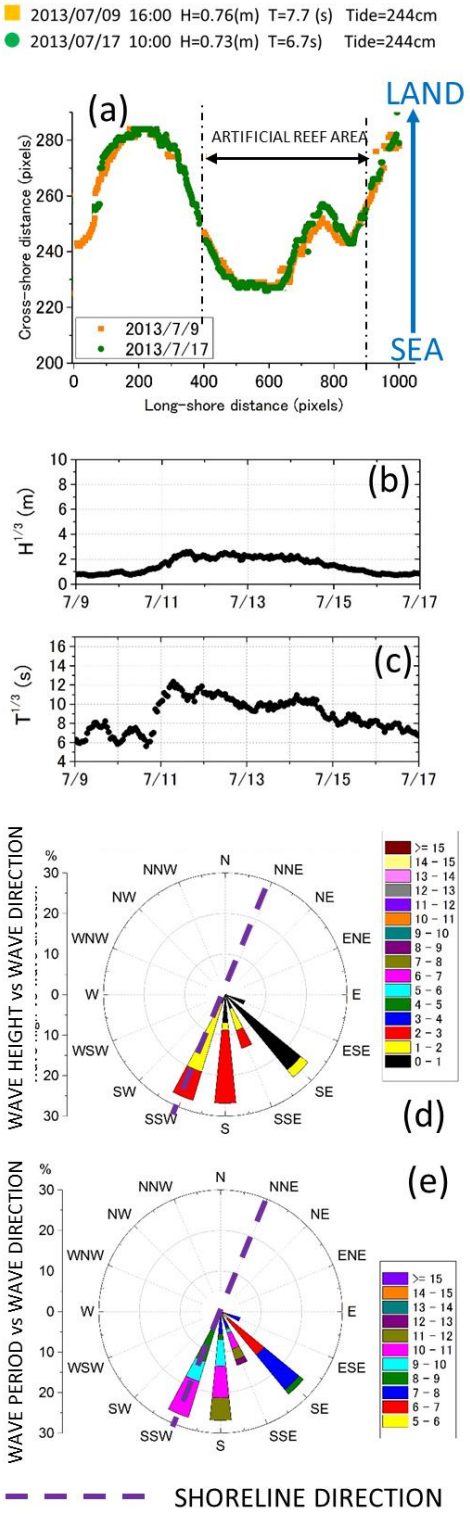

Figure 2.21 Shoreline change during 2013/07/09~2013/07/17

than increase to highest point in the middle of period, and decrease to less than 1m in the end (Figure 2.22b). This wave condition caused the retreat of in the area without artificial reef. In the area behind artificial reef the left side retreat, while the right side forward. During 2014/05/10 ~ 2014/05/07 and 2014/05/19 ~ 2014/05/23, income wave show the similar behavior, in which wave period is 4s to 10s income wave direction extend from SE direction to SSW direction. This wave direction results a long-shore current on south to north direction, i.e. sediment have moved from south to north, caused shoreline retreat in the left side of study are and forward in the right side of study area (Figure 2.23a, Figure 2.24a). However, during 2014/05/19 ~ 2014/05/23, high wave came from ESE, SE, SSE direction (Figure 2.24d), while in 2014/05/10 ~ 2014/05/07, high wave came from S direction (Figure 2.23d). Moreover, in 2014/05/19 ~ 2014/05/23, 9s-10s wave period was 15% (Figure 2.24e), while during 2014/05/10 ~ 2014/05/07, only 1% wave had 9s-10s period. Hence, retreat distance during 2014/05/19 ~ 2014/05/23 is larger than that one 2014/05/10 ~ 2014/05/07.

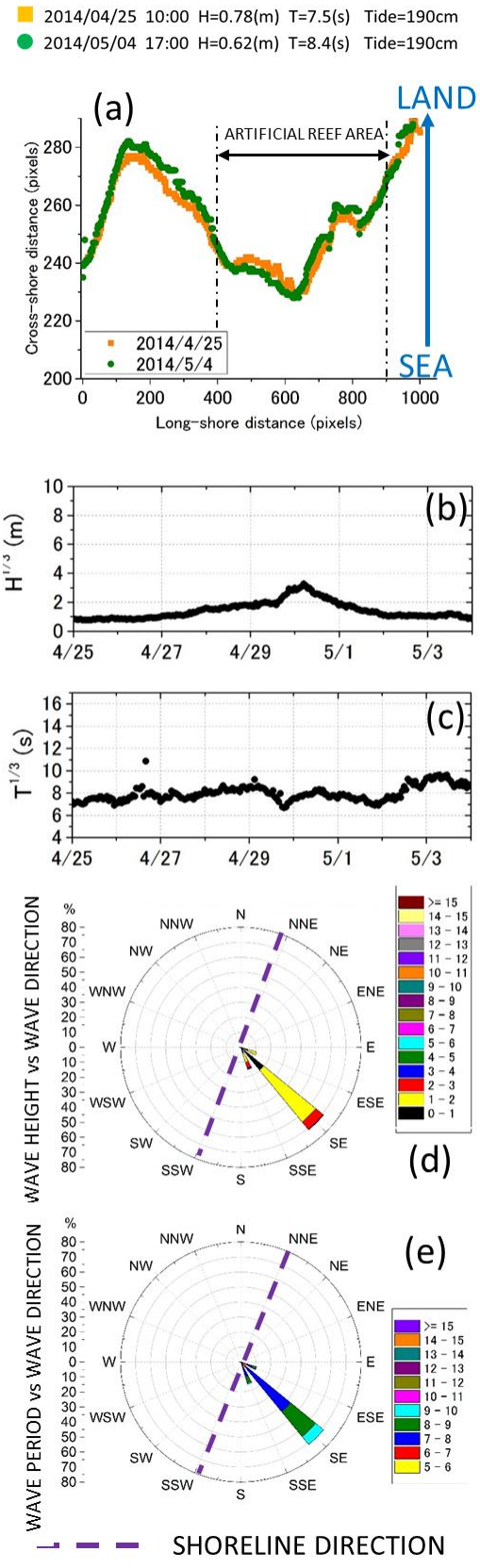

Figure 2.22 Shoreline change during 2014/04/25~2014/05/04

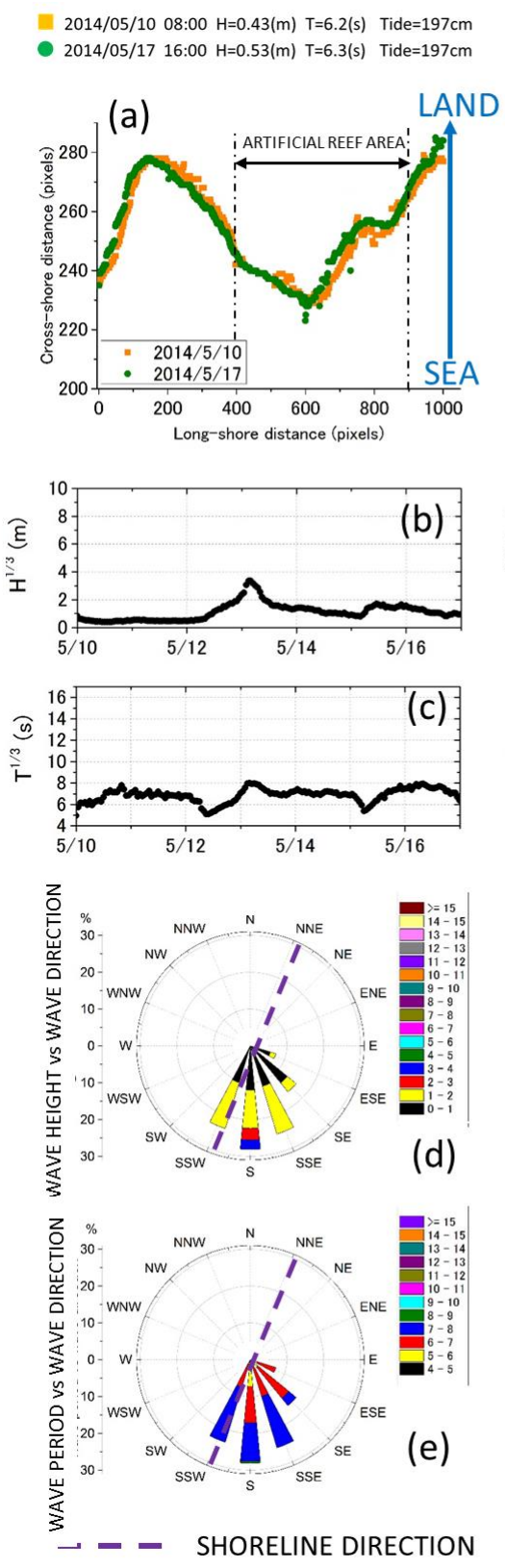

Figure 2.23 Shoreline change during 2014/05/10~2014/05/17

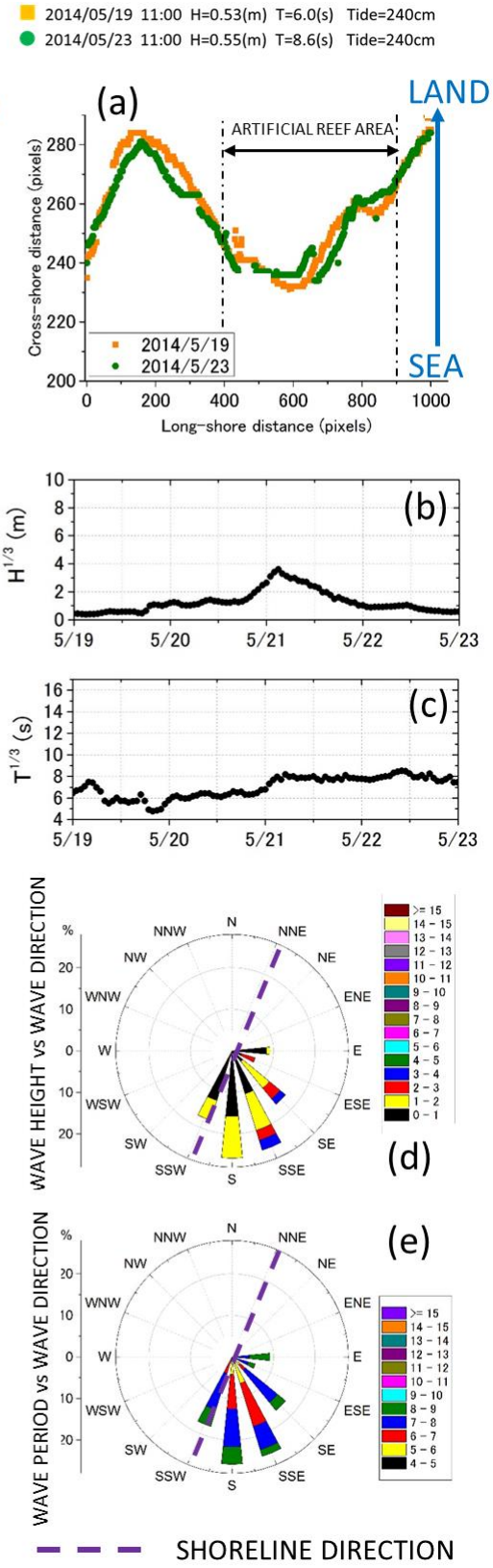

Figure 2.24 Shoreline change during 2014/05/19~2014/05/23

2.4.2.3 Shoreline change due to wave 4m-6m high

Figure 2.25 shows shoreline change during 2012/07/30~2012/08/10. In this period, after a high energy wave caused by a large wave, which highest wave high was 4.8m and highest wave period was 11.5s, off to the coast SE direction on 1st August, 2014, a number of waves with wave high around 2.5m and wave period about 9s continue attack to the coast until 6th August, 2014. This wave conditions lead to shoreline retreat about 4m entire the study area, even in the area behind artificial reef. In contrast with previous case, during the period from 2012/11/15 to 2012/11/19 (Figure 2.26) and from 2012/11/19 to 2012/11/30 (Figure 2.27), low energy wave extend on the whole period, with wave's height less than 1m, and wave period less than 10s, except a single large wave energy in the middle of period. Hence, the shoreline retreat was not large in compared with previous case. Moreover, since wave direction was S and SSW, shoreline retreat occurs only on the area without artificial reef.

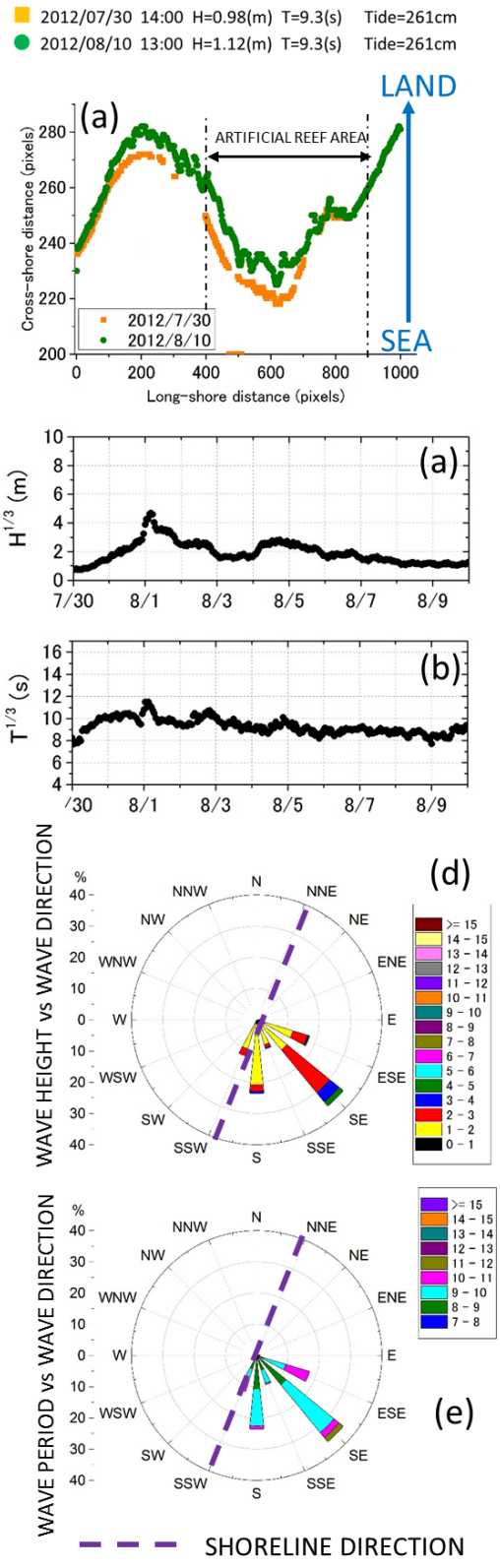

Figure 2.25 Shoreline change during 2012/07/30~2012/08/10

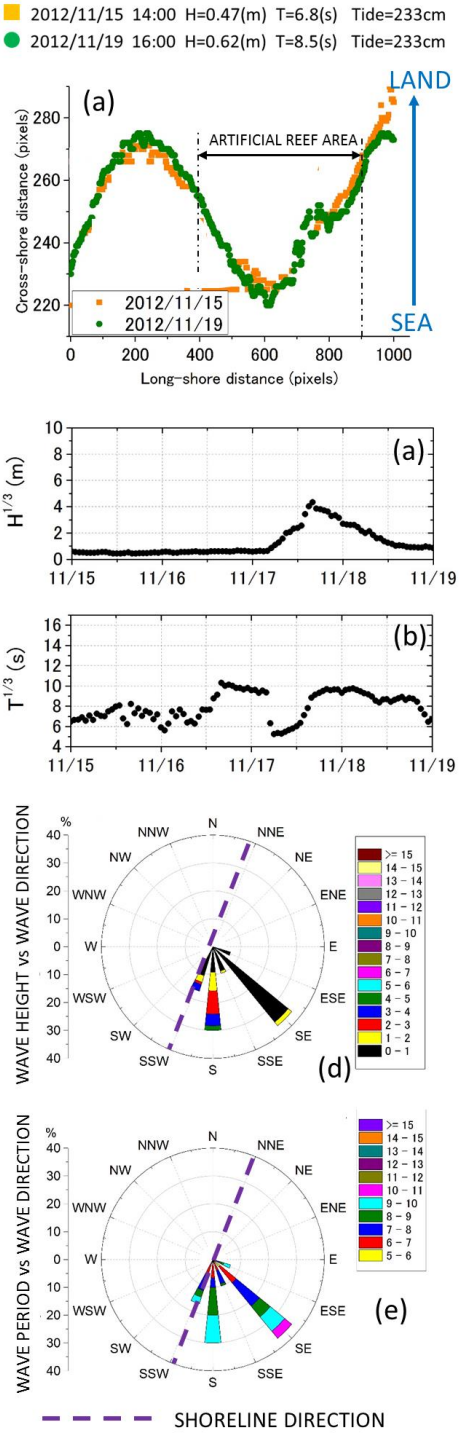

Figure 2.26 Shoreline change during 2012/11/15~2012/11/19

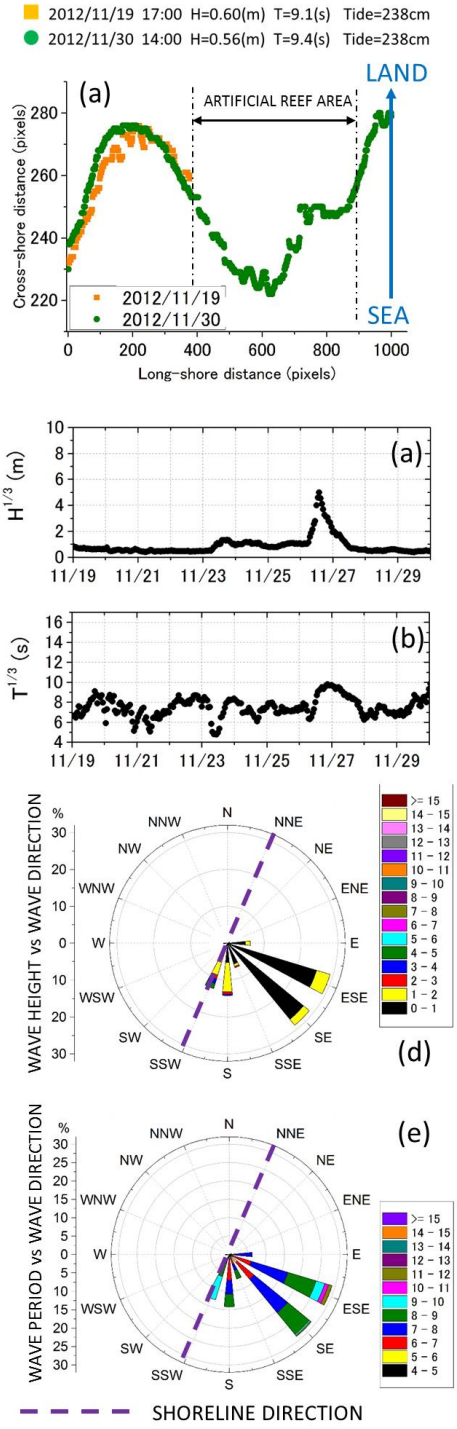

Figure 2.27 Shoreline change during 2012/11/19~2012/11/30

2.4.2.3 Shoreline change due to larger 6m wave high

From Figure 2.28-Figure2.30, it can be said that the shoreline will significant retreat after income wave with wave's height higher than 6m off to the coast. Wave occurred during 2013/09/11~2013/09/20 (Figure 2.28b, Figure 2.28c) have smaller energy than another two waves occurred on 2013/06/17~2013/06/25 (Figure 2.29b, Figure 2.29c) and 2013/10/12~2013/10/17 (Figure 2.30b, Figure 2.30c). However, in the period from 2013/09/11 to 2013/09/20, shoreline retreat 8m, the largest retreat distance among 3 study periods. Because, in this time the highest wave off to the coast from SSE direction, while during 2013/06/17~2013/06/25 the highest wave was from SSW direction (Figure 2.29d), and during 2013/10/12~2013/10/17 the highest wave approached to the coast from S direction (Figure 2.30).

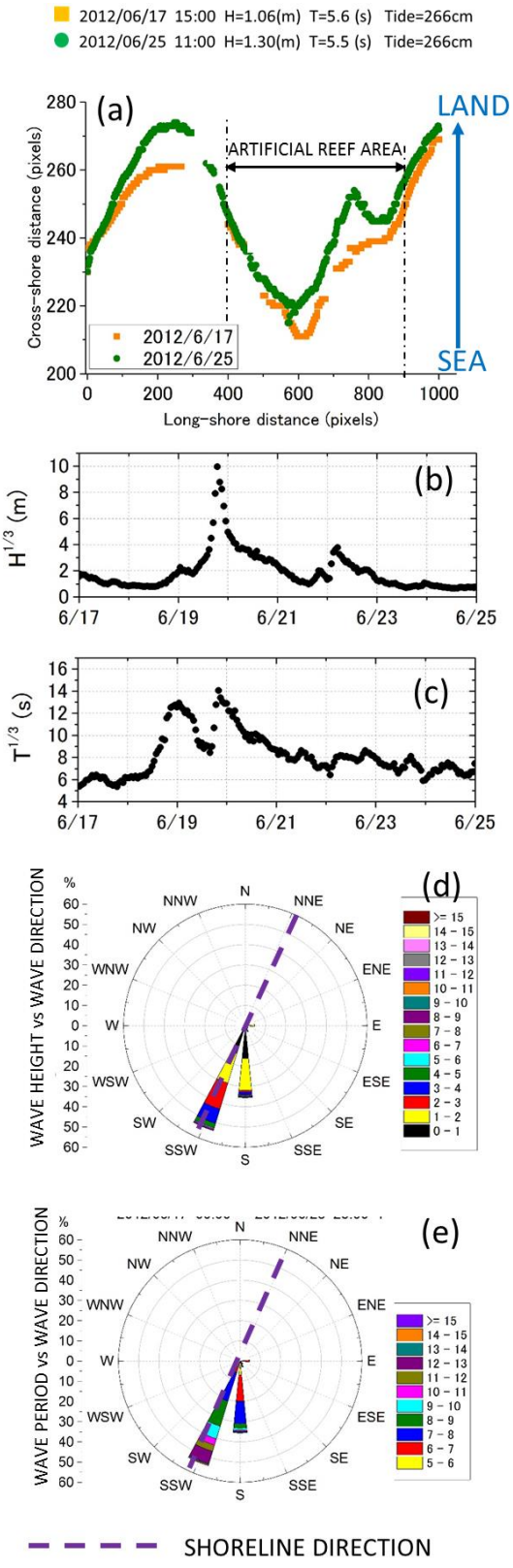

Figure 2.28 Shoreline change during 2012/06/17~2012/06/25

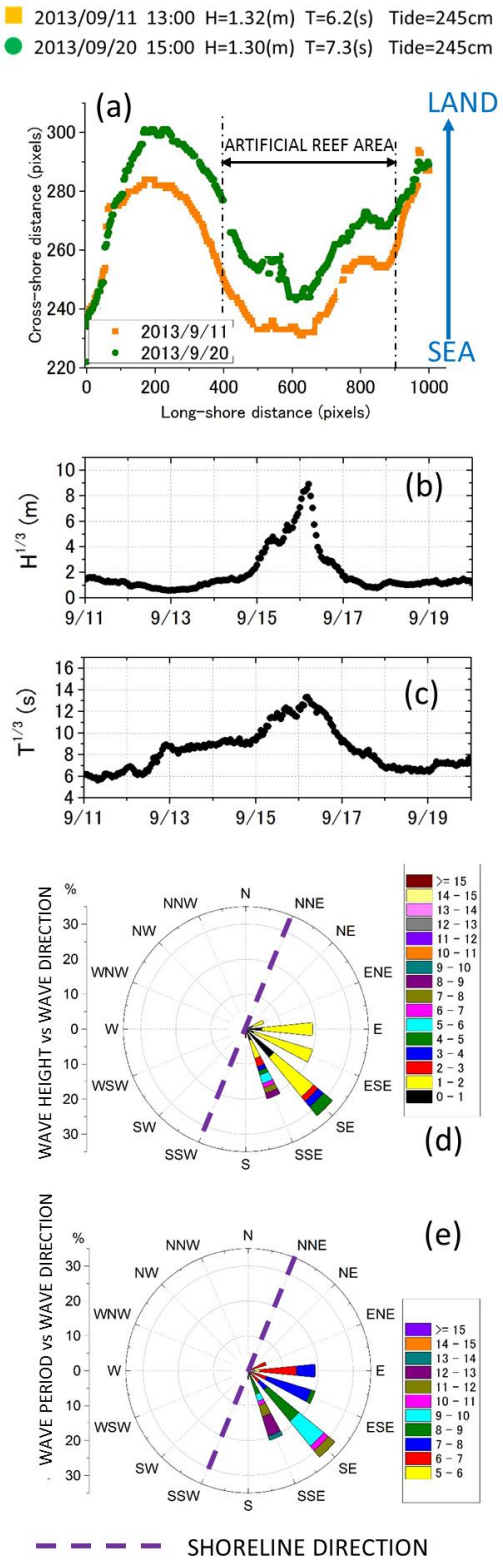

Figure 2.29 Shoreline change during 2013/09/11~2013/09/20

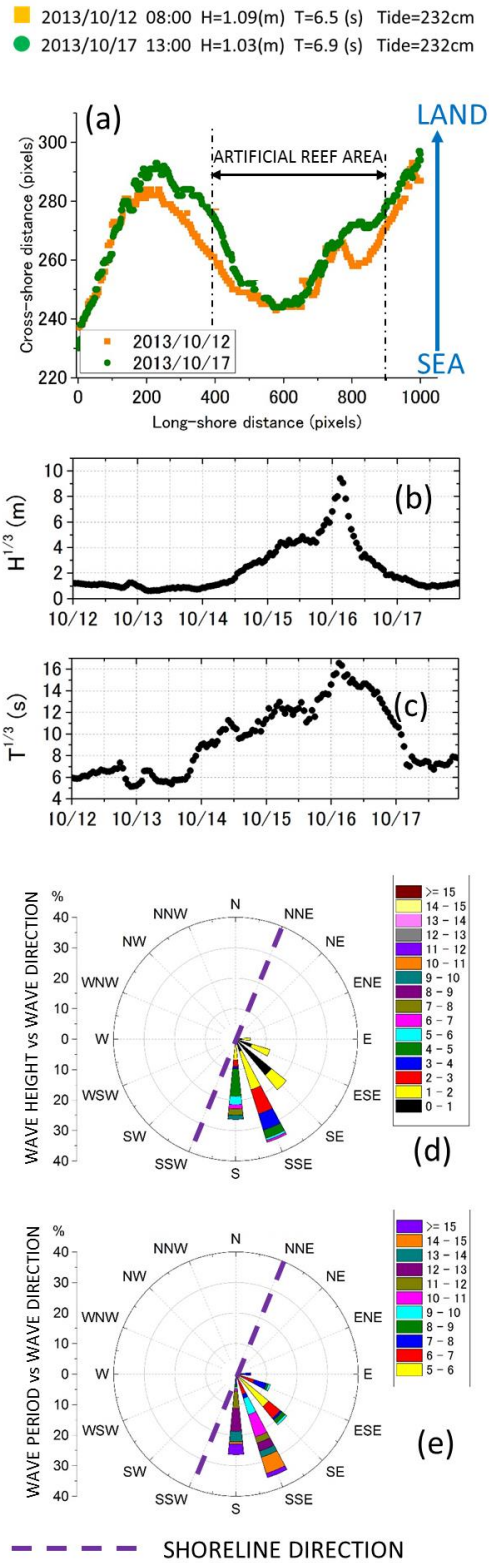

Figure 2.30 Shoreline change during 2013/10/12~2013/11/17

2.4.3 Long-term shoreline change

Long-term coastline change plays a significant role in long-term coastal management. In this section, shoreline season change was analyzed by using shoreline data from 1st March, 2013 to 28th February, 2014. Then the shoreline change during 2 years study period will be shown.

2.4.3.1 Shoreline change in spring

In spring, about 50% wave's height range from 1m-2m, 30% wave's height less than 1m, 5% wave's height range 2m-3m. About wave period, 20% was 6s-7s, 30% was-8s, 15% was 8s-9s, 5% was 9s-10s and 5% was longer than 10s. There is only one time when wave's height exceeds 5m, observed on 5th April, 2013. High wave high approached to the coast from ESE, SE, S, SSW direction (Figure 2.32c), while high wave period approached to the coast from E, ESE, SE direction (Figure 2.32d). Due to this wave direction, the shoreline fluctuation in the area without artificial is higher than that one in the area behind artificial reef. In the end of spring season, the largest shoreline retreat distance was 8m, located on the area without artificial reef. However in the area behind artificial reef, the shoreline forward about 2m.

2.4.3.2 Shoreline line change in summer

In early summer, most of wave high are higher than 1m, while in the later summer wave's height are almost smaller than 1m. In the summer, both high wave's height approached and high wave period approached to the coast from SSE, S, SSW direction (Figure 2.34c, Figure 2.3d). Due to this wave direction, the shoreline fluctuation on the area behind artificial reef is larger than the area without artificial reef. In the end of summer, the shoreline on the area without artificial reef forward about 1m (Figure 2.33). In the area behind artificial reef the shoreline in right side retreat about 1~2m, while the left side forward about 1~2m. From Figure 2.32a and Figure 2.34a, it can be understand that wave high in summer is smaller than waves in spring, hence the shoreline fluctuation in summer are smaller than that one in spring.

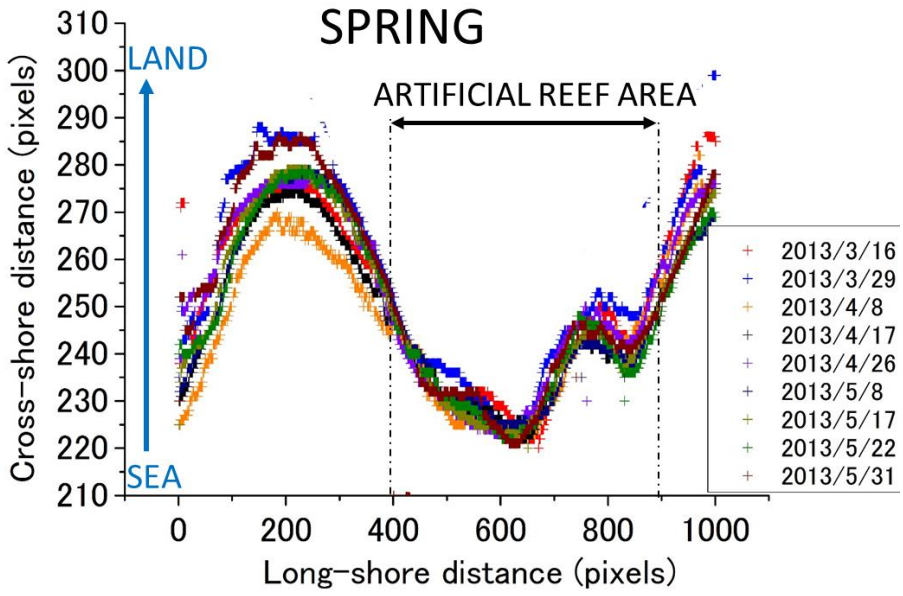

Figure 2.31 Shoreline change in spring

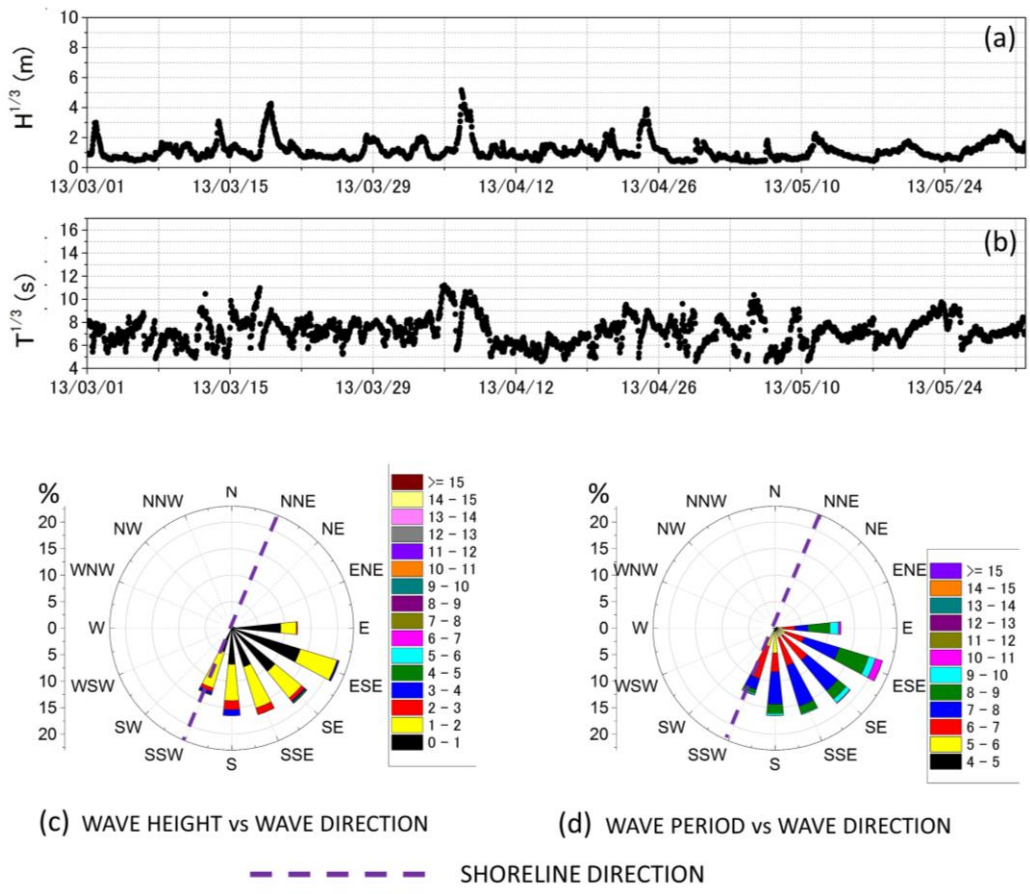

Figure 2.32 Wave condition in spring

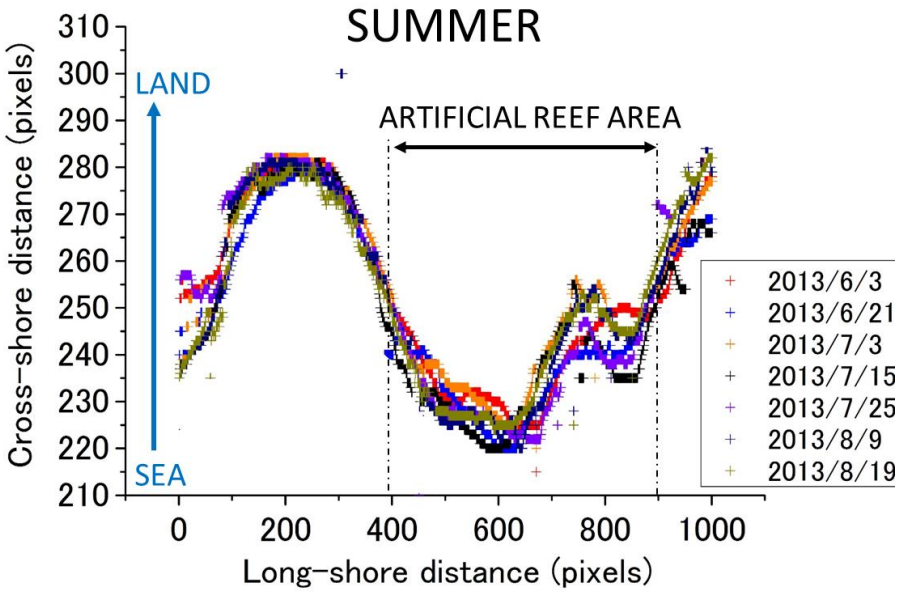

Figure 2.33 Shoreline change in summer

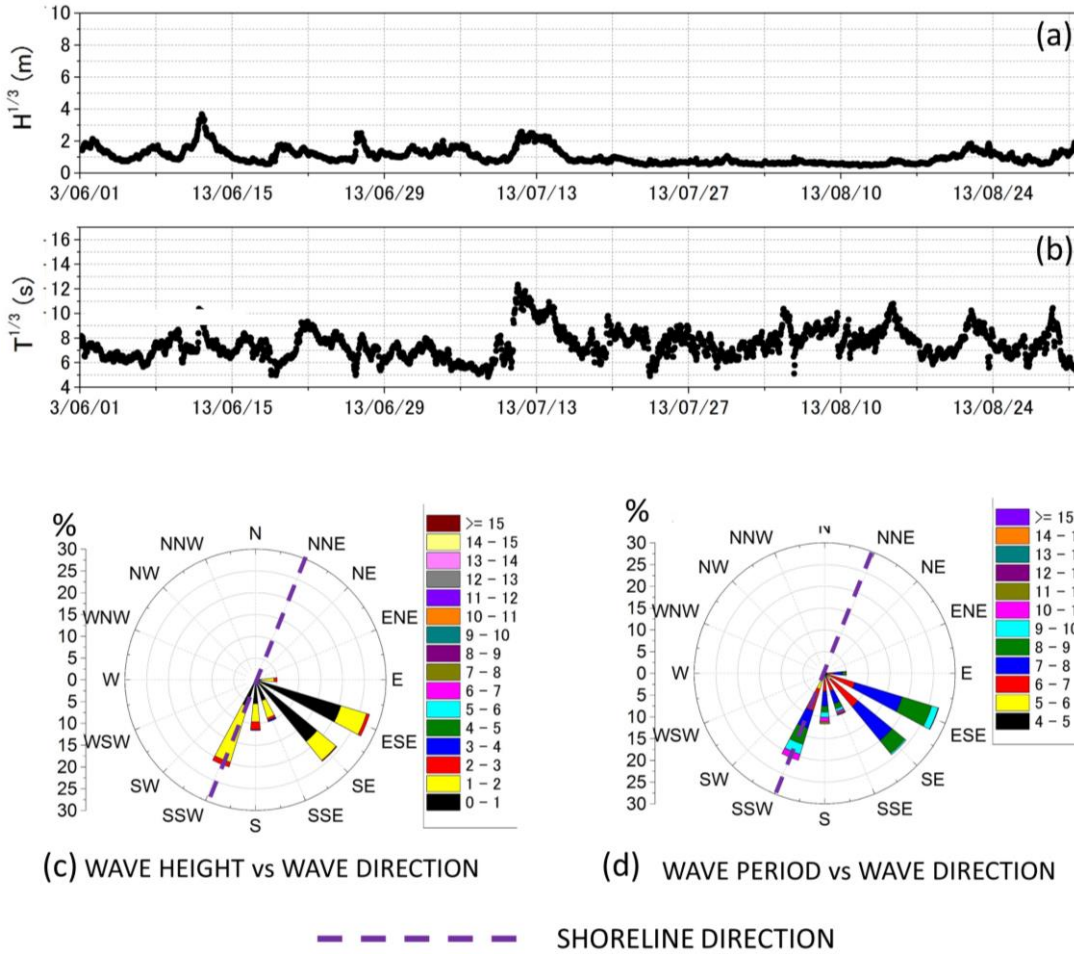

Figure 2.34 Wave condition in summer

2.4.3.3 Shoreline line change in fall

In fall season, high wave approach to the coast from all direction between E and SSW direction, hence the shoreline fluctuations on entire beach are larger than shoreline fluctuation on spring and summer. Because number of typhoons in fall season is larger than another seasons (Table 2.1), the most violent shoreline change during a year occurs in this season. The largest shoreline retreat was on 16th September, 2013 due to the typhoon No.1318 (Figure 2.35), with the center pressure was 975hPa (Figure 2.36). Comparing the shoreline position before (day 2013/09/10 in Figure 2.37) and after (day 2013/09/19 in Figure 2.37), shoreline entire the beach retreat about 6m after this storm off to the coast. After this storm, shoreline gradually forward, but retreat again due to 9m wave high off to the coast on 16th October, 2013.

Table 2.1 Number of typhoon during 2013 and 2014
(Source: JAPAN Meteorological Agency)

Year	Month											
	1	2	3	4	5	6	7	8	9	10	11	12
2013	1	1				4	3	6	7	7	2	
2014	2	1		2		2	5	1	5	2	1	2

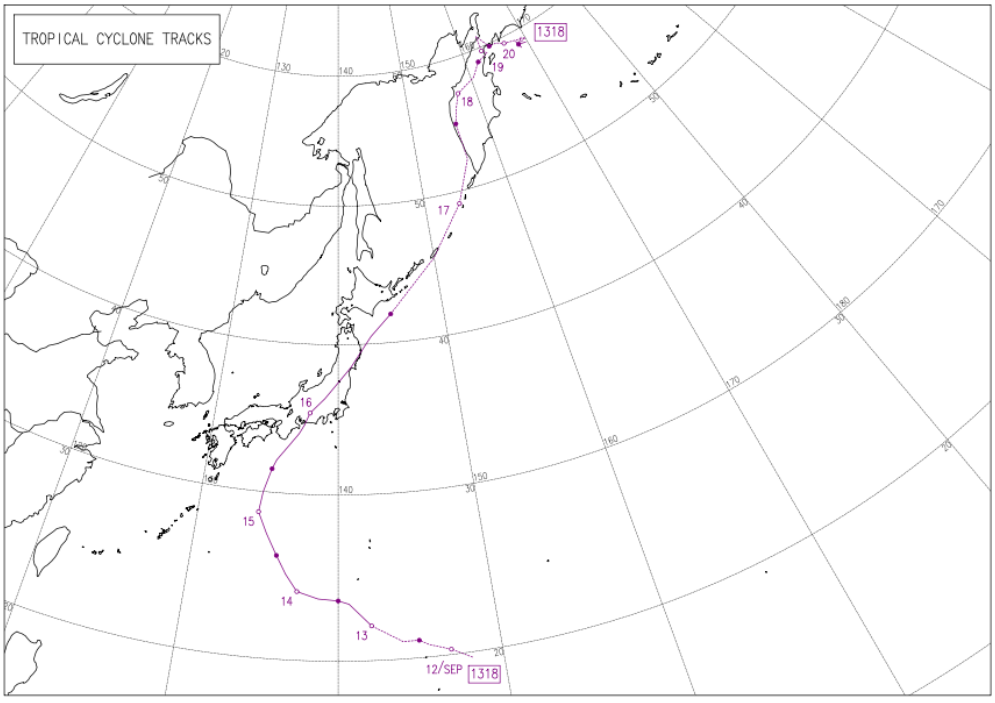

Figure 2.35 Route of storm No.1318 (Source: JAPAN Meteorological Agency)

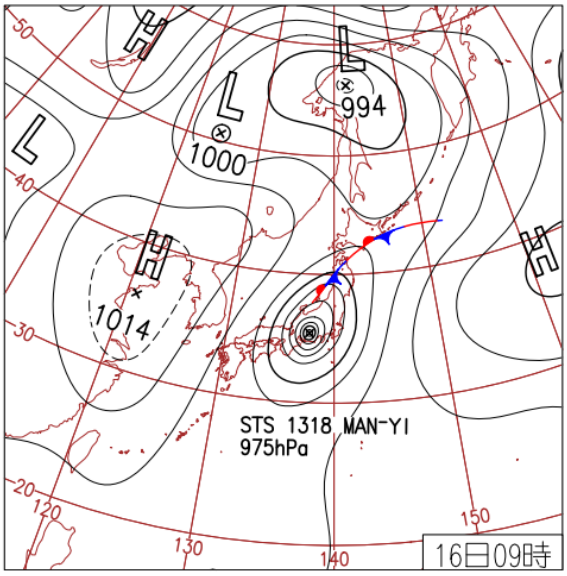

Figure 2.36 Pressure field due to No.1318 (Source: JAPAN Meteorological Agency)

2.4.3.4 Shoreline line change in winter

Figure 2.37 shows that in the area without artificial reef, shoreline retreat in early winter but forward form 24th January to the end of winter (day 20114/02/04, 2014/02/18, 2014/02/25 in Figure 2.38), while shoreline in the area behind artificial reef almost stable in early winter and retreat in the 24th January to the end of winter.

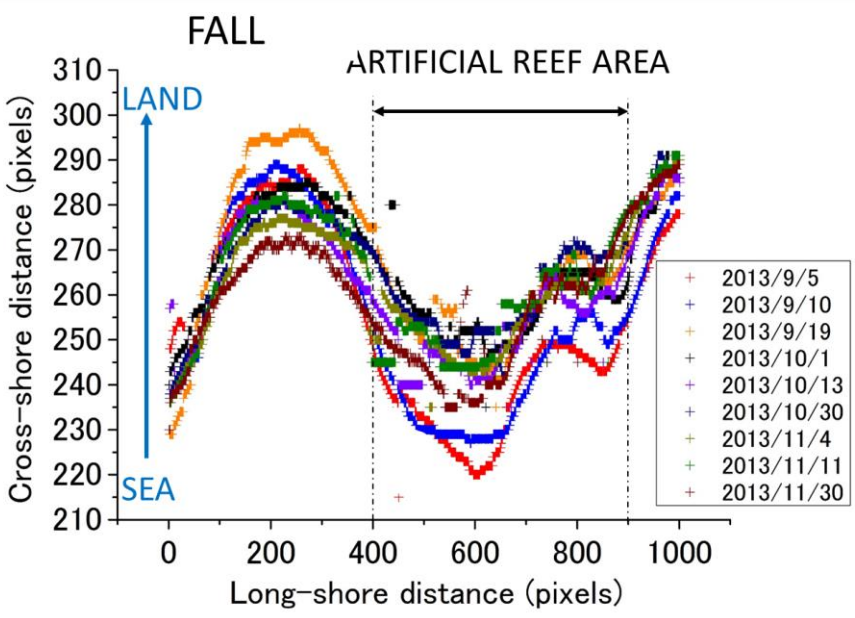

Figure 2.37 Shoreline change in fall season

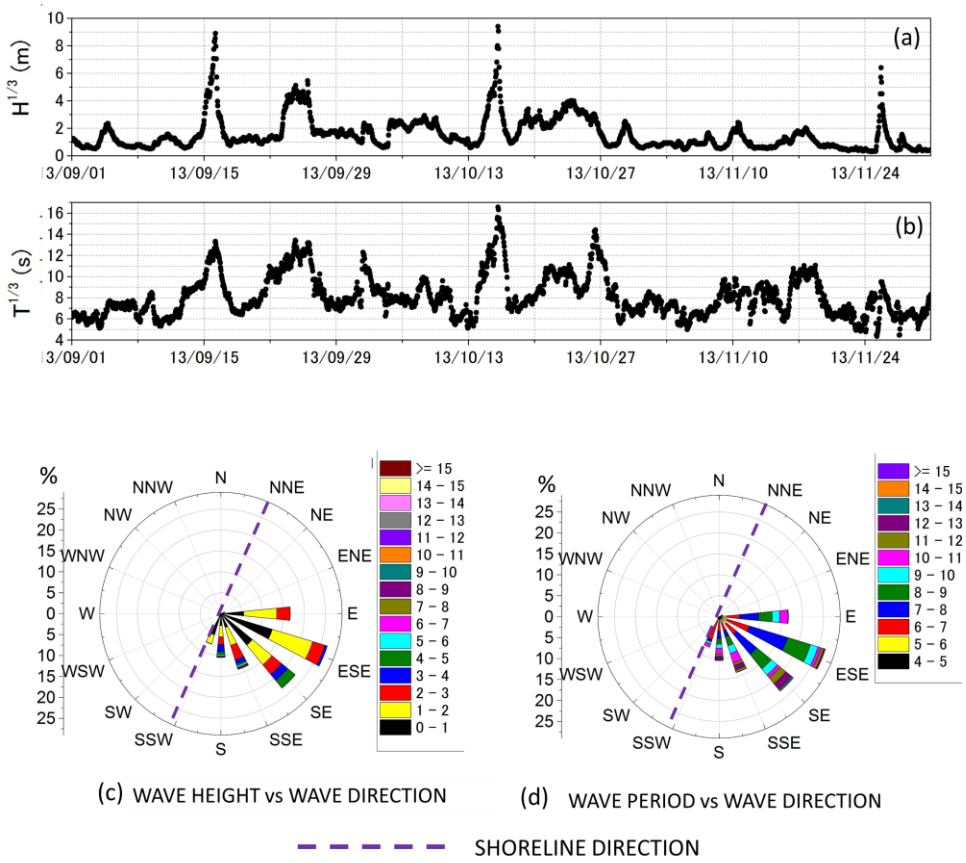

Figure 2.36 Wave condition in fall

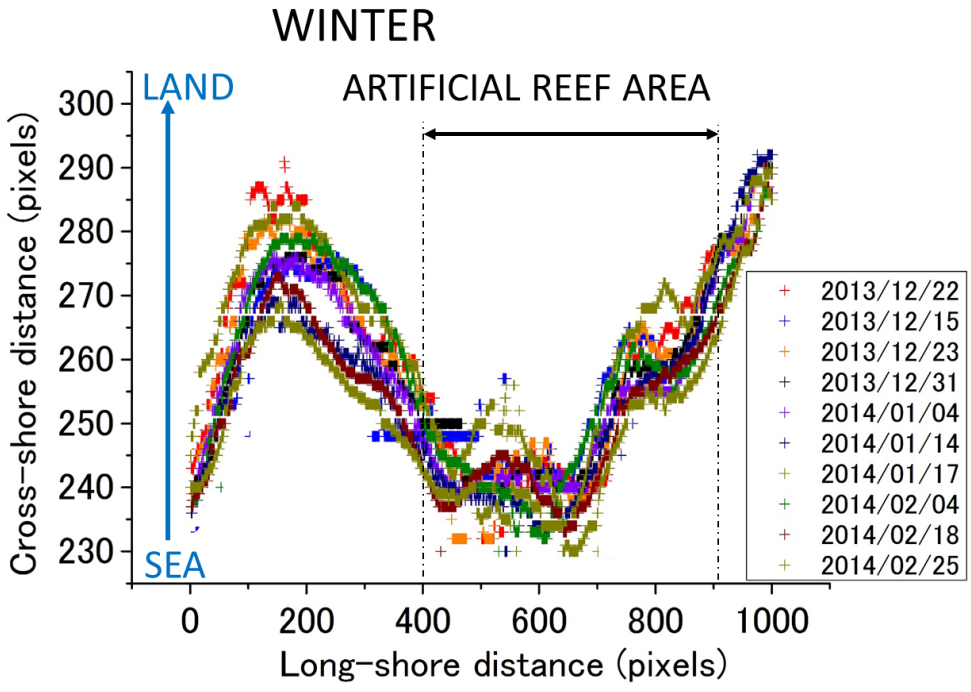

Figure 2.38 Shoreline change in winter season

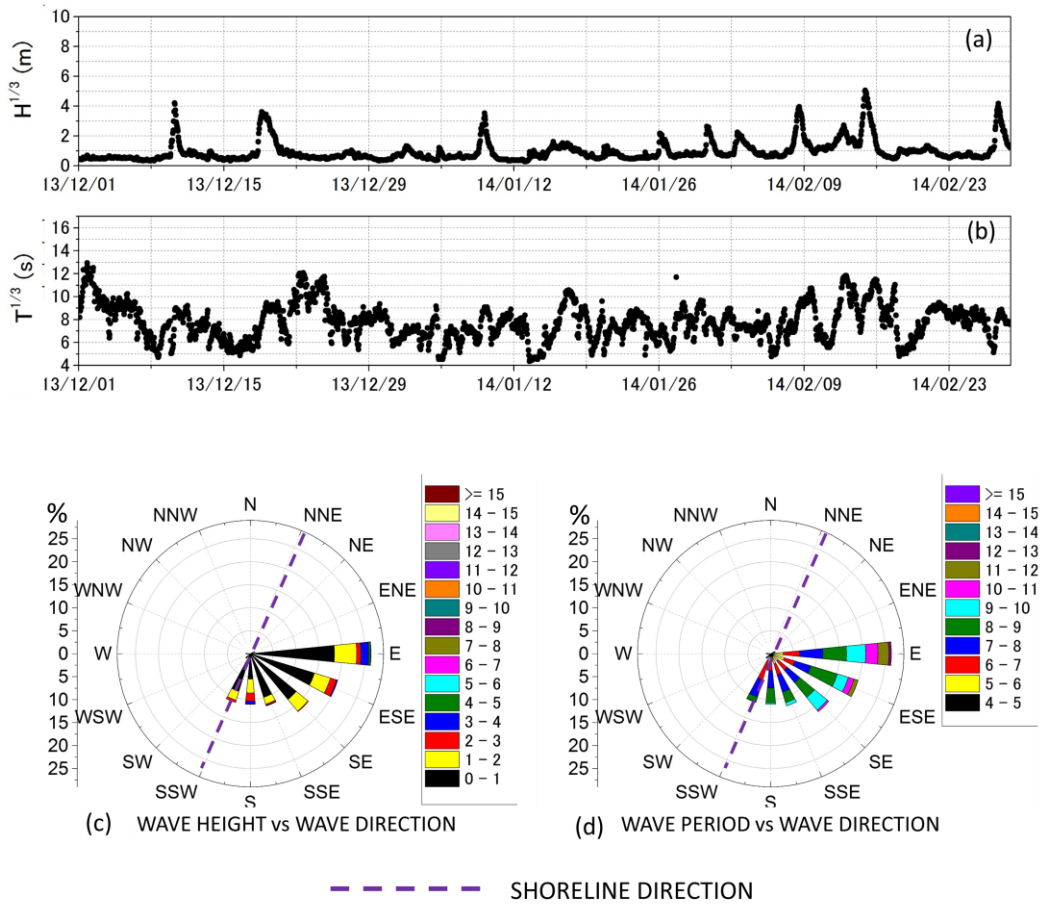

Figure 2.39 Wave condition in winter

2.4.3.5 Shoreline change during the 2 year study period

Figure 2.39 shows shoreline over 2 years data taken under condition with 1m wave height and 7 second wave period at 81cm tide level. In general, shoreline for entire beach has been retreated continuously from 2012. The most landward position of shoreline was recorded on 18th September 2013. This may be the results of shoreline retreat caused by high waves of 9m height with period of 13s on the tide level of 220cm on 15th September 2013 (typhoon 1318 in 2013). After this event, the shoreline is gradually recovering. However, in the end of the study period, the shoreline has retreat significant again. As mentioned before, the predominant wave direction in this area is southern directions which results in northern long-shore current. And serious shoreline retreat at the north of artificial reefs reflects an important role on the reduction of shoreline erosion of artificial reefs (Figure 2.40).

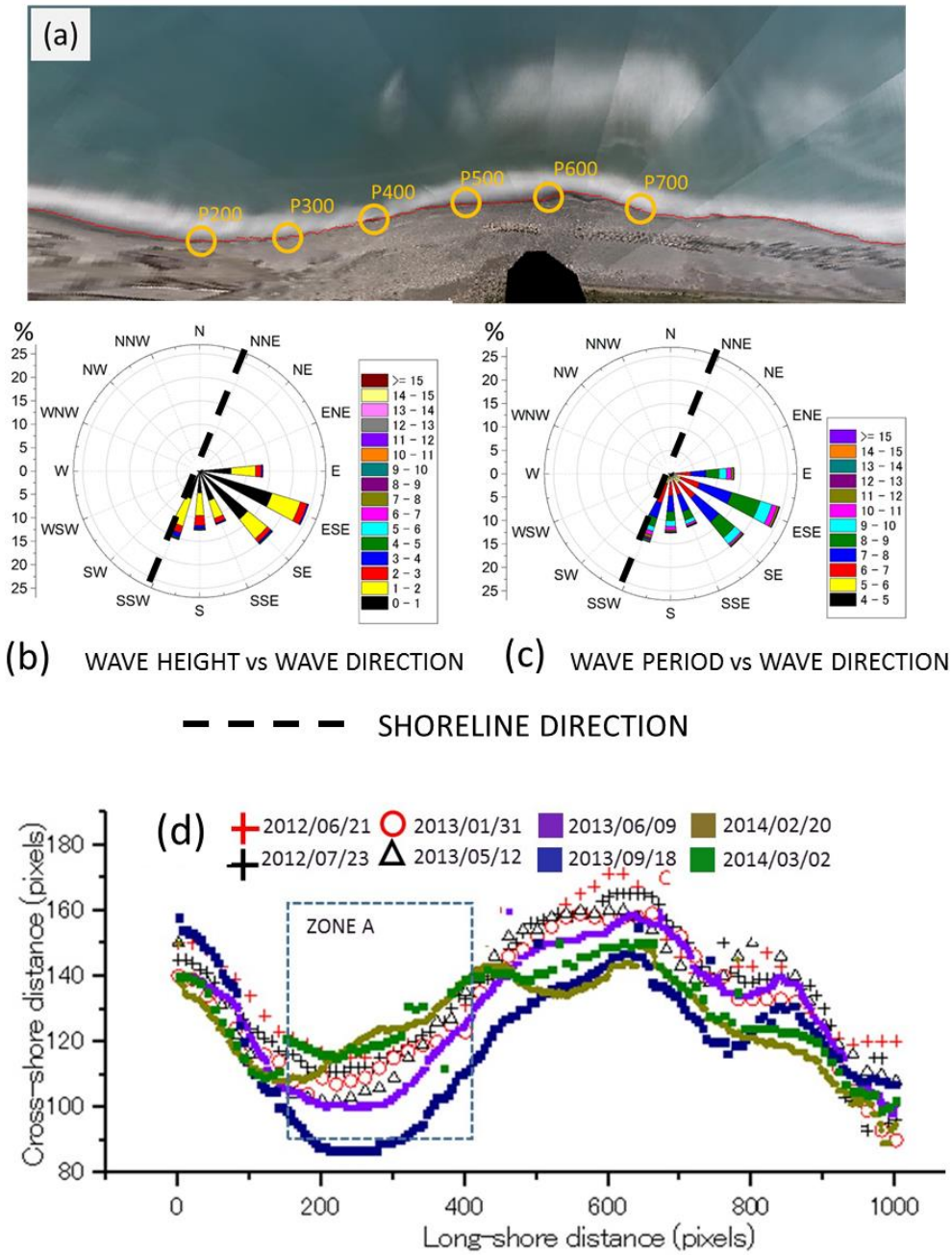

Figure 2.40 Shoreline change during 2012/06/08~2014/05/31

2.4.4 Effect of artificial reef on shoreline change

In order to investigate the effect of artificial reef on behavior of shoreline, the following six points were considered. Point 1 (P200), point 2 (P300), point 3 (P400) are located at the area without artificial reef. Point 4 (P500), point 5 (P600) and point 6 (P700) are located behind artificial reef. The fluctuations at P1and P2 are always large

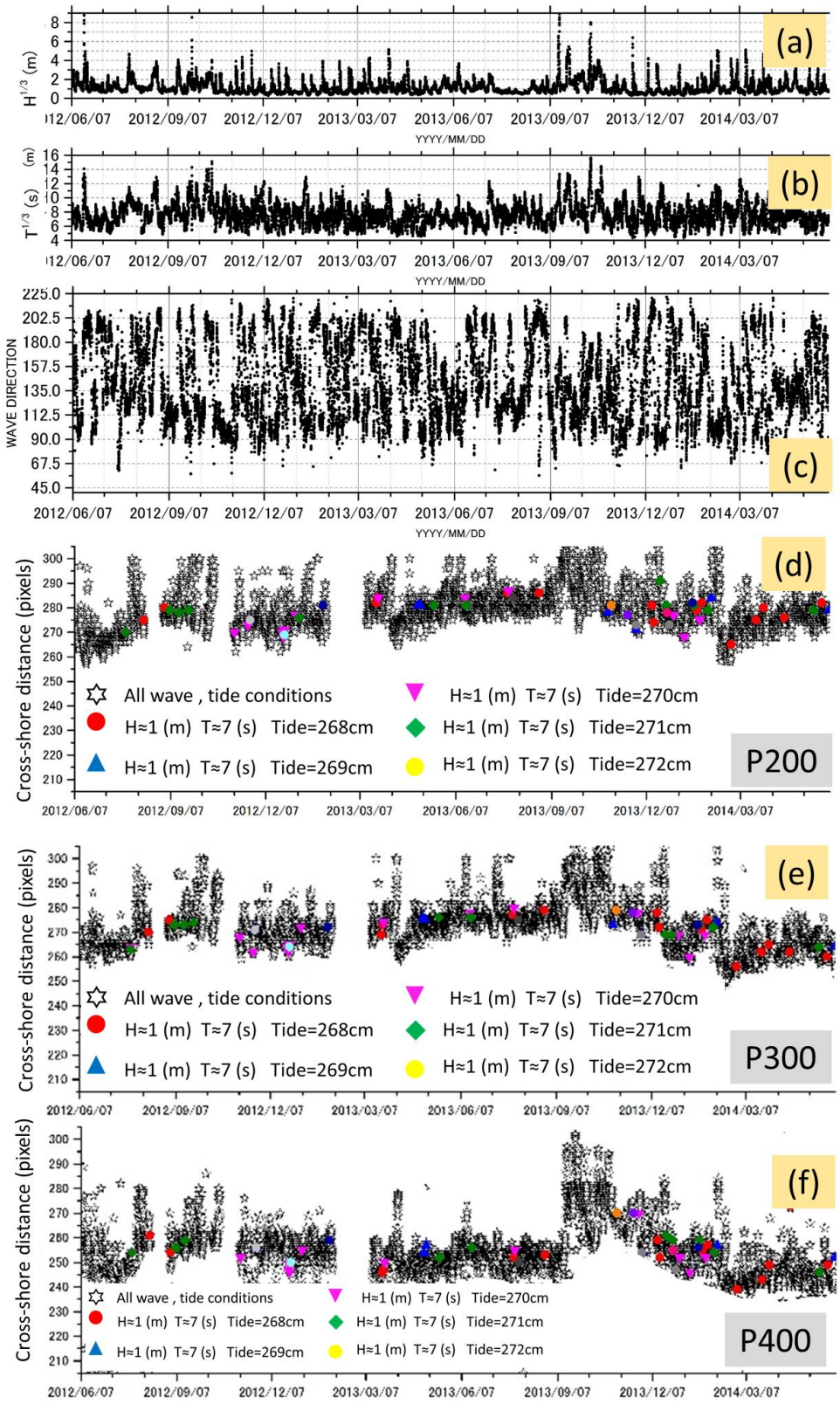

Figure 2.41 Shoreline change on the point without artificial reef

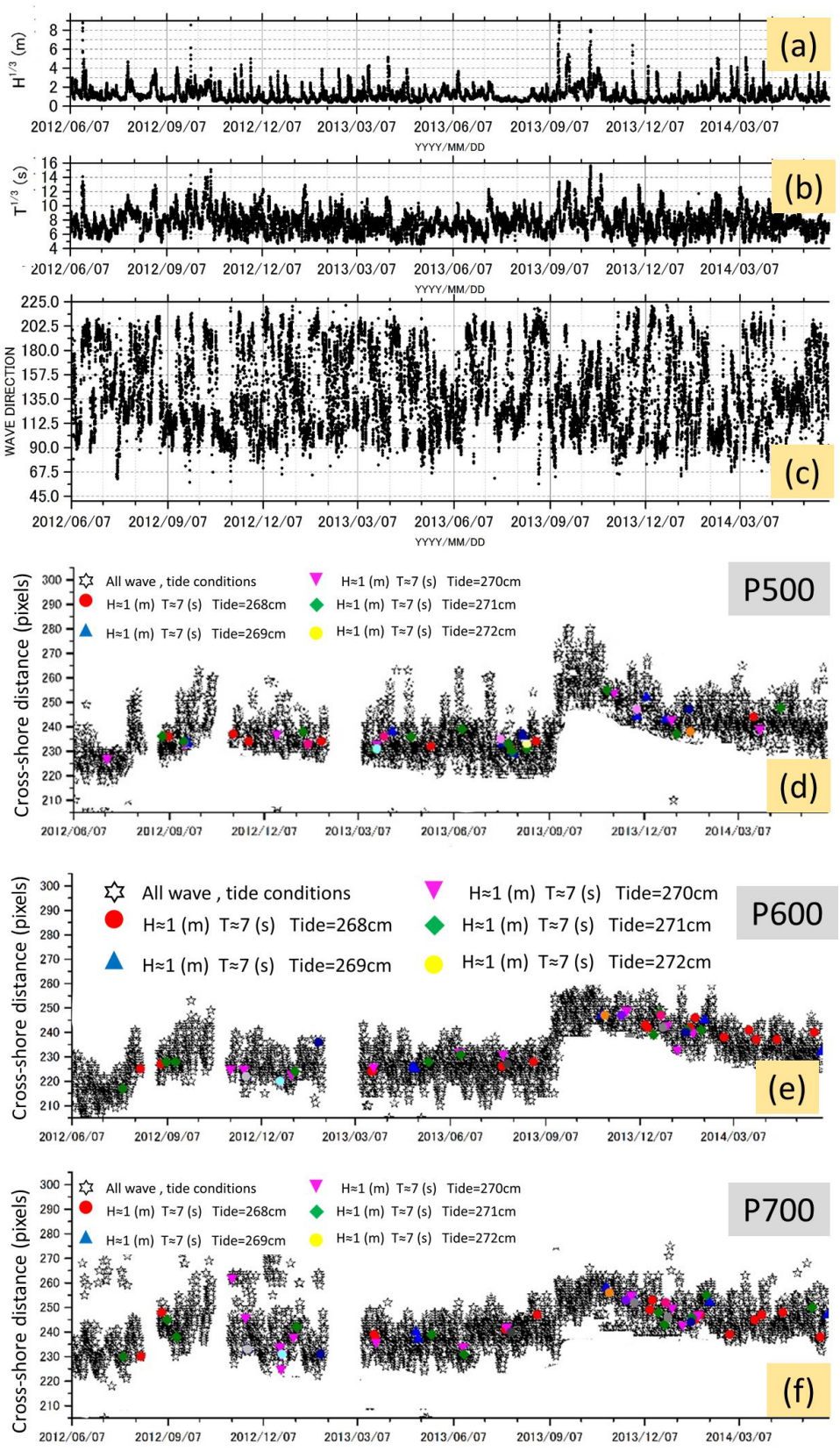

Figure 2.42 Shoreline change on the points behind artificial reef

even in the calm wave condition and larger than those at P3, P4, P5 and P6. After the largest retreat occurred due to typhoon 1318 in 2013, Point P2, P3, P4 and P5 are regularly recovering while those at P1 and P5 are standing still at shifted location. These results show that shoreline retreats rapidly during storm when wave's height larger than 6m and gradually advances after storm if wave's height less than 2m.

2.5 Summary

This section demonstrates the mechanism of shoreline change by using data of WEB camera system. The results show that:

(1) The new method can extract shoreline more stable than CCD method.

(2) Continuously data set of WEB camera system is a high-efficient tool for investigating the mechanism of shoreline change for both short-term change and long-term change.

(3) When wave which wave's height larger than 6m and wave period longer than 10s off to the coast, shoreline retreat.

(4) When wave which wave's height smaller than 1m a wave period smaller than 8s off to the coast, shoreline will forward at the area behind artificial reef, and stand still in the area without artificial reef.

(5) For other cases of wave condition, shoreline can be forward or retreat due to the change of wave direction.

(6) Artificial reef can help to reduce beach erosion, however in Shichirimihama it is still need to conduct more researches to improve the present artificial reef function.

Chapter 3

CHARACTERISTIC OF SHORELINE CHANGE

3.1 Overview

This chapter demonstrates the characteristic of topography change on Shichirimihama beach during the period from 30th January, 2014 to 20th August, 2014, focusing on berm development, beach profile change, beach slope change and beach volume change.

Firstly, study results about berm formation will be shown. As mentioned before, high permeability of gravel beach results in asymmetry on swash cycle. So the large gravel that moved onshore in up-rush phase will stay along the top of beach slope and berm will be created. In other word, berm is special morphology feather of gravel beach. Usually, berm was formed by high energy wave. Hence, it is difficult for observing berm data by field survey. In this chapter, formation of berm will be discussed by analyzing snapshot image data from Shichirimihama camera system with income wave data, in order to understand the wave condition that lead to the development of berm. The second part discuss about quantitative of beach profile change, beach slope change and beach volume change. In Shichirimihama beach, beside artificial reefs, there is another regular anti-erosion measurement has been adopted, that is beach nourishment. In spite of that, nourishment work has been done without the assessment of beach profile change as well as amount of sediment loss. In order to organize higher efficient nourishment work, understanding of changing on beach profile and beach volume are required. In this study, beach profile change, beach slope change, and beach volume change were obtained by analyzing field survey

topography data which collected by terrestrial laser scanning system

3.2. Wave condition during study period

As shown in Figure 3.1 (c, d), in this period, wave approached to the coast with a very wide angle extending from E to SSW direction. About 45% wave's height were less than 1m, 35% wave's height were 1m-2m, 10% wave were 2m-3m, 5% wave were 3m-4m, and 5% wave higher than 4m. There were about 24% wave came from SE direction, 20% wave came from ESE direction, 17% wave came from SSW direction, and 12.5% wave came from each E,SSE, S direction. Most of high wave approached to the coast from E, S, SSW direction. The highest approached from SSW direction was obtained on 10th August, 2014 with 7.087m wave height and 10.767s wave period.

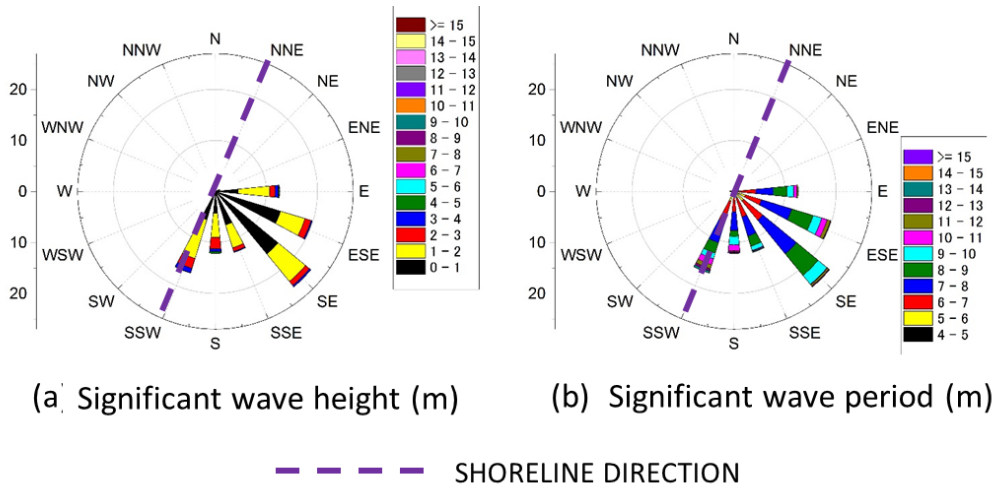

Figure 3.1 Wave condition during 2014/01/30~1014/08/05

3.3. Relationship between berm formation and income wave condition

One second interval snapshot image data were used to capture the fine shape of berm and income wave data during the period from 31st January, 2014 to 31st August, 2014 were used. Then the whole period was divided in small period in which wave height, wave period or wave direction presented nearly the same value. Figure 3.2 shows the berm formation from 31st January to 07th February. From 31st January to 2nd February 6:00, wave approached to the coast mostly from SSE with less than 1m wave

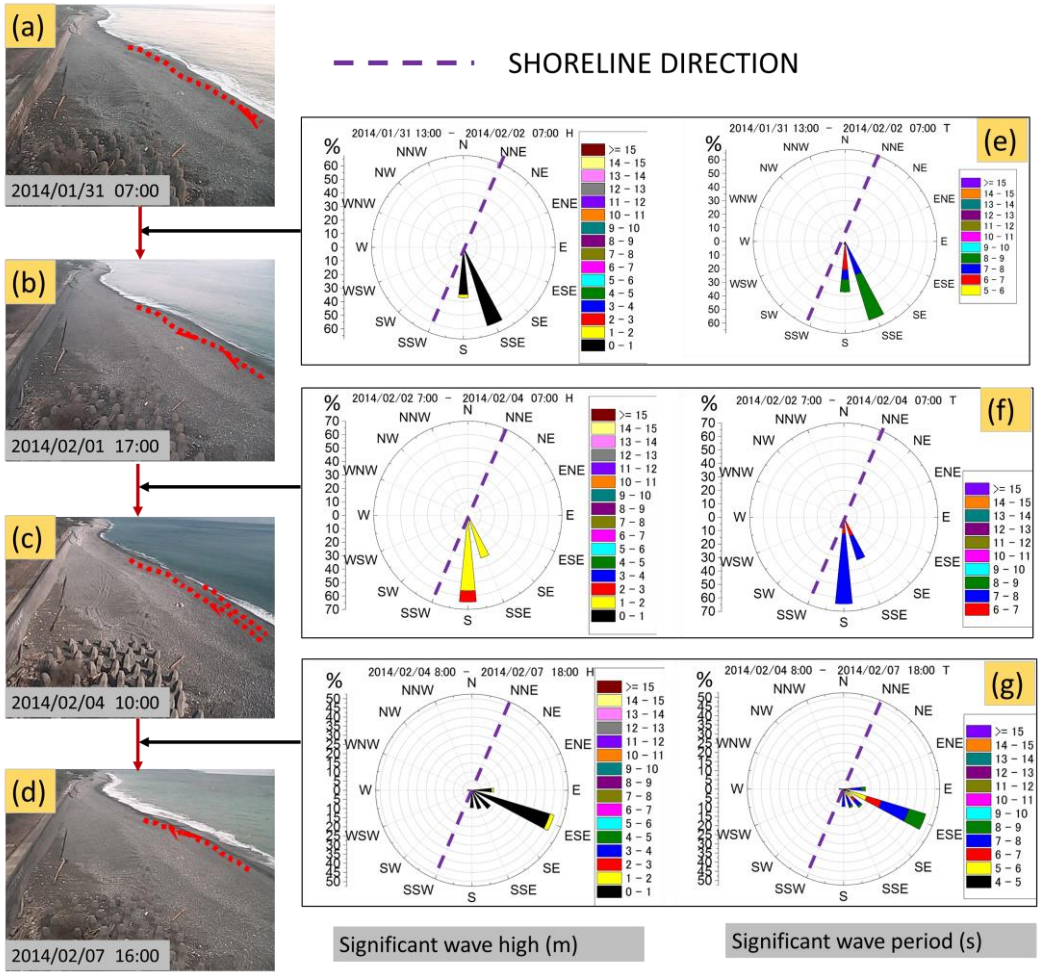

Figure 3.2. Berm formation during 2014/01/31~2014/02/07

high and 6-9s wave periods. Figure 3.2a and Figure 3.2b shows that berm height did not change during this period. From 2nd February 7:00 to 4th February 7:00 mainly wave direction change to S direction, and wave's height range from 1m to 2m with wave period 6s-8s. The highest wave was 2.23m on 2nd February 14:00. After this wave off to the coast, small berm occurred below previous berm (Figure 3.2c). From 4th February 8:00 to 7th February 18:00, wave direction change to ESE, with less than 1m wave high and4s-9s wave period. In this end of this period, small berm disappeared (Figure 3.2d). From 7th February to 10th February, storm occurred and the highest wave high was 3.94m with 9s wave period (Figure 3.3 a). Wave approached to the coast from E and ESE direction, with maybe cause slightly southern alongshore current, then result a large berm as shown in Figure 3.3c (brown ellipse). During 10th February to 13th February, wave's height was ranged 1.3~2.5m, and wave period was

8~12s, main wave direction was E. After this period, a very long berm occurred as shown in Figure 3.4b. On 14th February, the coast experienced a very high energy wave with 5.05m wave high and 9.97s wave period

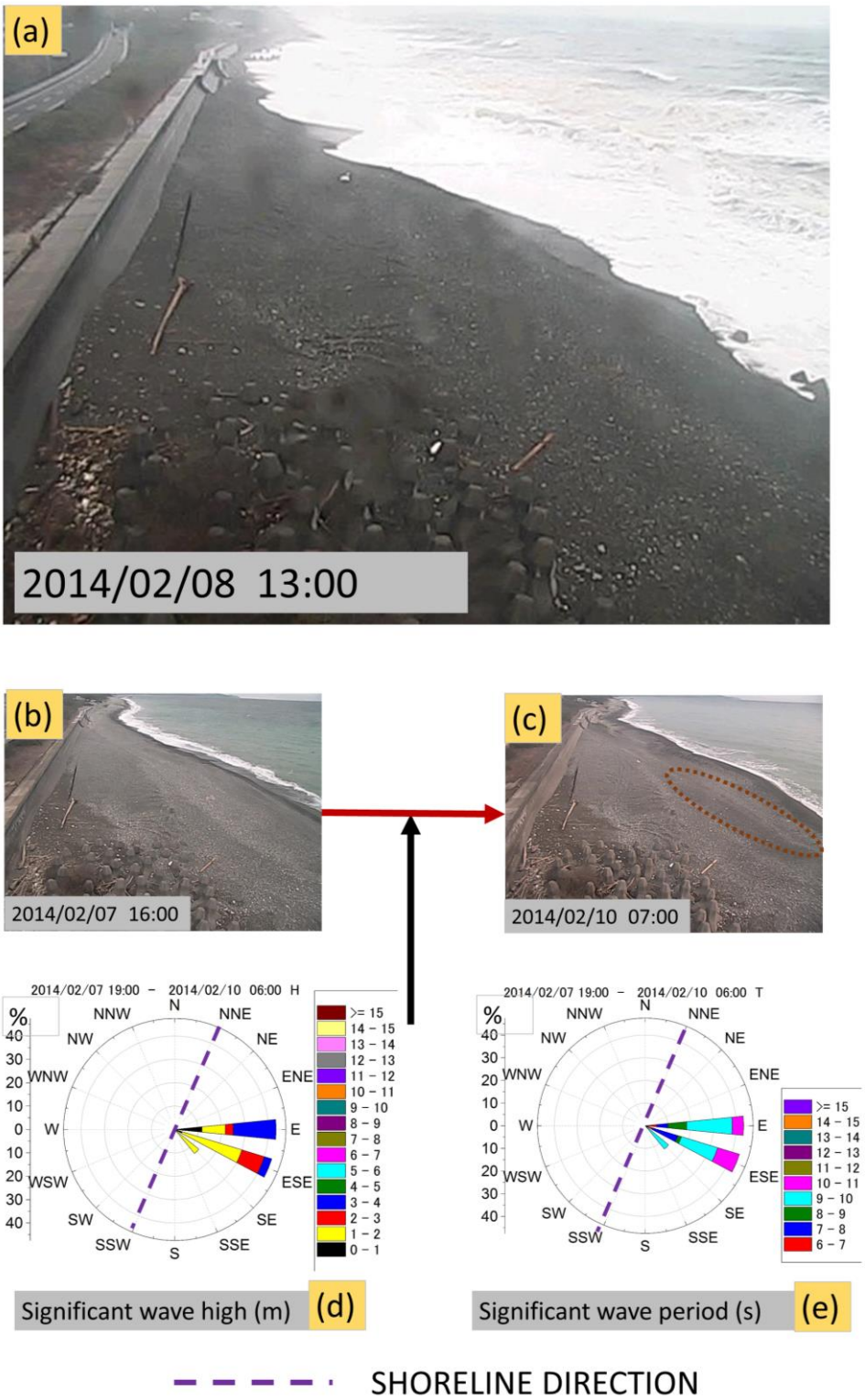

Figure 3.3. Berm formation by storm on 8th February

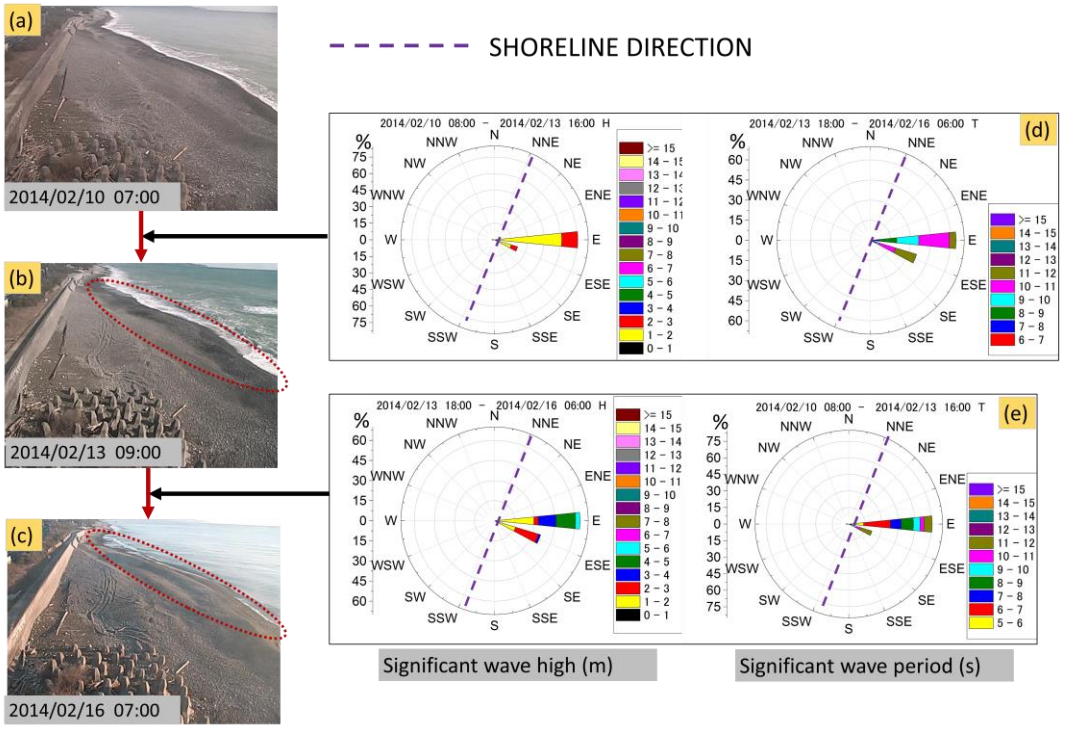

Figure 3.4. Berm formation by storm on 14th February

from E caused by the storm on 14th February. This results a firmly berm on the entire area without artificial reefs (red ellipse in Figure 3.4 c). In the period from 16th February to 26th February, wave approached to the coast E, ESE, SE with wave's height less than 2m and wave period was 4s-10s. Under this wave condition, berm height decrease a little and beach face became smoother (Figure 3.5 a). From 27th February to 2nd March, there was a 4.2m high wave with 8.2 wave period off to the coast from SSE direction, result in a new berm on the coast (brown ellipse in Figure 3.5 b). After that, on 03rd March ~06th March, wave direction changed to E direction, which the highest wave was 2.84 height and 7.4s period, contributed to the development of berm on the other side of beach (blue ellipse in Figure 3.6 b). In period from 6th March to 12th March, wave's heights were less than 1m. However, wave periods were long, from 9s-12s. In this period, berm development did not occur. Comparing Figure 3.6 b and Figure 3.7 a, it can be said that the beach face became more moderate. Figure 3.7 shows the berm shape change during 12th March ~ 15th March. From Figure 3.7 a and Figure 3.7 c, it can be said that in this period even the wave's height reached to 5.123m with 10.43s wave period, the berm did not occur on

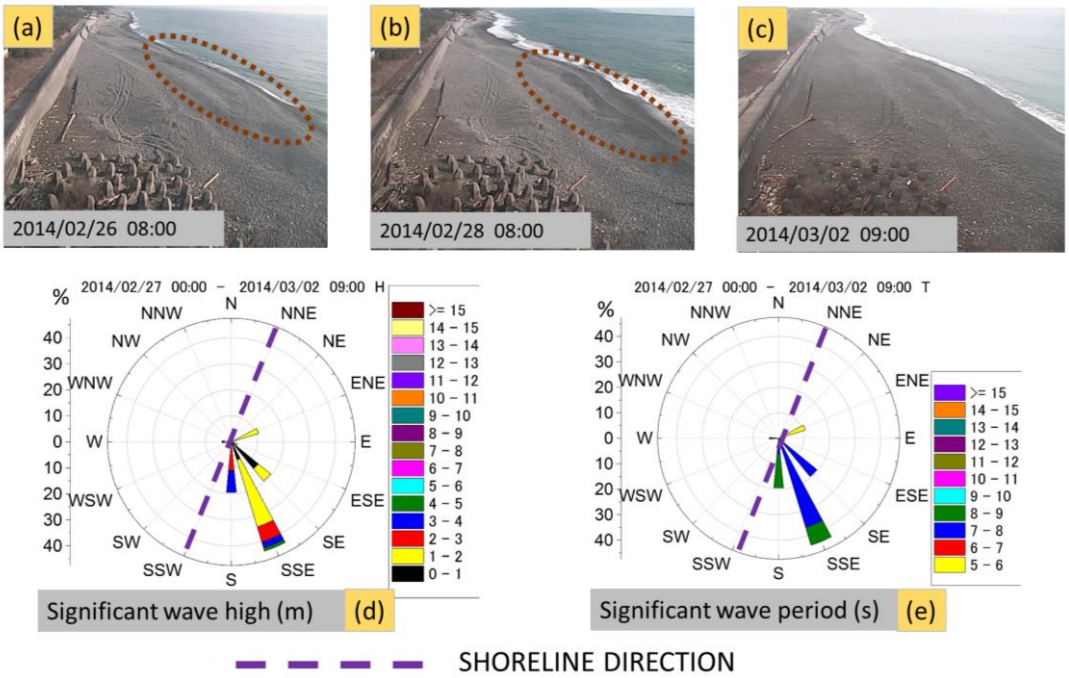

Figure 3.5. Berm formation during 27th February ~ 02nd March

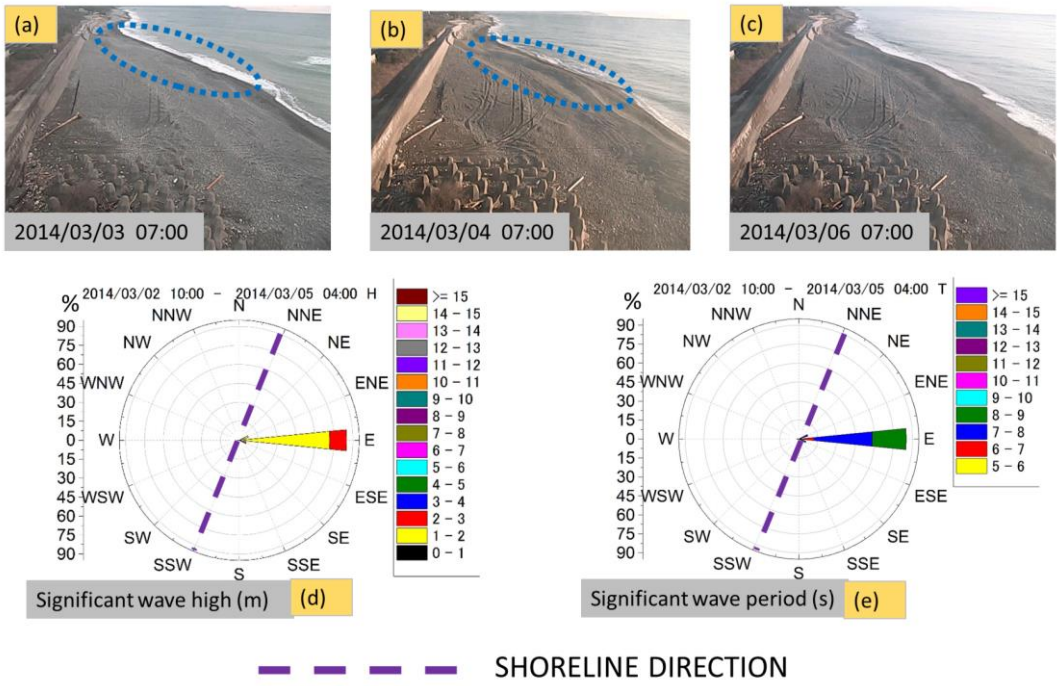

Figure 3.6. Berm formation during 3rd March ~ 06th March

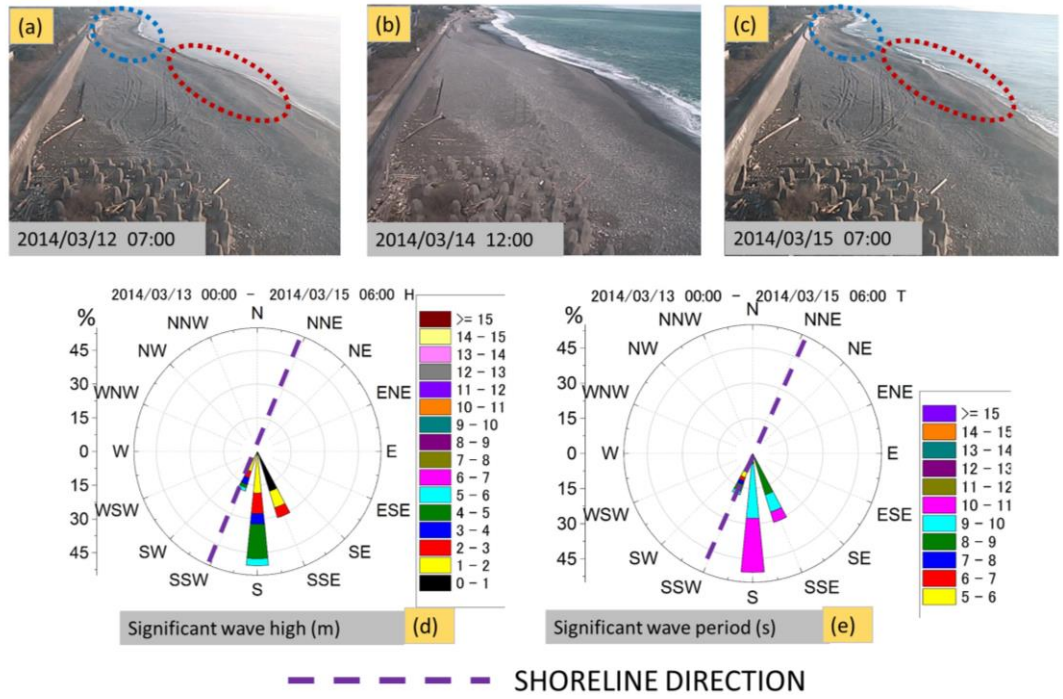

Figure 3.7. Berm formation during 12th March ~ 15th March

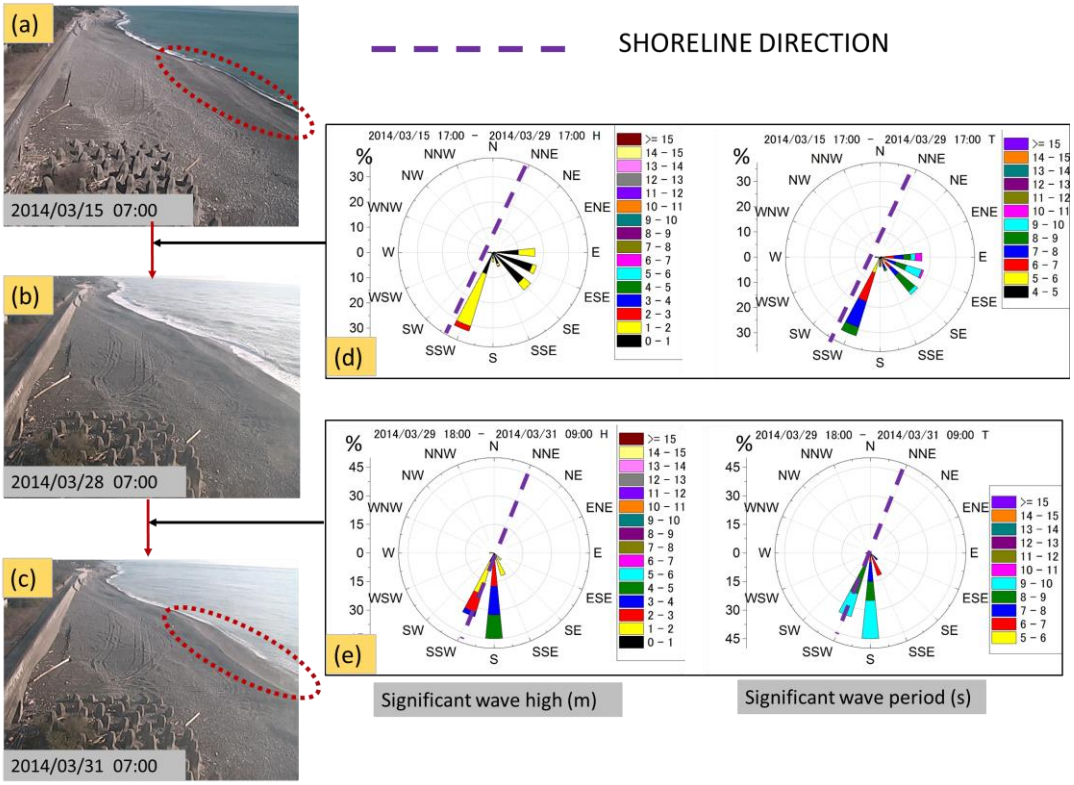

Figure 3.8. Berm formation during 15th March ~ 31st March

along shore direction (red ellipse in Figure 3.6 c) that shows different trend in compared to previous cases (Figure 3.3 c, Figure 3.4c, Figure 3.5d, Figure 3.6b. This result occurred because wave approached to the coast with a very small angle from southern direction (Figure 3.7d). This small approaching angle caused a northern long-shore current and gravel sediment was washed out along-shore as corollary. This trend appeared clearly when wave off to the coast from SSW direction, which coincided with beach direction.

3.4. Beach profile change

3.4.1. Terrestrial laser scanning system description

In this study, a three-dimensional (3D) laser imaging scanner named RiSCAN PRO was used for collecting topography data (Figure 3.9 a). This equipment with a hybrid sensor consisting of a high-performance 3D imaging laser sensor and a high-resolution digital camera is expected to provide high measurement accuracy. Moreover, because of a wide field of view as well as efficient performance of RiSCAN PRO, entire coastal topographic data can be collected in only one day work. In this study, the laser imaging scanner was made from a laser scanner, a digital camera mounted to the laser scanner, GPS receiver and an antenna. All of these equipments are mounted on an affirmative tripod. A computer connected to the system by a cable was used to operate the data collecting process and stored data. Figure 3.9b shows coordinate system of

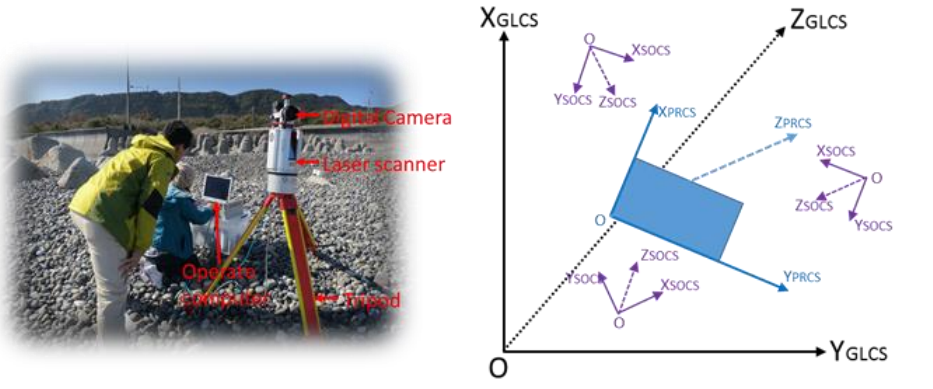

(a) Component of laser scan system (b) Coordinate system of RiSCAN PRO

Figure 3.9. General of RiSCAN PRO 3D imaging scanner system

RiSCAN PRO. In order to capture the whole studied objects, data acquisition was taken from different locations, named Scan Position. Each Scan Position has own coordinate system called Scanner's Own Coordinate System (SOCS), which stored the position and orientation of each scan position. SOCS can be registered to Project Coordinate System (PRCS) to make a single object presentation by using tie points, i.e., position of reflectors. PRCS can be converted to Global Coordinate System (GLCS). True color of studied object can be obtained digital camera image. This camera has its own coordinate system, called Camera Coordinate System (CMCS). At every scan position, optional number of images, which covered 360 degree view, will be taken, then image coordinate calibration (convert image from CMCS to PRCS) were done automatically at site.

3.4.2. Topography data acquisition process

Figure3.10. View of slope face at Shichirimihama Beach

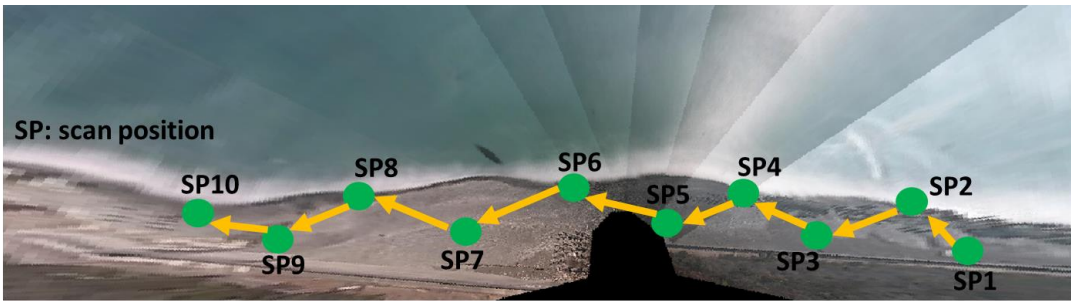

Figure 3.11. Data acquisition route

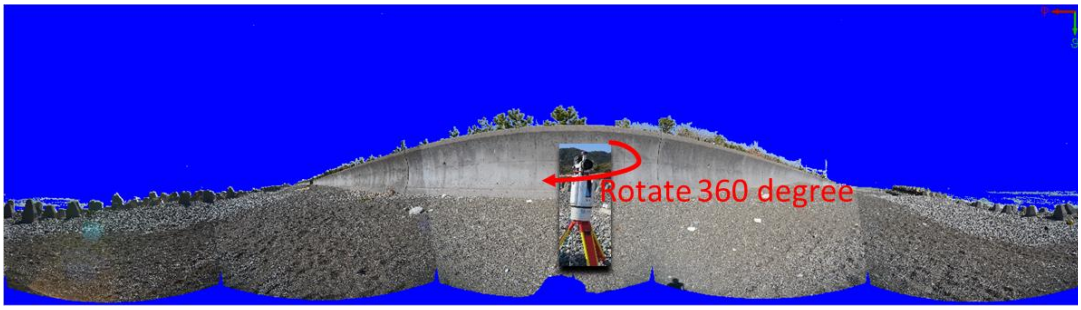

Figure 3.12. 2D view of image taking at scan position 3 (2014/02/21)

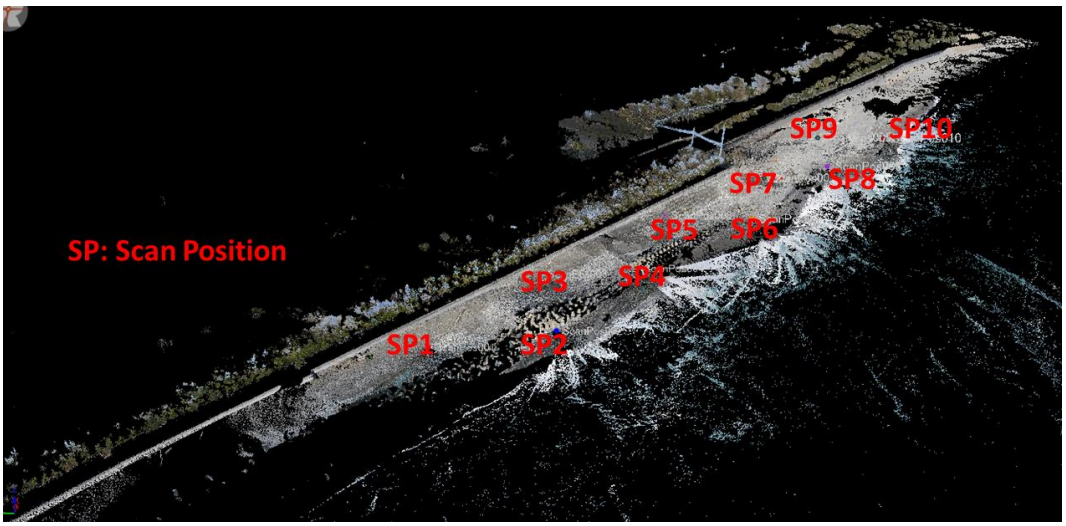

Figure 3.13. Combined data

Topography data was collected over 2km area in front of the camera station. Three times of data collection were conducted during period from January 2014 to August 2014. At each time of field survey, about 8 to 10 scan positions were to set up to collected the entire studied area. Shichirimihama is quite flat beach. However, there is a steep slope in the end of beach (Figure 3.10). So, in order to remove the effect of shadow and capture, the whole slope faced a zigzag path was used (Figure 3.11).

Data acquisition process at every scan position is as follow:

(1) Setting scanner system.

(2) Connect scanner system to outer computer.

(3) Setting reflectors. In this study, 10cm cylinder reflectors were used.

(4) Topography data acquisition

(5) Tie points acquisition.

(6) Digital image taking. In this study, 360 degree view of each scan position was obtained by 5 image frame (Figure 3.12)

(7) Assign object color.

3.4.3. Topography data analyzing process

The field observations were carried out on 31st January 2014, 21st February 2014 and 5th August 2014. Raw data was stored as point cloud. Then data analyzing was operated in laboratory. Data analyzing process has 4 main steps, they are: (1) converting Project Coordinate System to Global Coordinate System; (2) combining all single scan position into one object, i.e., register every single scan position to Project Coordinate System, (3) data cleaning, (4) making TIN data. At first, Project Coordinate System was converted to Global Coordinate System. Then, all scan positions were registered to Project Coordinate System by tie points list, which obtained at each scan position using reflectors. Figure 3.13 shows the data result of whole Shichirimihama Beach after step 2. Then useless data, such as tree point cloud, dust points… were cleaned to obtain accuracy topography data. TIN data were created in the final step (Figure 3.14).

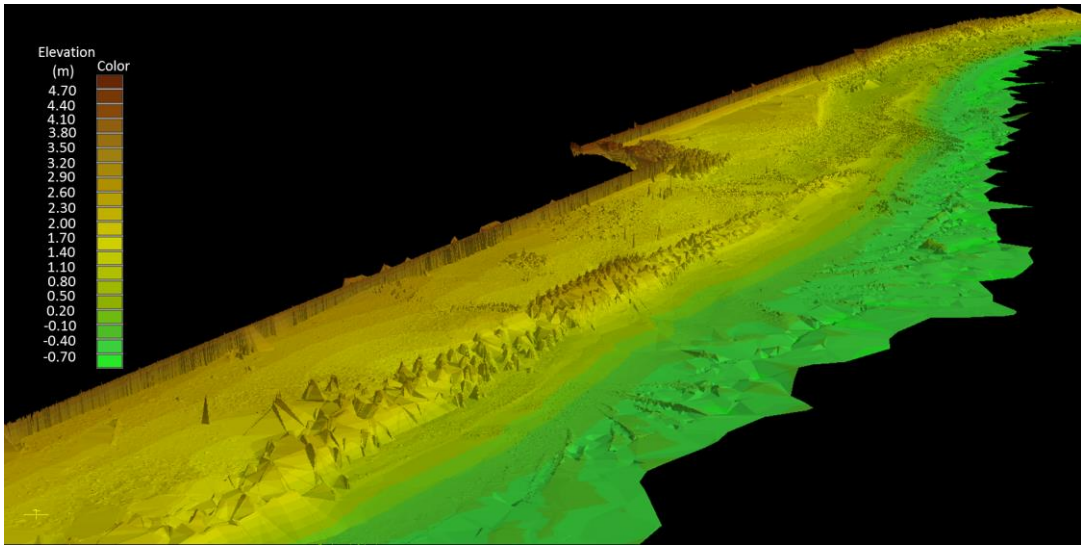

Figure3.14. Output TIN data

3.4.4. Beach profile change

Figure 3.15(a) shows a comparatively straight beach profile. In contrast, Figure 3.15b shows curly shape profile with 2 peaks, one is located behind and nearly on the end of artificial reefs, and another is formed at the location without artificial reef. The elevation of beach on 21st February is higher than that one on 31st January. From Figure 3.3d, Figure 3.4e, it can be understood that, during the period of 31st January ~ 21st February, high energy wave approached to the coast from E, ESE direction. So the berm development caused by cross-shore sediment transportation was the main reason that leads to high elevation of topography data on 21st February. The beach profile on 5th August shown in Figure 3.15c has a similar shape, but beach's width become smaller on entire coast in compared to beach profile on 31st January (Figure 3.15a. This change of morphology presents that large amount of sediment loss due to strong long-shore current caused by strong wave energy from S and SSW direction (Figure 3.1). Figure 3.15b shows a 5m long berm formed in the area without artificial reefs (dot circle). It was though that the low pressure weather occurred on 15th February 2014 lead to this berm formation. Then the berm extended toward the north and reached to 12m long after a typhoon 1408 past by on 10th July 2014 (dot circle in Figure 3.15c).

3.4.5. Beach volume change

Volume change of sediment was estimated through the difference of elevation for the period from 21st February to 5th August. A 2m*2m mesh was used for calculate the difference of elevation on interested area (Black color mesh in Figure 3.16d. Figure 3.16e shows beach volume change between 21st February 2014 and 5th August 2014. Green color indicates the decrease while the red color indicates the increase of volume at calculation cell. In the end of study period, the southern beach volume becomes higher while the northern part becomes lower except the location of the berm.

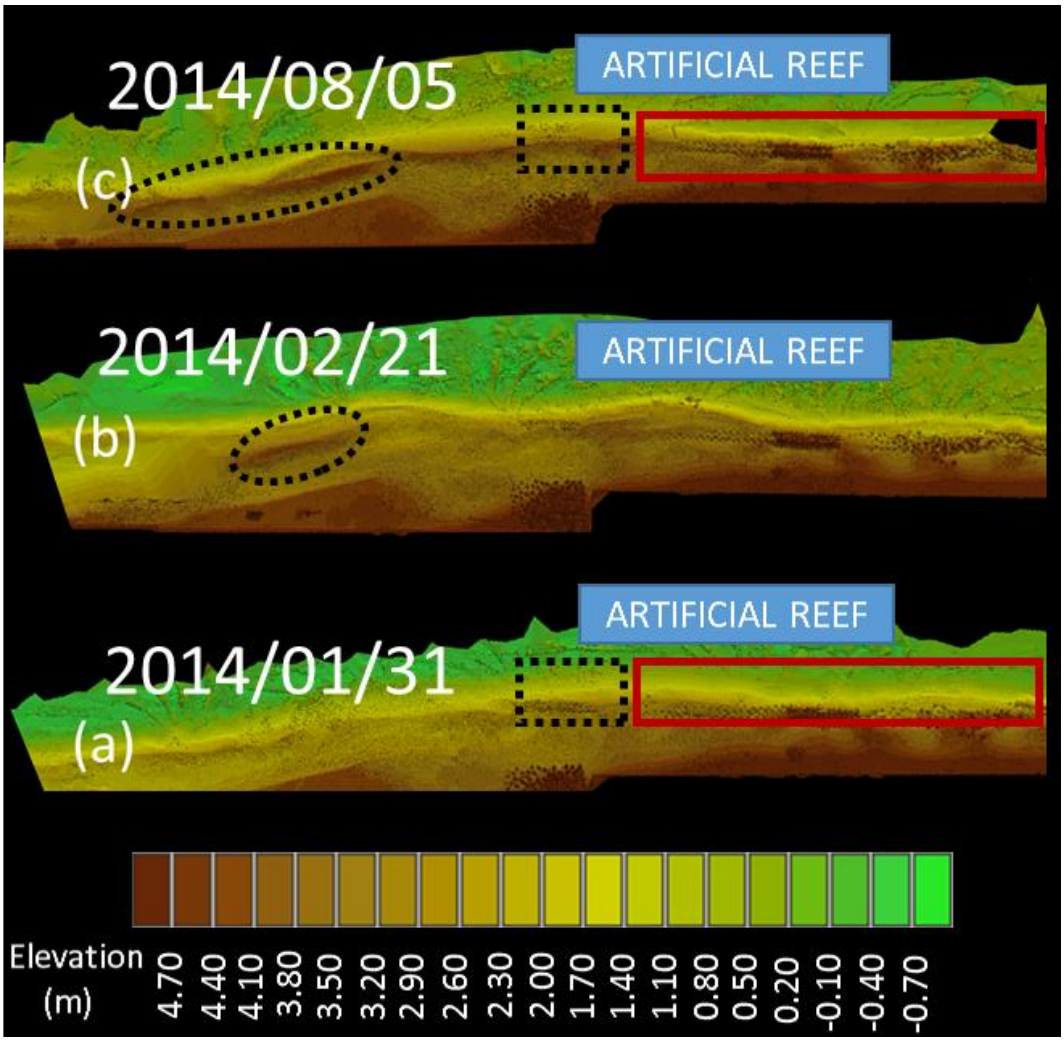

Figure 3.15. Beach profile change during studied period

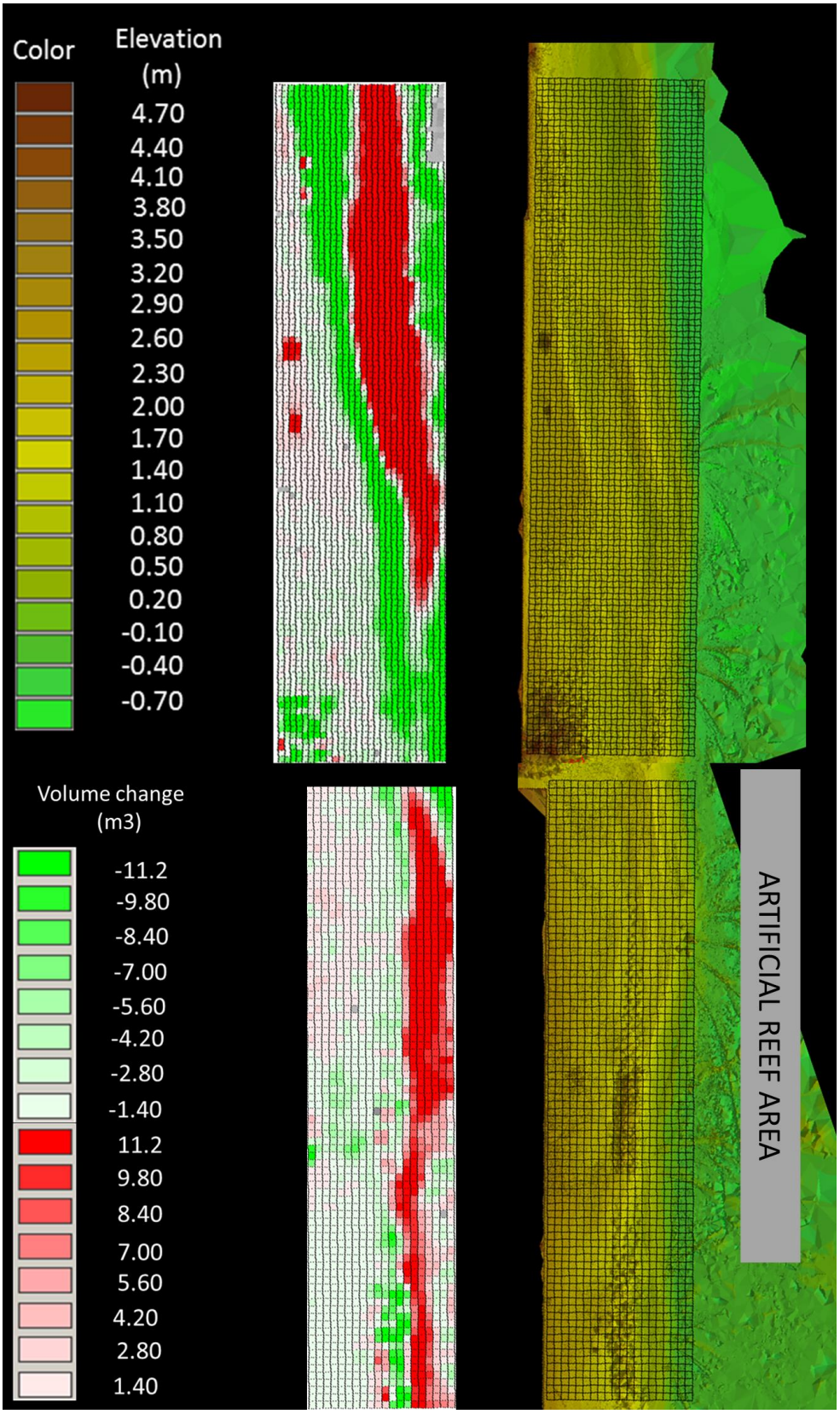

Figure 3.16 Beach profile change during studied period

3.4.6. Beach slope change

Figure 3.17 and Figure 3.18 show the change of slope during period of study. Along the beach, the slope on northern part of beach (Section I-I, Section II-II, Section IV-IV) is gentle in comparison with the southern part (Section VIII-VIII, Section IX-IX, Section X-X). The beach face becomes higher and steeper from south to north. During the period of study, the beach slope of the entire beach becomes steeper, especially in

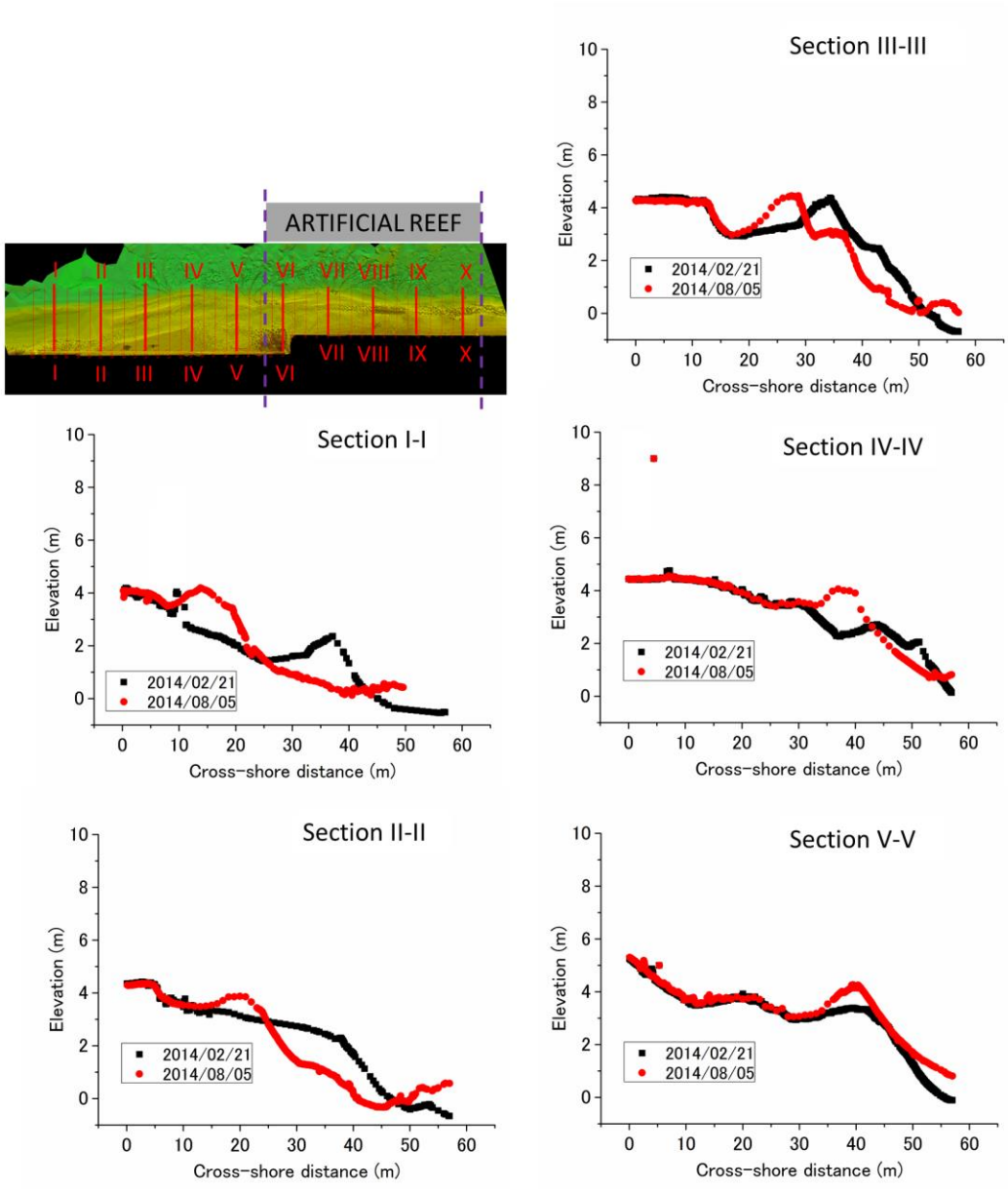

Figure 3.17. Change of beach slope at area without artificial reef

cross-section II-II, V-V which locates in the area without artificial reef. And high wave energy causes slope's crest to shift about 15m backward (Figure 4b and Figure 4c). Moreover, loss of large sediment amount leads to significant reduction on beach width along entire beach

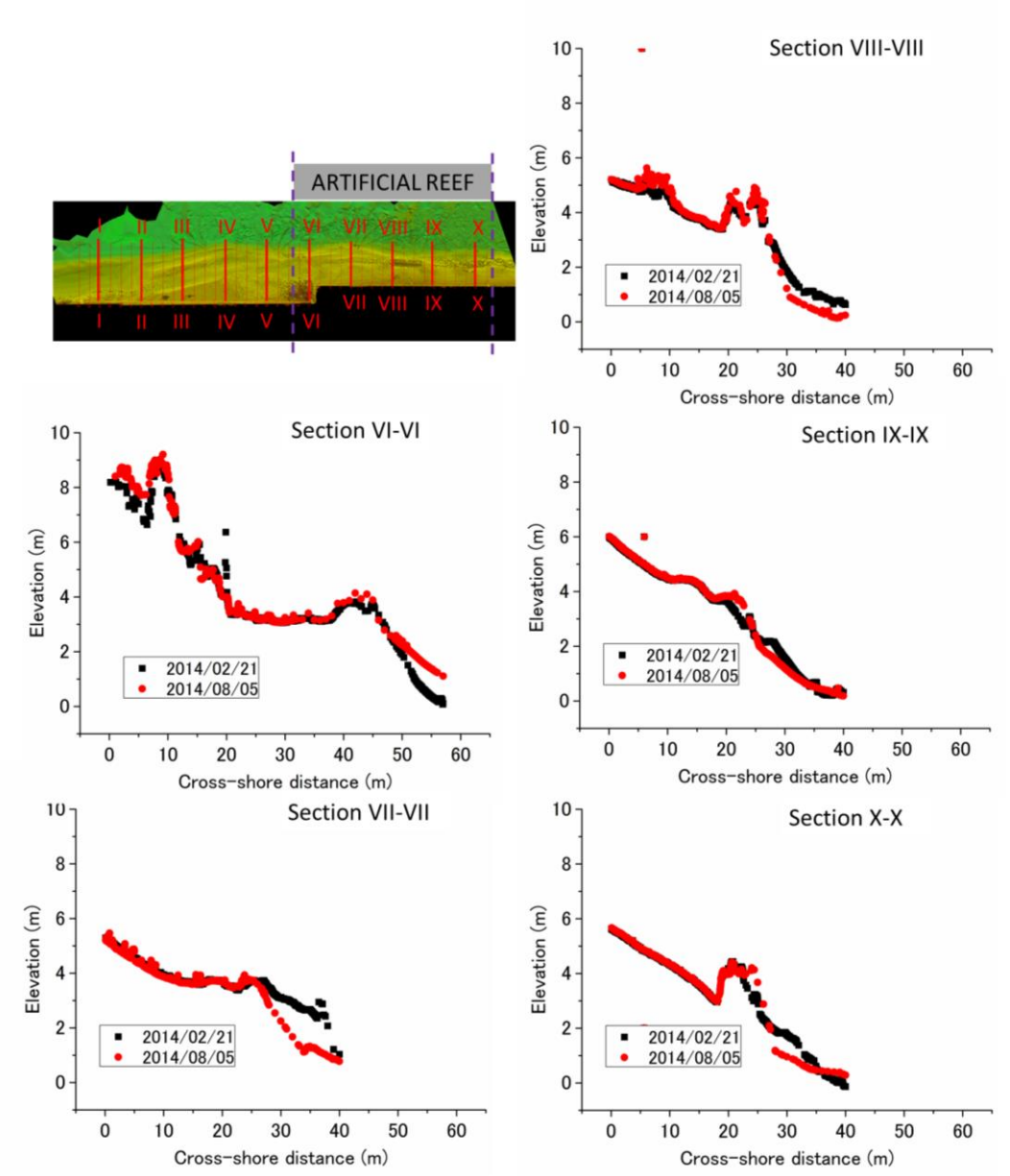

Figure 3.18. Change of beach slope at area without artificial reef

3.5. Relationship of shoreline change and topographic change

In this section the relationship between shoreline change and topographic change will be discussed. It should be noted that, in each figure of this section, view 1 shows the area without artificial reef, and view 3 shows the area behind artificial reef.

3.5.1 Relationship of shoreline change and topographic change due to wave high less than 1.3m

During the period from 2013/07/26 to 2013/07/31, wave approached to the coast from ESE, SE direction with wave period ranging from 4s to 9s. This wave condition did not result in any change of topography. And as showed in Figure 3.19, there is a slight shoreline retreat in the right side of area behind artificial reef. While the shoreline in the area without artificial reef stands stable during entire period. This was thought that under this low wave energy condition, energy due to wave breaking is not strong enough to cause strong sedimentary transport, so the beach topography as well as shoreline did not show the significant change during study period.

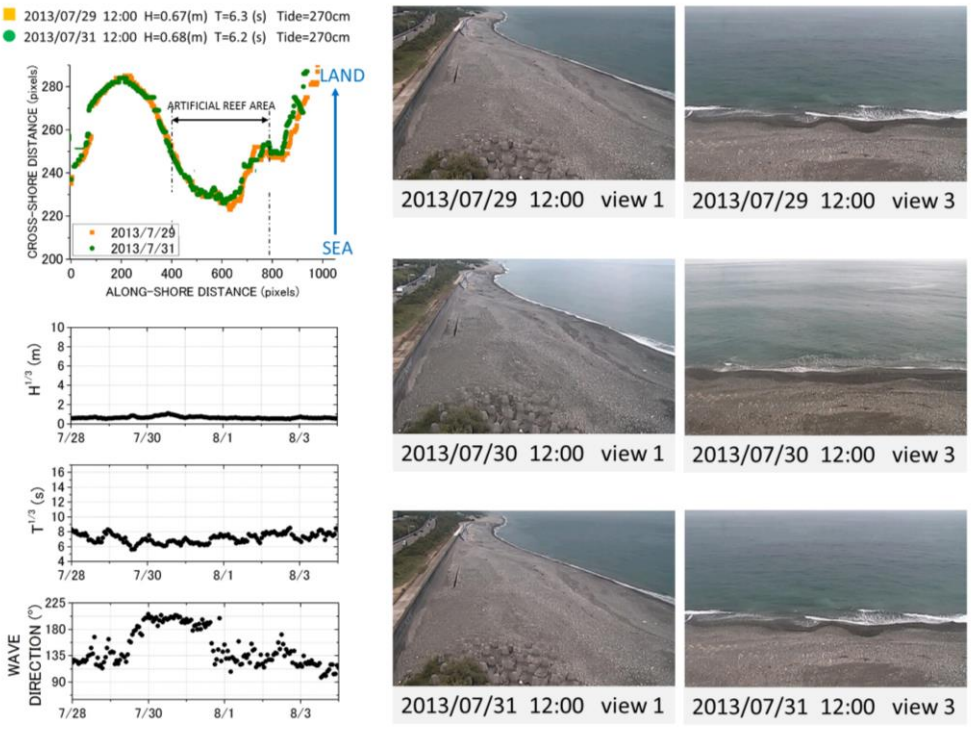

Figure 3.19 Shoreline change and topographic change during 2013/07/29~2013/07/31

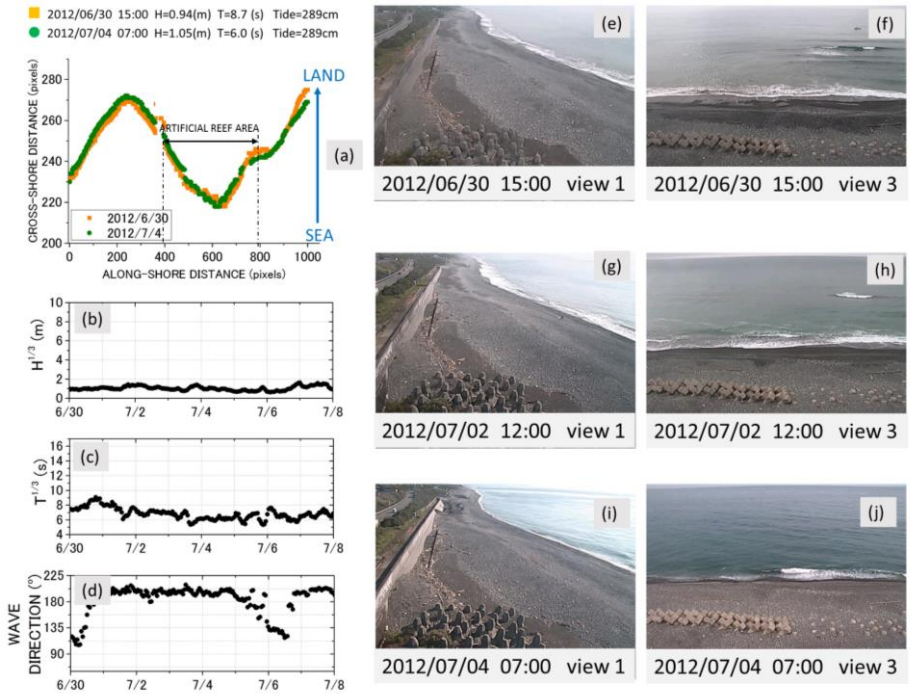

Figure 3.20 Shoreline change and topographic change during 2012/06/30~2013/07/04

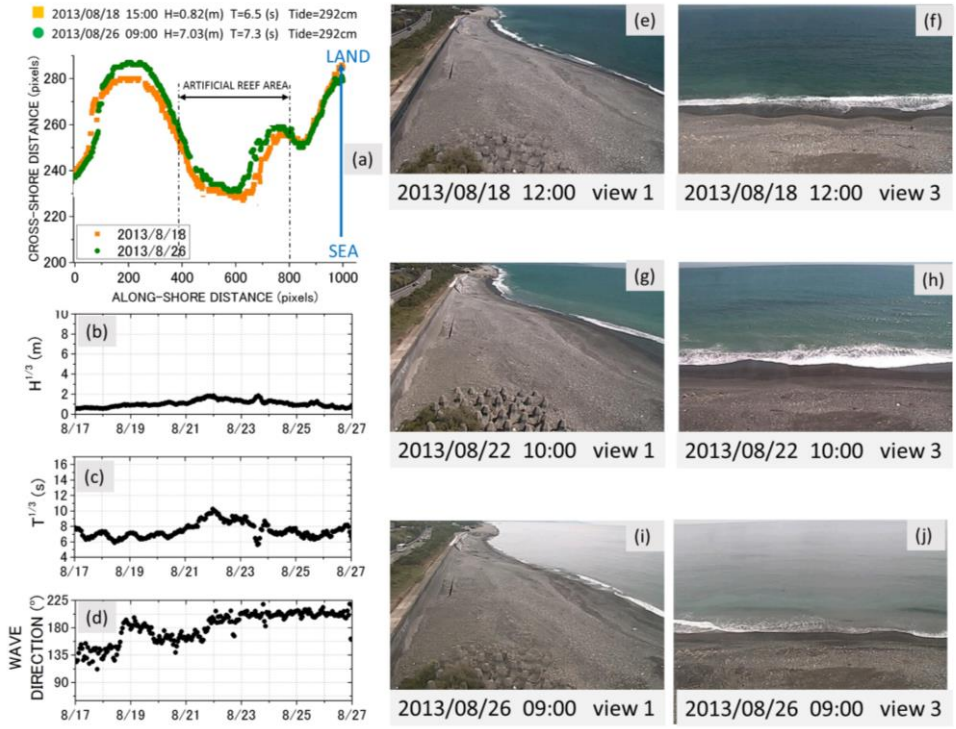

Figure 3.21 Shoreline change and topographic change during 2013/08/18~2013/08/26

3.5.2 Relationship of shoreline change and topographic change due to 1m-2m wave high

In the period from 2012/06/30 to 2012/07/04, and 2013/08/16 to 2013/08/26 waves approached to the coast from SSW (Figure 3.20d, Figure 3.21d). After wave with wave height about 1.7m off to the coast sediment on the southern part of beach face is removed (Figure 3.21h, Figure 3.21j). In addition, right hand side of Figure 3.21g and Figure 3.21i have a dent, while left hand side seem become higher than before. It was thought that this wave condition results a long-shore current on south to north direction, hence the sediment on southern part of beach was removed and deposited on northern part of the beach. This sediment transport process then results shoreline retreat entire study area (Figure 3.21a).

3.5.3 Relationship of shoreline change and topographic change due to 2m-3m wave high

During 2013/01/12~2013/01/20 wave approached to the coast from E, ESE (Figure 3.22d), result along-shore berm extend from the area without artificial reef (Figure 3.22i) to the area behind artificial reef (Figure 3.22j), and shoreline forward on entire study area (Figure 3.22a). From 3.13/07/09 to 2013/07/17 wave approached to the coast from SSE, S, and SSW (Figure 3.23), and similar with the case in Figure 3.21, there is a dent on right hand side of Figure 3.23g and Figure 3.23i have a dent, while left hand side seem become higher than before. In the end of study period, shoreline forward on both side of study area and forward on the middle part of study area.

3.5.4 Relationship of shoreline change and topographic change due to 3m-4m wave high

During 2014/05/11 ~ 2014/05/14, incoming wave direction change from SE direction to SSW direction (Figure 3.24d). In the early stage of period when wave offed to the coast from SE direction, along-shore direction berm was created (Figure 3.24g, Figure 3.24h). After that, when wave direction change to S, SSW direction, berm was washed out by long-shore current (Figure 3.24i). Shoreline forward on both side of study area and forward on the middle part of study area (Figure 3.24a).

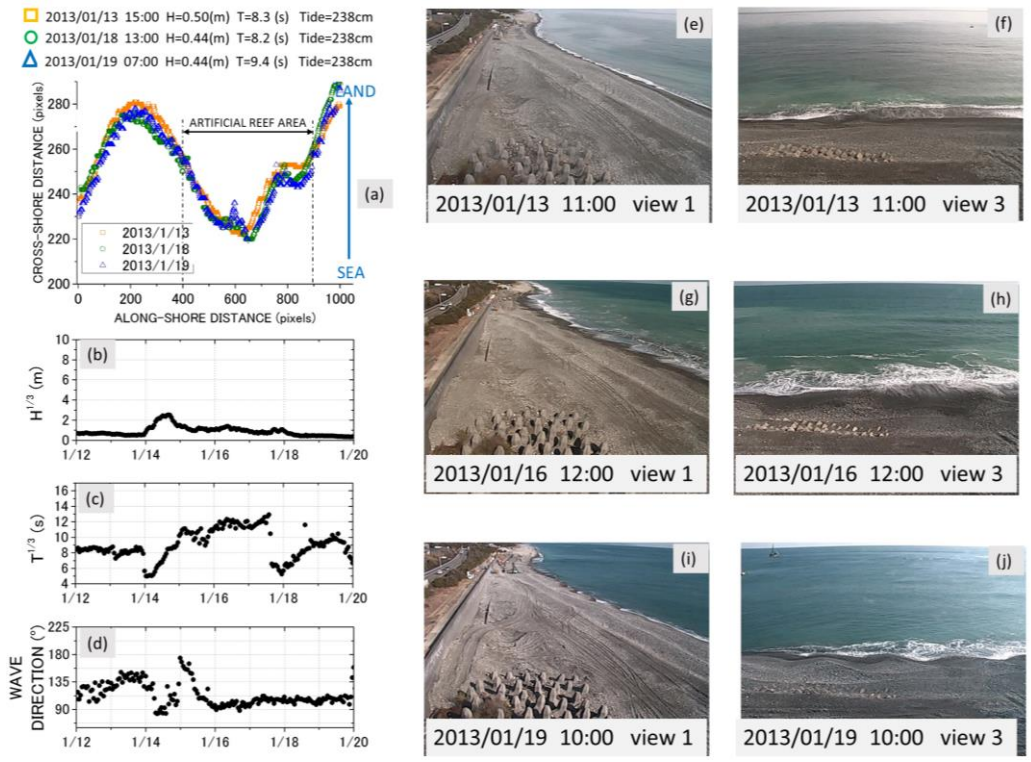

Figure 3.22 Shoreline change and topographic change during 2013/01/11~2013/01/19

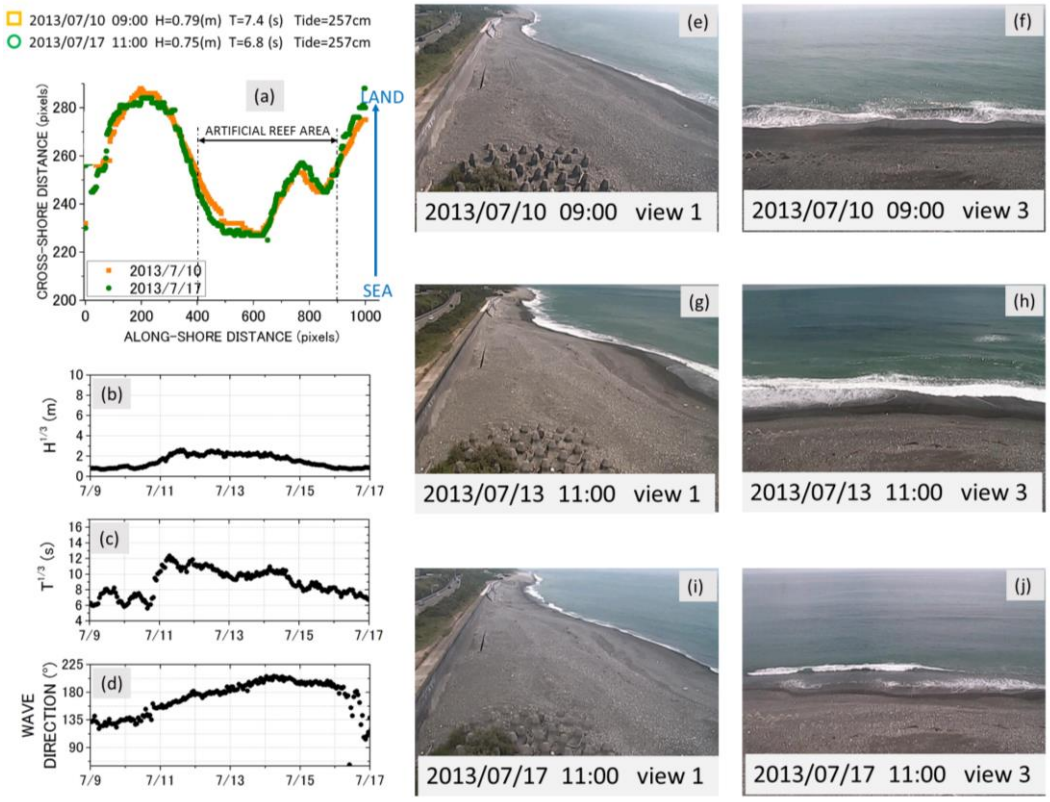

Figure 3.23 Shoreline change and topographic change during 2013/07/10~2013/07/17

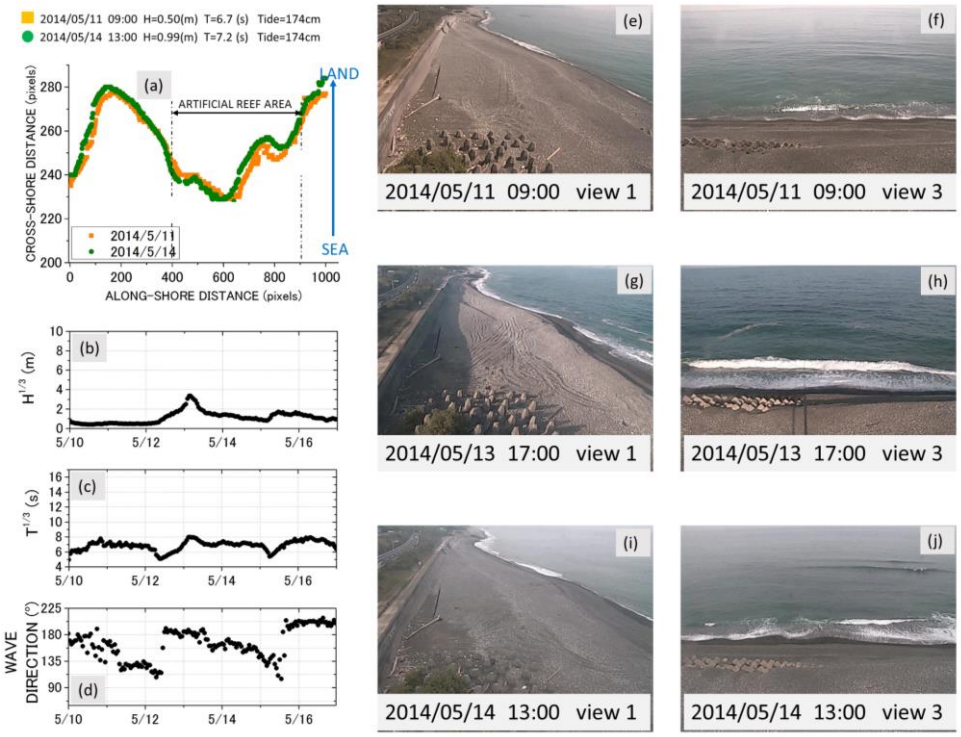

Figure 3.24 Shoreline change and topographic change during 2014/05/11~2014/05/14

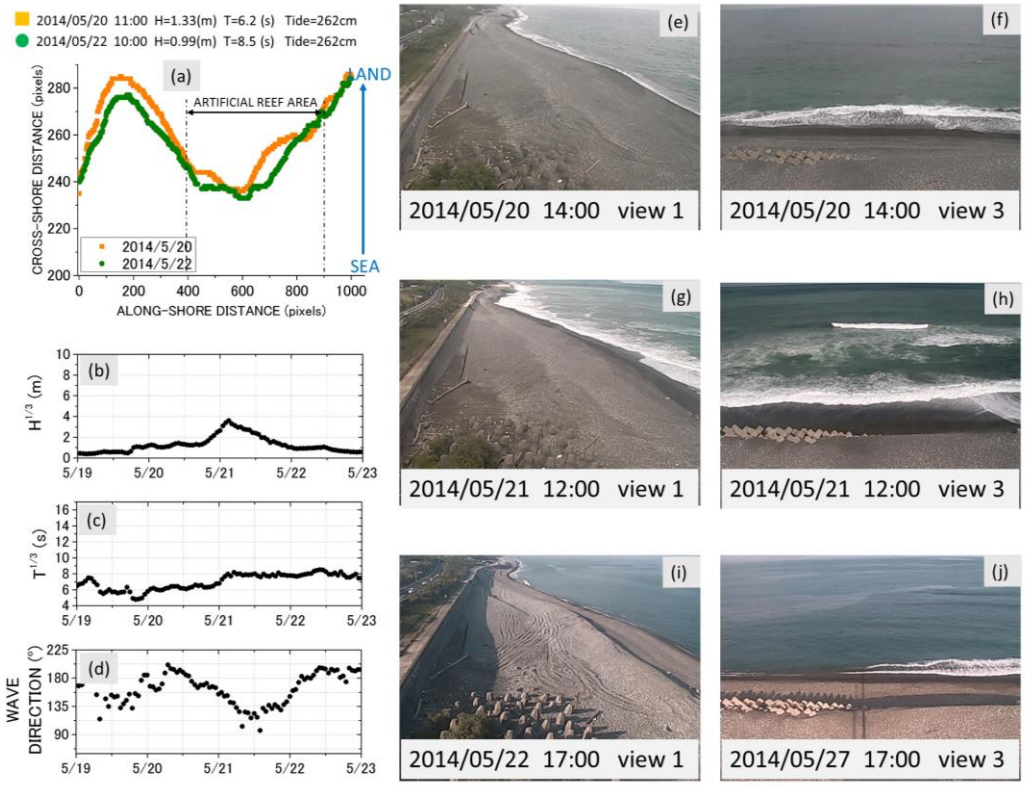

Figure 3.25 Shoreline change and topographic change during 2014/05/20~2014/05/22

From 2014/05/20 to 2014/05/22 waves approach to the coast from SE, SSE direction (Figure 3.24d) result a large long-shore berm (Figure 3.25i, Figure 3.25j), and shoreline forwards on the entire beach (Figure 3.25a).

3.5.5 Relationship of shoreline change and topographic change due to wave which wave high from 4m to 6m

During the period from 2012/11/19 to 2012/11/30, low energy wave extend on the whole period, with wave height less than 1m, and wave period less than 10s, except single large wave energy in the middle of period. Moreover, since wave direction was S and SSW, the original berm (Figure 3.26g, Figure 3.26h) was washed out (Figure 3.26i). Then shoreline retreat slightly in the area without artificial reef and forward on the area behind artificial reef (Figure 3.26a).

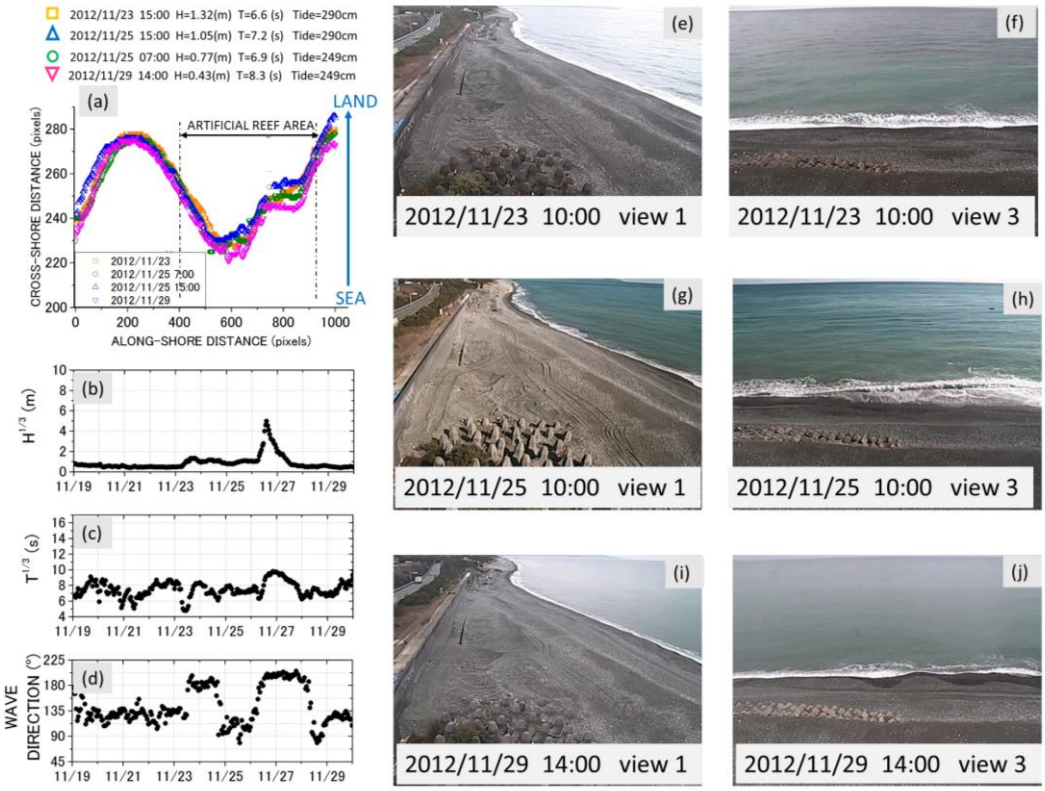

Figure 3.26 Shoreline change and topographic change during 2012/11/23~2012/11/29

3.5.6 Relationship of shoreline change and topographic change due to wave which wave high larger than 6m

From Figure 3.27 and Figure 3.28, it can be said that the shoreline retreat significantly after income wave with more than 6m wave's height approached to the coast. In the period from 2013/09/11 to 2013/09/20, shoreline retreats 8m, the largest retreat distance among 2 study periods. In this time, because the highest wave off to the coast from SE, SSE direction, while during 2013/06/17~2013/06/25 the highest wave was from SSW direction. Moreover, due to very strong wave energy, large amount of sediment was washed out leading to the original berm disappeared.

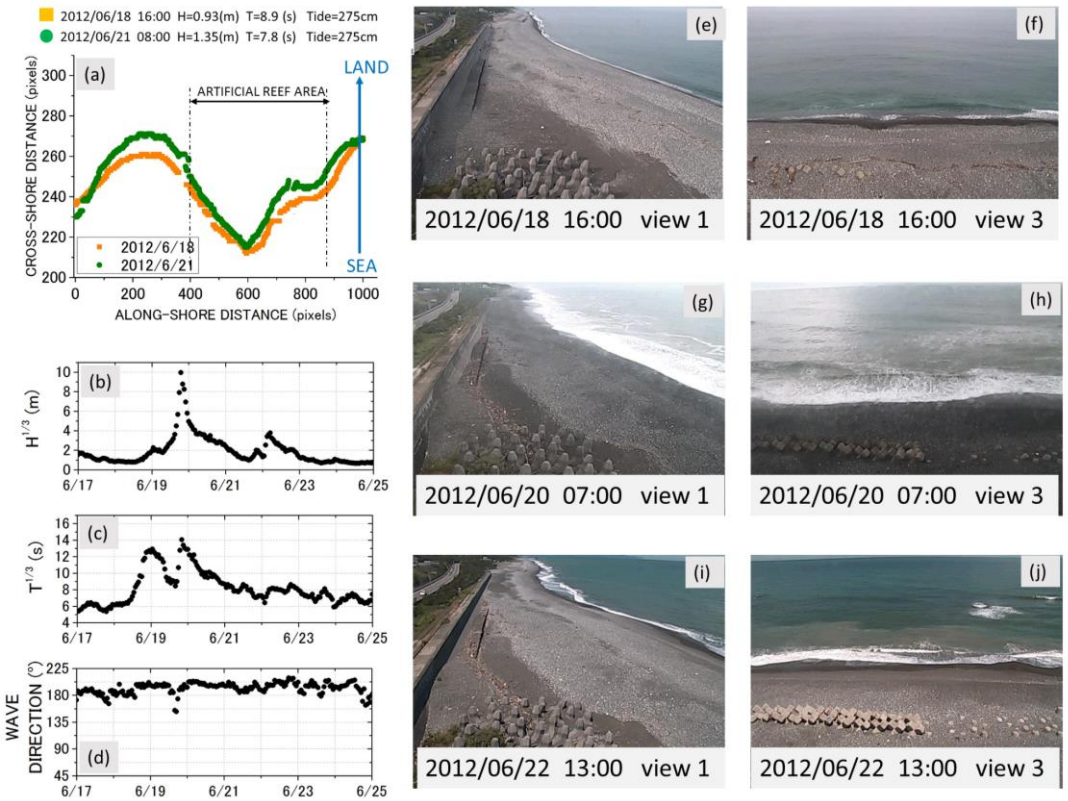

Figure 3.27 Shoreline change and topographic change during 2012/06/18~2012/06/21

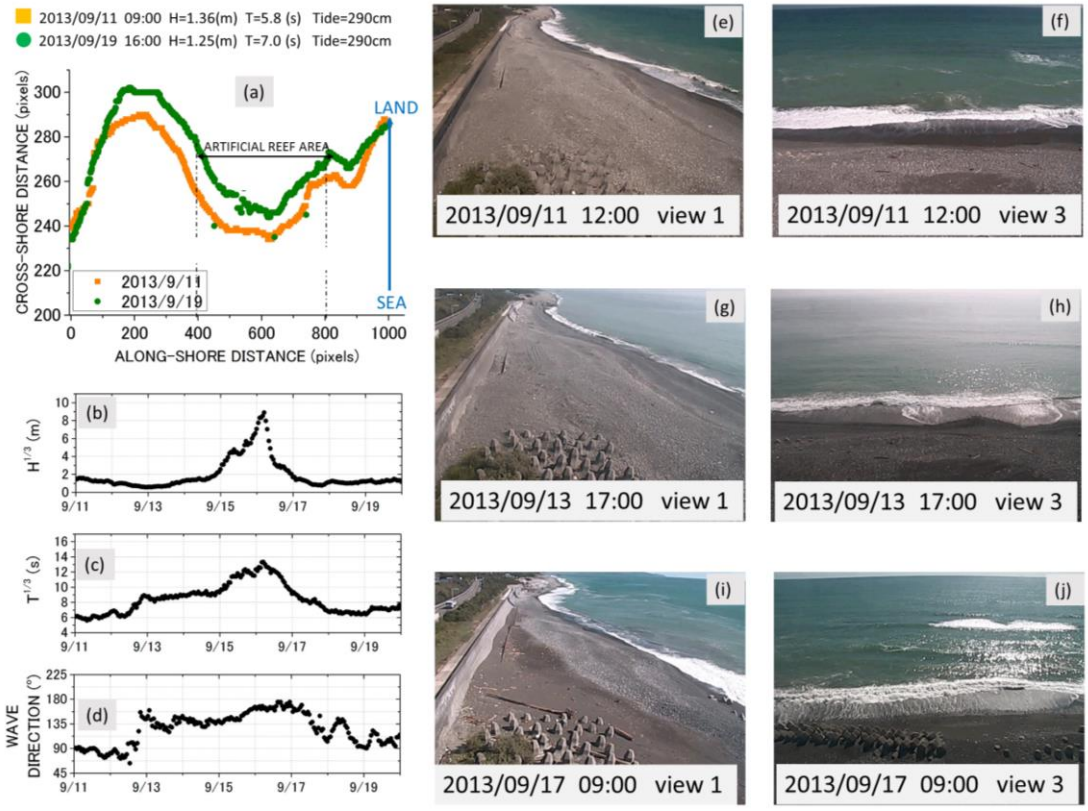

Figure 3.28 Shoreline change and topographic change during 2013/09/11~2013/09/19

3.6. Summary

This chapter presented the topography change during 31st January, 2014 ~ 21st February, specially focus on berm formation and beach profile change, by using image data from WEB camera system and topography data observed 3D imaging scanner system.

(1) The image analyzing results indicated that berm development did not occur when wave's height less than 1m. When wave's height is ranged from 1m-2.5, berm was formed on low area of beach face (See Figure 3.2 c, Figure 3.2f). When wave high exceed 3m, berm was located on the top of beach face (Figure 3.3c, Figure 3.4c, Figure 3.5b, Figure 3.7c). The relationship between berm formation and wave period was not clearly.

(2) Topography data shows that the beach width as well as beach volume decrease significant when wave approach to the coast from S, SSW direction with

wave’s height higher than 3m. Beach slope become steeper when moving from south to north on long-shore direction. On the area without artificial reef, beach slope become steeper and berm was retreated about 10~20m. On the other hand, on the area behind artificial reef, beach slope did not change dramatically.

(3) From topographic change and shoreline change it can be said that under the incoming waves with wave height less than 1.3m and wave period smaller than 8s, there is no significant change of beach morphology as well as shoreline position. However when wave height is larger than 2m and wave period larger than 8s, berm development has begun and shoreline position has changed significantly. The reason leads to such kind of differences might be the change on characteristic of flow field under low energy condition and high energy condition. And characteristic of flow field due to different wave conditons will be clarified in chapter 4.

Chapter 4

NUMERICAL SIMULATION

4.1 Overview

In chapter 2 and chapter 3, mechanism of shoreline change and topography change on Shichirimihama beach were discussed. The results show that artificial reef plays an importance role on reducing the wave energy off to the coast, hence it can prevent the coast from erosion. However, the continuously retreat of shoreline from 2012 also indicated that present artificial did not fulfill its function as expected. The reason of this was thought that hydrodynamic behavior around artificial reef is not fully understood yet. In order to find a method that can improve the present artificial function and create more stable beach, the behavior of flow field around the present artificial reef should be reassessed considering the permeability of gravel sea bed. This chapter aims to investigate the mechanism of flow field around artificial reef over a permeable seabed through numerical simulations. Firstly, the effect of seabed permeability on the behavior of hydrodynamic field around artificial reef will be discussed. Then, the relationship between permeability of artificial reef and hydrodynamic change will be investigated. The validation the function of present artificial reef in Shichirimihama beach by comparing the hydrodynamic behavior of two scenarios: with and without artificial reef. In the last section, changing of hydrodynamic varies with offshore distance of artificial reef will be investigated to search for a more effect arrangement method for future artificial reef construction.

4.2 Numerical model description

This study used the FSSM model investigated by Nakamura et al. (2012), in which permeability of beach, sea bed, and artificial reef are considered. The primitive equations are the equation of continuity (Eq.4.1), equation of momentum (Eq.4.2), equation of interface motion (Eq.4.3)

$$\frac{\partial\left(mv_j\right)}{\partial x_j} = q^* \tag{4.1}$$

$$\begin{aligned}\left(m + C_A(1-m)\right)\frac{\partial v_j}{\partial t} + \frac{\partial\left(mv_i v_j\right)}{\partial x_j} = \\ \frac{m}{\rho}\frac{\partial p}{\partial x_i} + mg_i + \frac{m}{\rho}\left(f_i^s + R_i\right) \\ + \frac{\partial}{\partial x_i}\left(-m\tau_{ij}^a + 2m\mu D_{ij}\right) + Q_i + m\beta_{ij}v_j\end{aligned} \tag{4.2}$$

$$m\frac{\partial F}{\partial t} + \frac{\partial\left(mv_j F\right)}{\partial x_j} = Fq^* \tag{4.3}$$

In which

$$f_i^s = \sigma\kappa\frac{\partial F}{\partial x_i}\frac{\hat{\rho}}{\overline{\rho}} \tag{4.4}$$

$$R_i = -\frac{12C_{D2}\hat{\mu}(1-m)}{md_{50}^2}v_i - \frac{C_{D1}\hat{\mu}(1-m)}{2md_{50}}v_i\sqrt{v_j v_j} \tag{4.5}$$

$$Q_i = v_i q^* - \frac{2}{3}\frac{\partial}{\partial x_i}\left\{\hat{\nu}\frac{\partial\left(m v_i\right)}{\partial x_j}\right\} \tag{4.6}$$

$$\beta_{ij} = \begin{Bmatrix} \beta(x, y, z)\delta_{iz}\delta_{jz} \\ 0 \end{Bmatrix} \tag{4.7}$$

in which m is porosity $1 \le m \le 0$; v_i, v_j is fluid/seepage flow velocity vector; x_i, y_j are the position vector; q^* is the intensity of wave source per unit (Kawasaki, 1999); C_A is the add mass coefficient due to porous media; t is time; p is pressure; $g_i = -g\delta_{iz}$ is the gravitational acceleration; $\hat{\rho} = F\rho_W + (1-F)\rho_a$ is the density of fluid (subscripts of w and a indicate water and air, respectively); F is VOF function indicating the volume fraction of water in each cell ranging $0 \le F \le 1$ ($F = 0$ for air, $0 < F < 1$ for water surface, $F = 1$ for water) ; f_j^s is the surface tension force vector based on the continuum surface force (CSF) model (Brackbill et al., 1992); R_i is the laminar and turbulent drag force vector due to porous media (Mizutani et al., 1996); τ_{ij}^a is the anisotropic part of the turbulent stress tensor; $\hat{\upsilon} = F\nu_W + (1-F)\nu_a$ is the kinematic molecular viscosity of fluid; $D_{ij} = \partial v_i / x_j + \partial v_j / x_i$ is the strain rate tensor; Q_i is the wave generation source/sink vector; β_{ij} is the artificial damping factor matrix; σ is the surface tension coefficient; κ is the local surface curvature; $\overline{\rho} = (\rho_W + \rho_a)/2$ is the density of fluid at the air-water interface; C_{D2} and C_{D1} are the laminar and turbulent drag coefficient, respectively; d_{50} is the mean median size of particle; $\hat{\mu} = \hat{\rho}\hat{\nu}$ is the molecular viscosity of fluid; $\beta(x, y, z)$ is the artificial damping factor

4.3 Calculation condition

Calculating scenery is three dimension the near-shore area in which artificial reef was constructed. Calculation domain is shown in Figure 4.1. Size of artificial reef was scaled down from the real size of artificial reef in Shichirimihama beach, which 6m height, 200m long and 80m width. Calculation scale is 1/25. Water deep is 8m. Beach slope is 1/7. Artificial reef slope is 1/2 for all sides. Two damping zone are set at landward and seaward boundary to prevent the effect of reflected waves. In order to clarify the effect of bed permeability, two types of bed porosity, 0.0, and 0.37, were calculated. Two scenarios of wave condition were calculated, that were regular wave with 10cm incident wave height 1.8s, wave period and regular wave with 4 cm incident wave height 1.6s wave period. Calculation mesh in computation domain was uniform mesh with 4mm, 4mm, 3mm for X direction, Y direction and Z direction, respectively. In remainder domain, non-uniform mesh was used to reduce the computation load. Flow velocity boundary condition was: the slip condition for bottom. Pressure boundary conditions were: the Sommerfeld radiation condition for the seaward and landward boundary, constant-pressure condition for the top boundary. For VOF function, the gradient-free condition was used

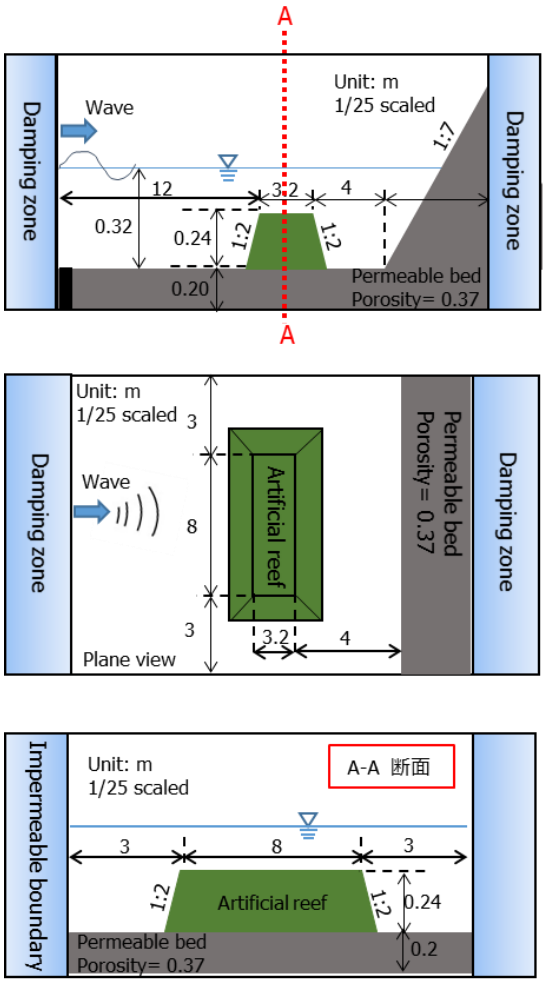

Wave high(H) Wave period (T)	H=4.0(cm) T=1.6(s)
	H=10.0(cm) T=1.8(s)
Bed porosity (m1)	0, 0.37
Artificial porosity (m2)	0.45, 0.55
Artificial reef average sediment size (cm)	2.0

Figure 4.1 Calculation area and calculation condition

for all boundaries.

4.4 Numerical results

4.4.1. Berm formation under different wave condition

Chapter 2 and chapter 3 discussed about changes of shoreline as well as beach topography in different incoming waves. The results show that after low energy wave approached to the coast, beach topography doesn't change significantly, and shoreline stands by at its original position. On the other hand, after wave's height larger than 2m off to the coast, the significant change of topography as well as shoreline are confirmed, especially in the area without artificial reef. According to experiment results of Eguchi et al (2004), development of berm strongly depended on income wave condition (Figure 4.2). In this section, in order to understand the development of

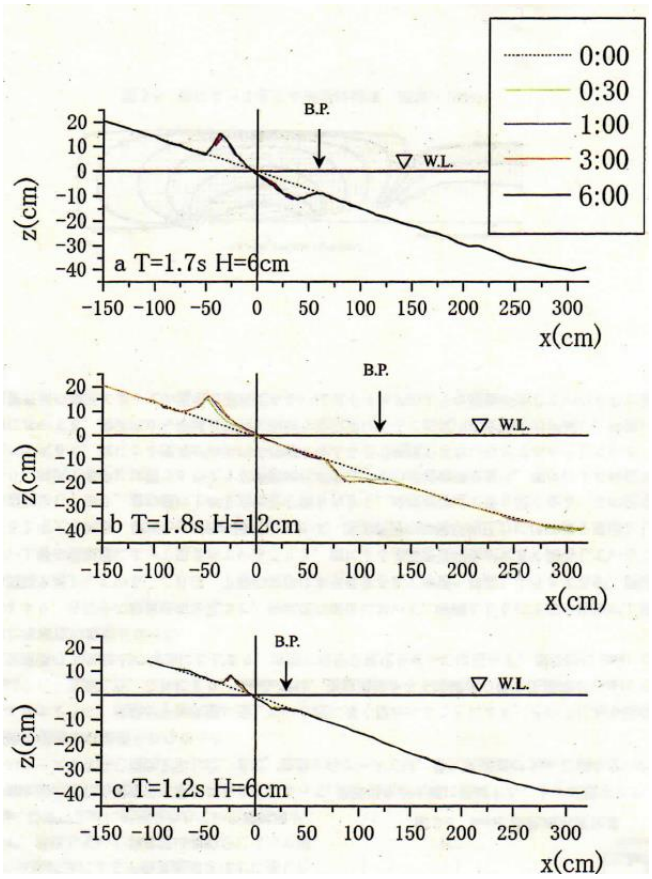

Figure 4.2 Berm formation under various income wave condition (Source: Eguchi, 2004)

berm under different wave conditions, characteristic of flow filed under high wave energy condition and low wave energy condition will be analyzed based on two dimension calculation results.

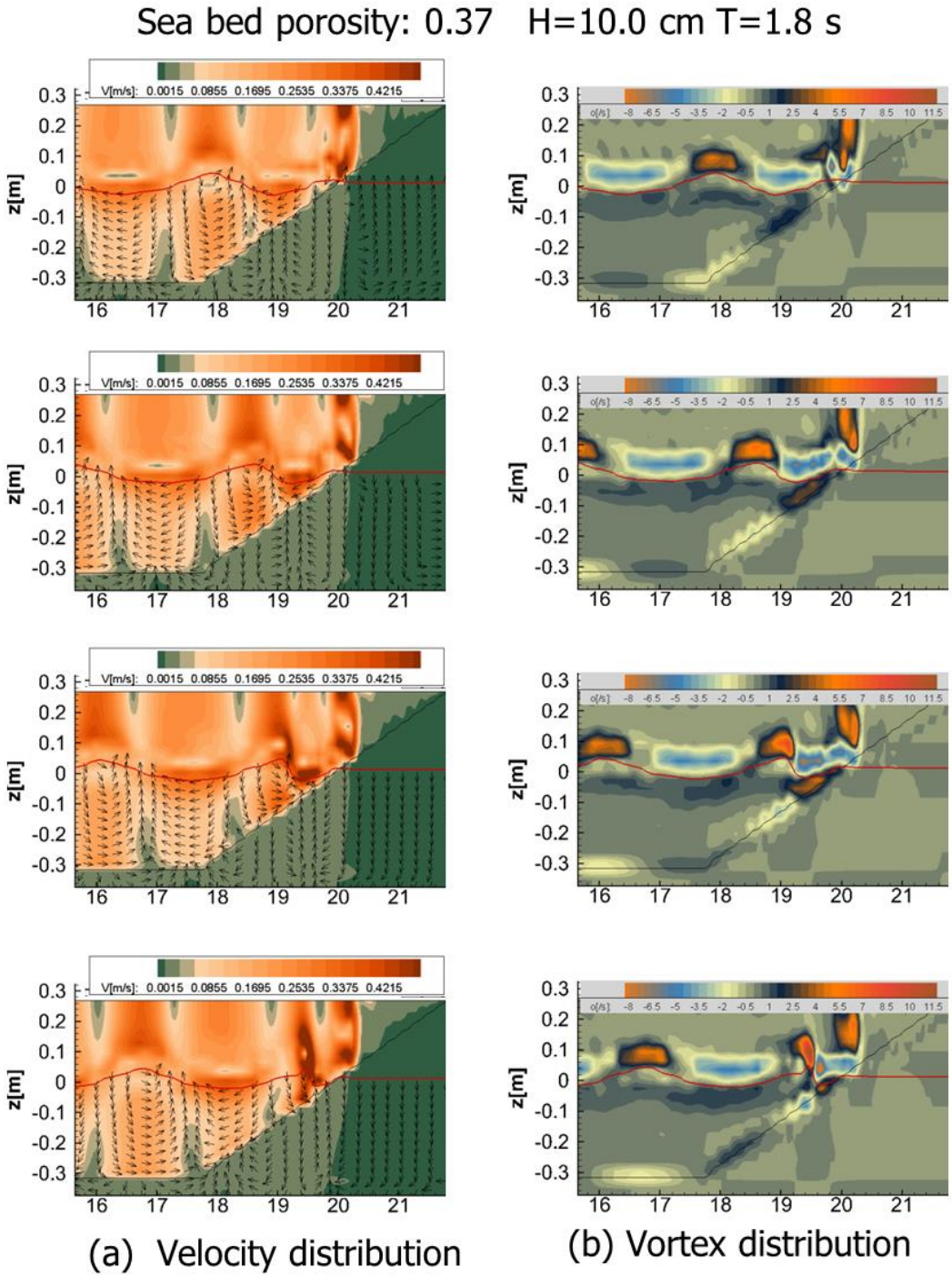

Figure 4.3 Characteristic of flow field under high wave condition

Figure 4.3 and Figure 4.4 illustrate velocity distribution and vorticity distribution in swash zone of two cases: H=4.0 cm, T=1.6s and H=10.0cm, T=1.8s. From these results it can be understood that in the case of H=10.0cm, T=1.8s wave breaking reveals a strong velocity field on swash zone and results large vortex near from beach face. Hence sediment on the lower part of beach face will be rolled up and moved to the top of the beach results by the onshore surface flow and berm will be created. The results show the same behavior with the experiment results done by Eguchi (2004, (Figure 4.5)). Moreover as showed chapter 3, there is a significant difference on berm development in the area behind artificial reef and in the area without artificial reef. It was though that because in the area behind artificial reef, wave breaks over artificial reef and reduced wave energy off to the coast. Then the flow field in near shore area in case with artificial reef (Figure 4.6) is more moderate thsn the case without artificial reef (Figure 4.3).

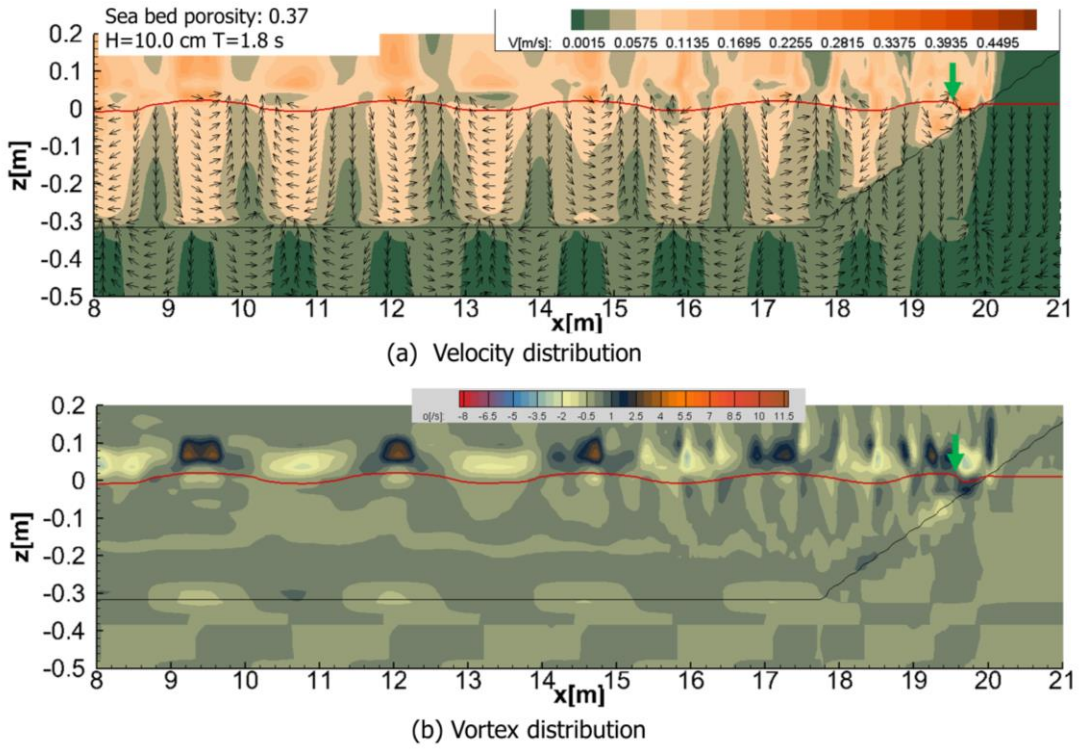

Figure 4.4 Characteristic of flow field under low wave condition

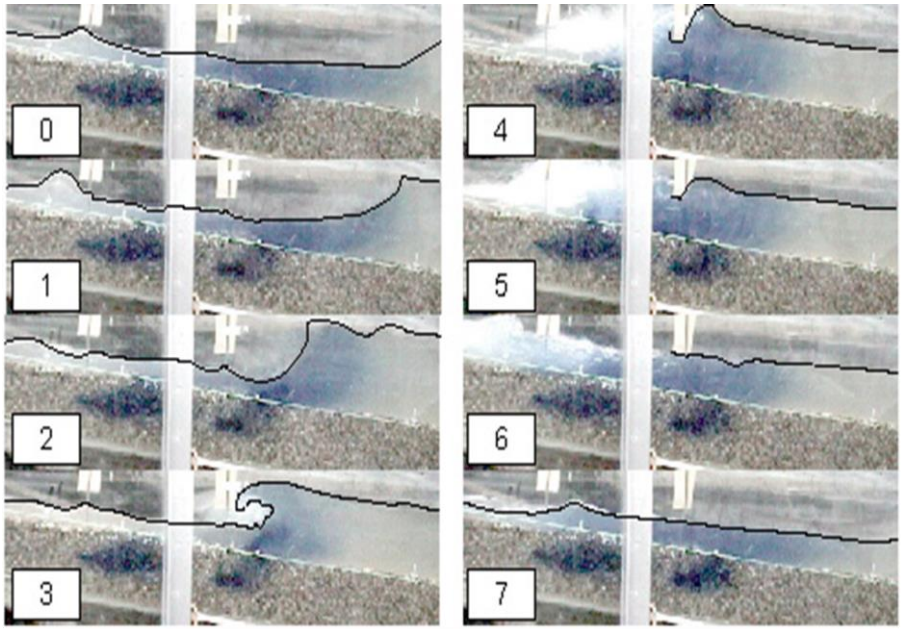

Figure 4.5 Experiment results of flow field various with income wave condition (Source: Eguchi, 2004)

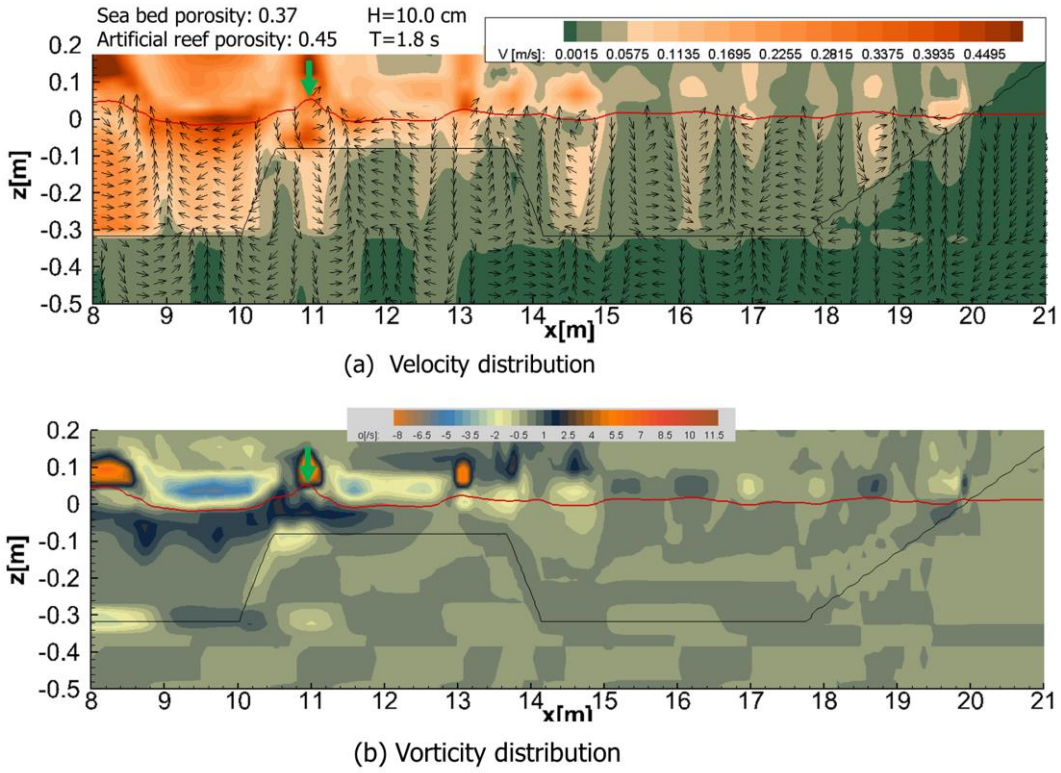

Figure 4.6 Characteristic of flow field under high wave condition with artificial reef

4.4.2 Effect of bed impermeability on near-shore flow field

4.4.2.1 Effect on wave breaking point

According to the simulation results done by Ma et.al (2004), there is an upward flow inside gravel beach under wave breaking point, and it plays an important role on swash zone sediment transport process. Therefore, permeability of the seabed is considered that also affect the wave breaking point. It should be noted that the breakings point was defined as the location of the highest water level. Figure 4.7 illustrates the velocity field together with changing on wave shape over artificial reef of two cases: Figure 4.7a shows the result of impermeable case, Figure 4.7b shows results of permeable bead case. From these figures, it can be confirmed that when considering the bed permeability, the wake breaking point moving to onshore side comparing with the case of opaque. Moreover, when the bed is permeability, the flow field spreads into the bed and return flow inside the bed was formed.

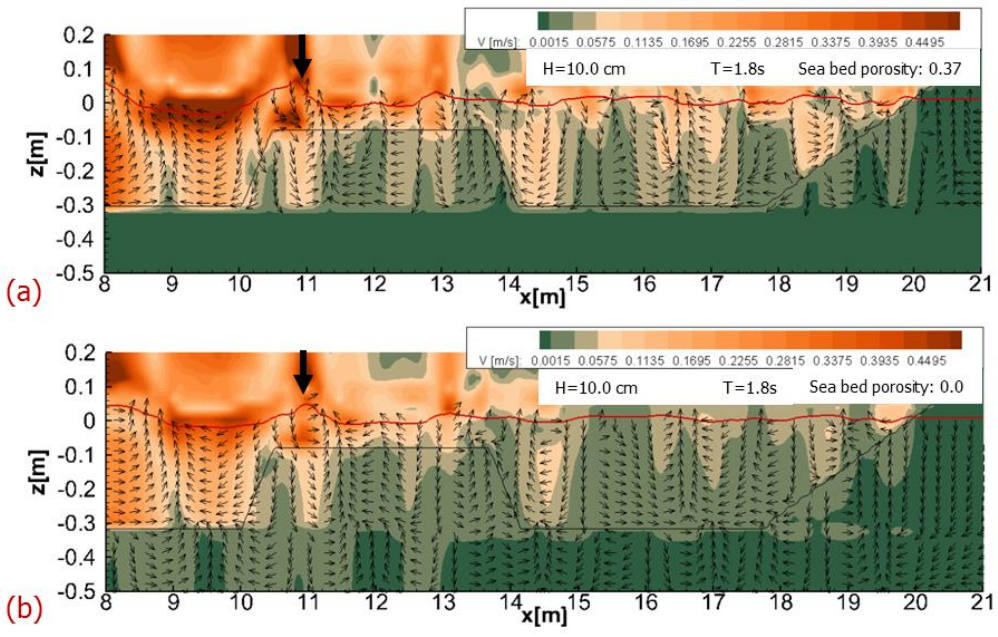

Figure 4.7 Change on wave breaking point when consider bed permeability

4.4.2.2 Effect on distribution of wave high and water level

Flow field on near-shore zone was created by the different on spatial distribution of water level. Figure 4.8 illustrates spatial distribution of maximum water level and wave high on entire computation domain. From Figure 4.8, it can be said that water level on swash zone of the case with permeable bed (Figure 4.8b) is lower than the case with impermeable bed (Figure 4.8d). And the spatial wave high distribution also shows the same trend (Figure 4.8a, Figure 4.8b).

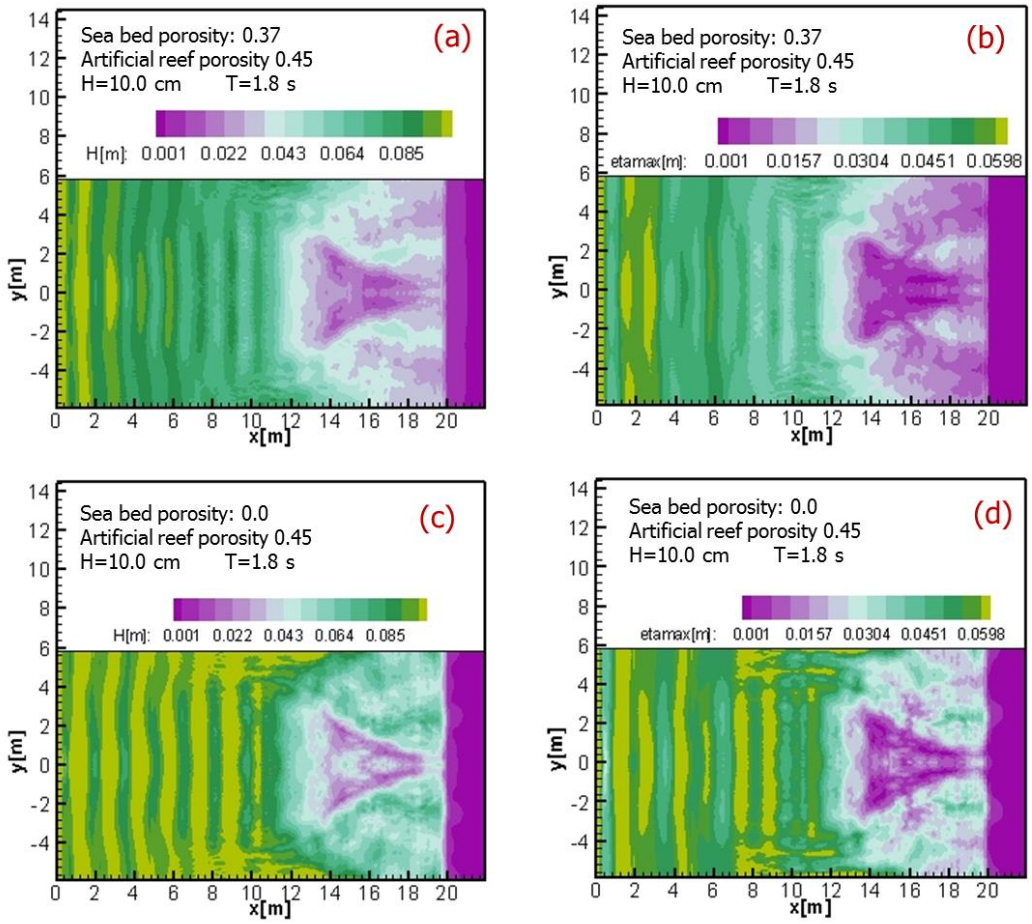

Figure 4.8 Change on distribution of wave high and water level when consider bed

4.4.3 Three dimensional flow field in swash zone

4.4.3.1 Three dimensional flow field inside and outside artificial reef

As mentioned above, by field survey in 1993 Shimizu et al. reported that erosion occurred in the artificial reef lee after artificial reef installation. Regarding characteristics of the flow field around the artificial reef, several studies have been carried out in the past (for example, Kawashima et al., 1992; Sumi et al. 1997; Torii et al., 2003). However, most of studies were conducted by two-dimensional numerical calculation. As described above, characteristics of the flow field of the horizontal and vertical directions play a significant role on the deformation of the beach topography, thus the three-dimensional flow field characteristics are required. Therefore, this section performs the three dimension flow field around the artificial reef. Figure 4.9 shows the instant velocity field when the wave breaking occurs over artificial reef. From this figure, it can be confirmed that there is an upward flow under wave breaking point. Figure 4.10 illustrates the spatial distribution of the average

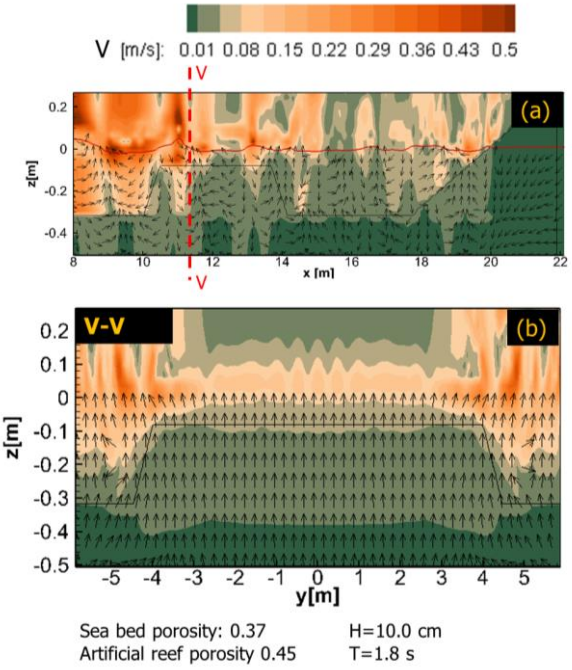

Figure 4.9 Flow field when wave breaking

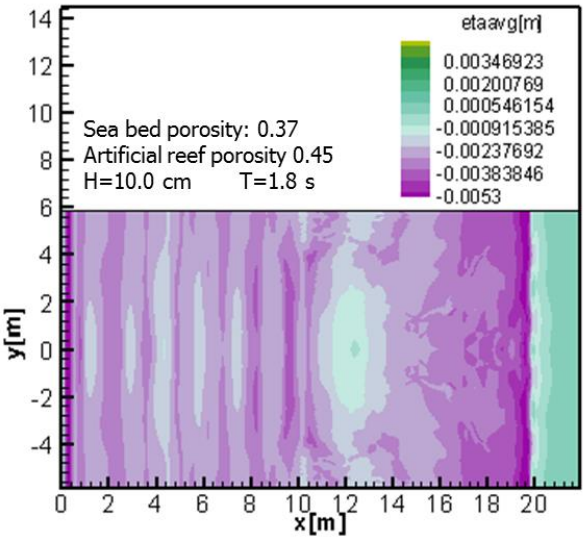

Figure 4.10 Flow field when wave breaking

water level surrounding artificial reef waters. Waves are breaking in on the top that was shown by the dashed line, and therefore a high average water level on the artificial reef crest, lead to a strong flow toward to the beach after breaking. There is a quite high average water level zone behind artificial reef. Average water level on artificial reef lee also become higher, but decreases when the distance from artificial increases.

Figure 4.11 shows the distribution of the instant velocity over water depth in cross section I-I, II-II, III-III, IV-IV at wave breaking time. It can be seen from Figure 4.11a, Figure 4.11b, and Figure 4.11c that over water depth from the seabed to the crest of the artificial reef, there is a flow toward the beach. On the other hand, in the surface layer above artificial reef, the flow toward onshore exists entirely. Consequently, the onshore flow occurred when wave breaking will return to the sea through lower part artificial reef crest. These can be considered as a stream associated with the spatial distribution of the average water level due to the breaking waves on the artificial reef.

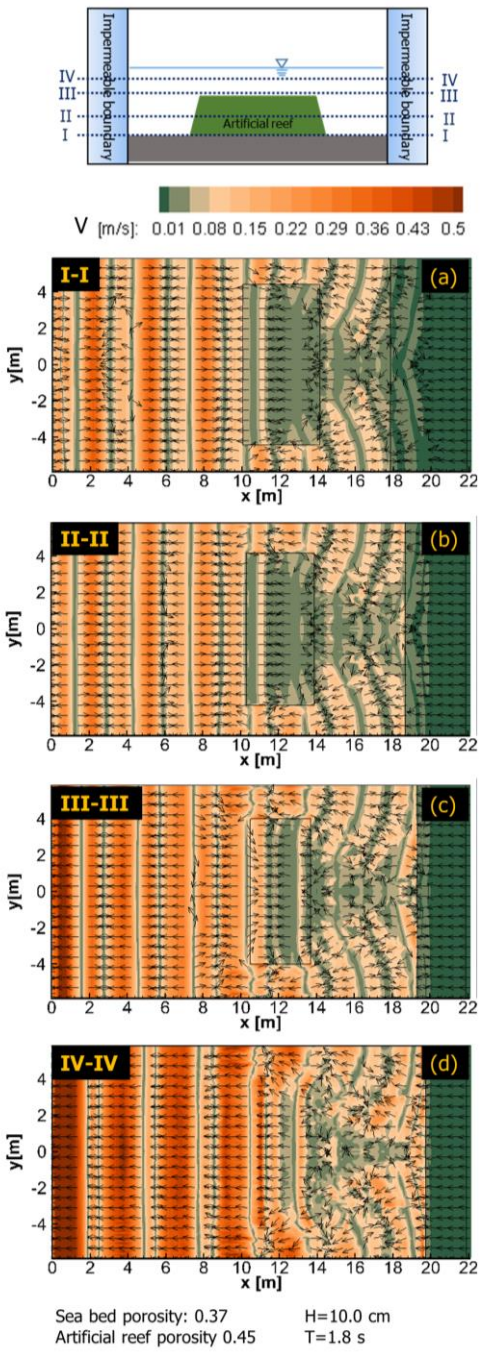

Figure 4.11 Flow field along water depth

Due to field survey in 1991, Uda et al. reported that the fluorescence sand that are submitted to the shore side of the artificial reef were flowing out to the offshore artificial reef, and from the results of numerical simulation, it can be

pointed out that the flow toward the sea on the gap between artificial reef may become a cause of the sand movement.

4.4.3.2 Three dimensional flow field in low wave condition and high wave condition

In case of H=10cm, T=1.8s, there is a circle flow extend from sea bed to water surface in the gap between artificial reef, and the high velocity area spreads entire the artificial reef (Figure 4.12a). Moreover, after passage through artificial, wave approach to the coast and wave breaking occur again in the area near from the beach, results in a high velocity field inside beach face (Figure 4.12b). In case of H=4cm, T=1.6s, velocity in the gap between artificial reef as well as inside the artificial reef is smaller compared to previous case (Figure 4.13a). Figure 4.14 and Figure 4.15 illustrate the average velocity over the water deep of two cases. Velocity behind artificial reef in case of H=4cm, T=1.6 is smaller than that one of H=10cm, T=1.8s. Hence, in case of H=10cm, T=1.8s there is a strong offshore flow in the gap between artificial reef.

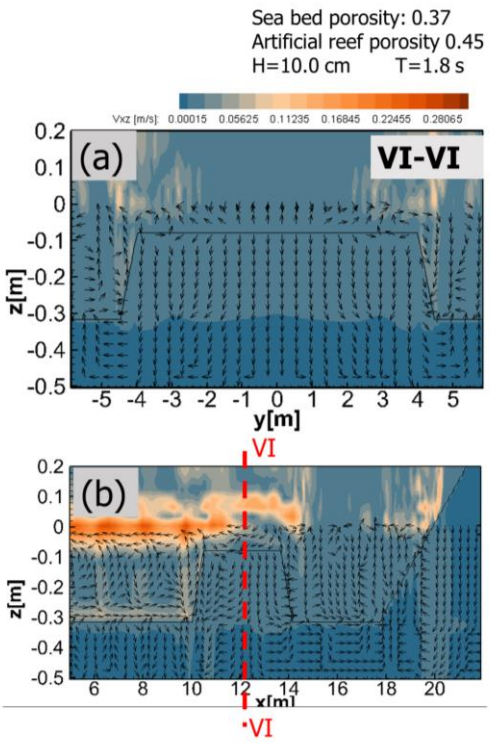

Figure 4.12 Flow field under high wave condition

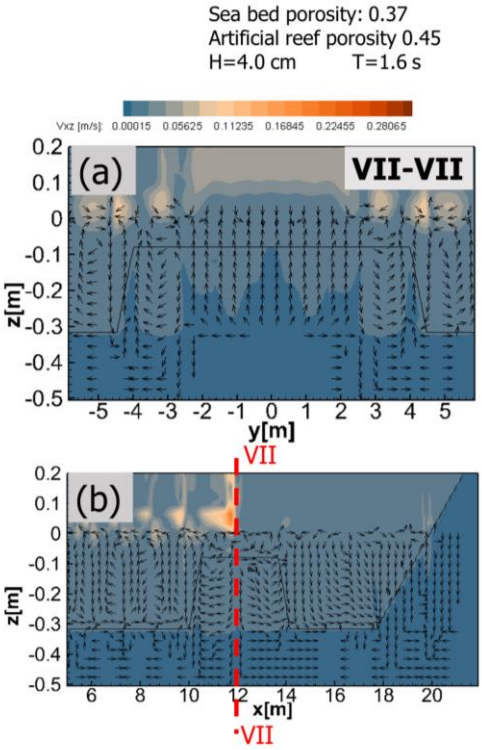

Figure 4.13 Flow field under low wave condition

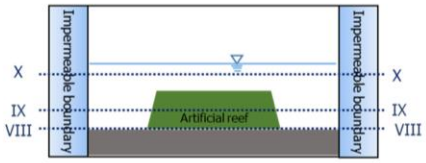

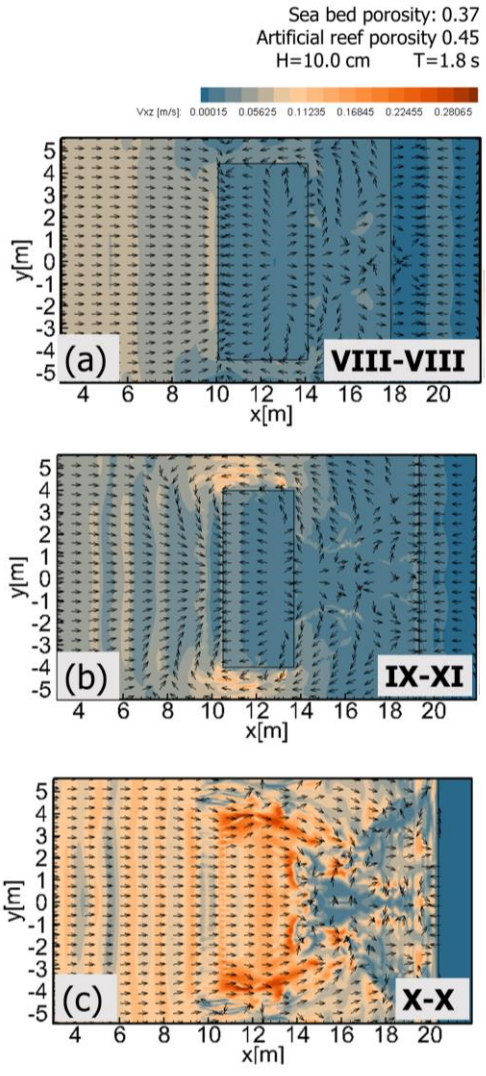

Figure 4.14 Return flow under high wave condition

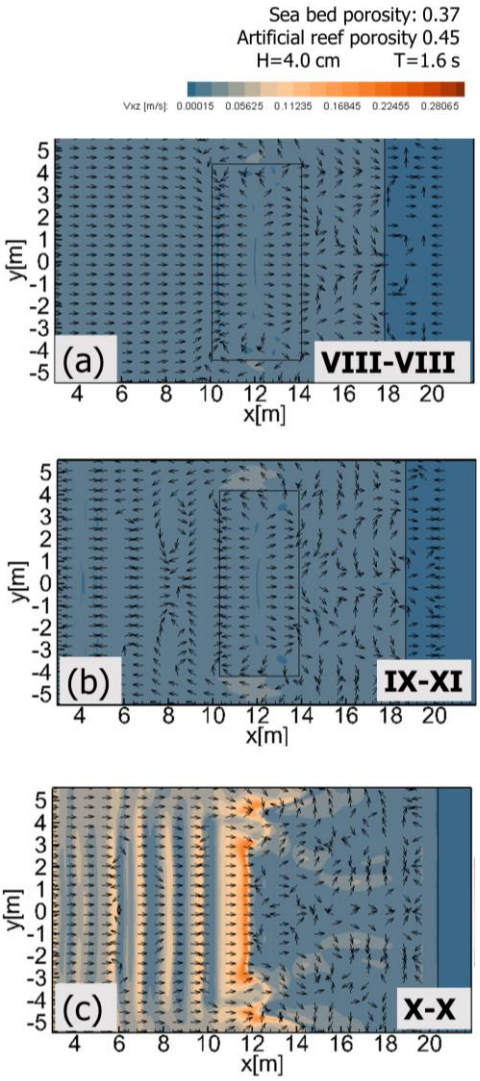

Figure 4.15 Return flow under low wave condition

4.4.4 Effect of artificial reef porosity on flow field in swash zone

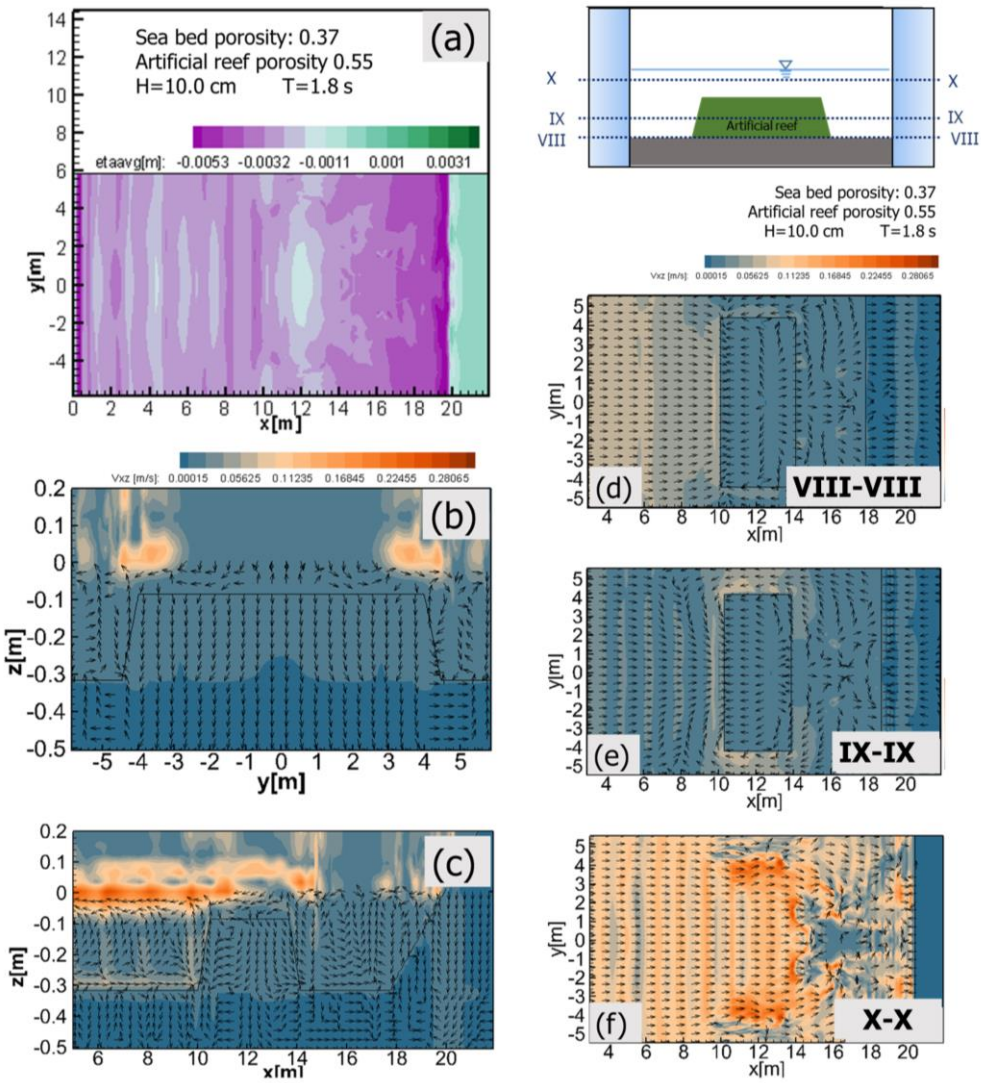

Figure 4.16 Flow field when porosity of artificial reef is 0.55

Figure 4.16 shows the average water level (Figure 4.11a) and average velocity (Figure 4.16 b-f) when artificial reef porosity was 0.55. From Figure 4.10, Figure 4.12, Figure 4.14, Figure 4.16, it can be concluded that average water level behind artificial reef will decrease when artificial reef porosity increase (Figure 4.10, and Figure 4.16a). Therefore, the velocity behind the artificial reef decreases when artificial reef porosity increase and the offshore flow between two artificial reefs will decrease (Figure 4.12, Figure 4.14, and Figure 4.16 b-f).

4.4.5 Effect of artificial reef location on swash zone flow field

In order to investigate the effect of artificial reef location on flow field, the numerical simulation, in which the distance between artificial and the beach reduces from 4m to 2m, was carried. Figure 4.17 illustrates the spatial distribution of the average flow velocity of the long distance case (4m) and short distance case (2m). When distance artificial reef is short, there is a circulation in the seabed there is a circulation extend the beach face to artificial reef (Figure 4.17c). In the view of the Ma's results (2004), this promotion of the flow inside permeable layer can reduce the offshore direction flow and reduce offshore sediment transport amount, so it can be expected to reduce beach erosion. On the other hand, paying attention to the planar mean flow distribution, the mean flow in the gap between artificial reefs will increase when the distance become smaller, therefore, it can also increase the erosion at artificial reef lee.

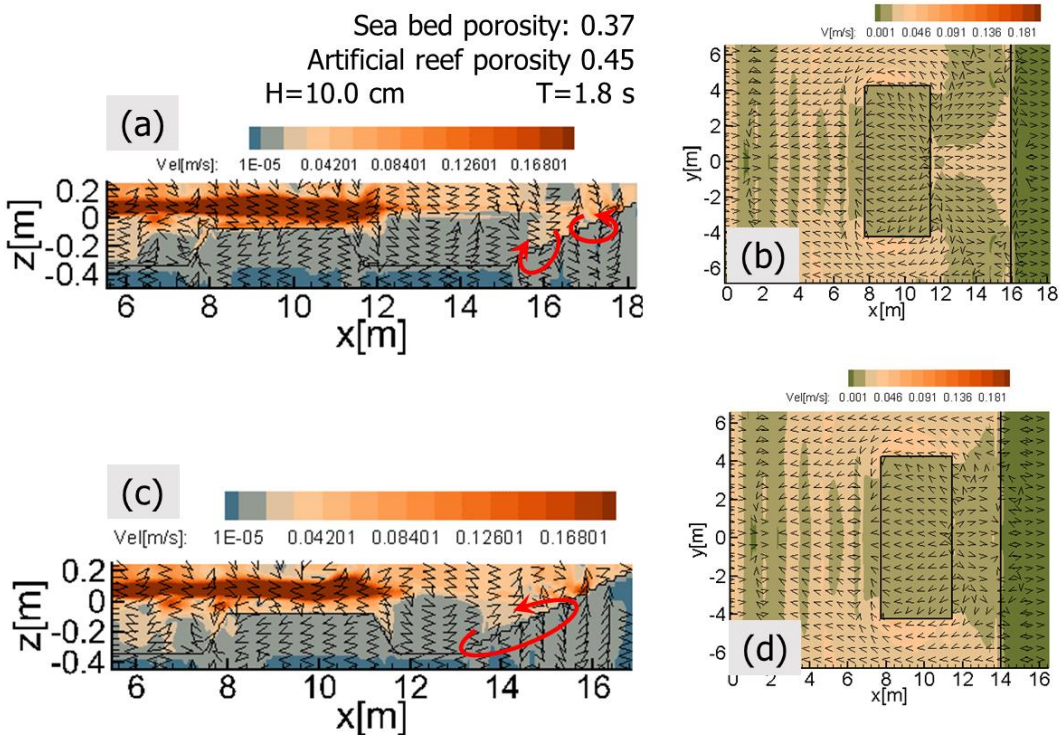

Figure 4.17 Spatial distribution of the average flow velocity of the long distance case (a, b) and short distance case (c, d)

4.5 Summary

This chapter discuss about the flow field in the swash zone, considering to the permeability of sea bed and artificial reef. The main conclusions are summarized as below:

1) When considering to the permeability, flow field extends to the permeable layer of the seabed. Accordingly, the difference is also found in the average flow field. In addition, such changes are associated with changes in the breaking point. Also, it was confirmed that the porosity artificial reef material also influences the breaking point.

2) Wave breaking on the artificial reef crest reveals a higher average water level on the top of artificial, and a relatively high average water level water is also formed in the area behind artificial reef. Water level on artificial lee also increases, but decrease far from artificial reef.

3) Onshore flow occurred when breaking wave will return to the sea through lower part artificial reef crest and through the gap between two artificial reefs.

4) When distance artificial reef is short, the flow inside permeable layer will increase, so reduce the offshore direction flow and reduce offshore sediment transport amount, and it can be expected to reduce beach erosion. On the other hand, the mean flow in the gap between artificial reefs will increase when the distance become smaller, therefore it can also increase the erosion at artificial reef lee.

Chapter 5

CONCLUSIONS AND DISCUSSIONS

People living on coastal zone have gaining their livelihood directly or indirectly from the coast through many kinds of economic processes. Certain human activities have negative impacts on the nature of coast environment. This close relationship between human activities and coastal zone environment leads to the requirement of a mode of exploitation which has less impact on natural coastal system. For that reason, from the past, artificial reefs have been used as an additive construction to reduce negative impacts caused by manmade near-shore facilities. In Shichirimihama Beach, artificial reefs have been constructed to reduce beach erosion caused by breakwater construction at Udono port. However, recent continuous shoreline retreat indicates that artificial reef did not function well as expected and it was thought that the lack of knowledge on hydrodynamic behavior around artificial reef is a major reason. In order to restore the original beach status and create a more stable beach, the behavior of shoreline change under the present of artificial reef should be re-assessed. On the other hand, artificial reef is still new measurement on coastal defense, and it requires more studies about flow field in swash zone in which artificial reef were constructed. Furthermore to gain an accurately knowledge about the flow field around artificial reef which constructed over a gravel beach like Shichirimihama, the permeability of gravel sea bed should be considered. Due to the complexity of nature hydrodynamic in swash zone, numerical simulation is the most efficiency method for investigating the near-shore hydrodynamic process. Consequently, this study aims to investigate the

function of artificial reef on Shichirimihama beach through analysis of the change of shoreline position and beach topography. After that the flow field of coast in which artificial reef has been installed as countermeasure against beach erosion was investigated by conducting numerical simulation, in order to clarify the mechanism of hydrodynamic changes on the swash zone as well as around artificial reefs. In numerical simulation model, the permeability of sea bed was considered to clarify the mechanism of hydrodynamic changes on gravel beach which has a high permeability as Shichirimihama beach.

In summary, this study aimed to: (1) Investigate the shoreline change based on the images obtained from coast based WEB camera system as well as propose new method of shoreline detection from the images. (2) Collect and analyze the changes of topography in Shichirimihama beach using 3D terrestrial laser scanning system. (3) Investigate mechanism of flow field around artificial reef in consider the effect of seabed permeability using numerical simulation. (4) Validate the present artificial reef in Shichirimihama Beach and investigate a more effective method to increase the function of present artificial reef.

WEB camera system along with image processing is a very efficient method for collecting continuous shoreline data with an efficient operation as well as a management cost. The proposal method can extract shoreline more stable than the existing CCD method, especially in bad weather when quality of images were not good. Hence using the proposal method shoreline in rain weather or storm event can be collected. And it helps to gain more knowledge about behavior of shoreline caused by special event, which cannot collect by filed survey or satellite image. Moreover continuously data set of WEB camera system is a very efficient tool for investigate the mechanism of shoreline change for both short-term change and long-term change.

According to image processing results when wave heights larger than 6m and wave periods longer than 10s off to the coast, shoreline retreated. When wave heights smaller than 1m and wave periods smaller than 8s off to the coast, shoreline will forward at the area behind artificial reef, and stand still in the area without artificial reef. For other cases of wave conditions, shoreline behavior strongly depends on wave direction, and shoreline can be forward or retreat due to the change of wave direction.

Topography data showed that the beach width as well as beach volume decrease significant when wave approach to the coast from S, and SSW direction with wave height larger than 3m. Beach slope became steeper when moving from south to north on long-shore direction. On the area without artificial reefs, beach slope became steeper and berm was retreated about 10~20m. On the other hand, on the area behind located artificial reef, beach slope did not change dramatically.

Berm development was investigated through snapshot image data. The results indicated that berm development did not occur when wave height less than 1m. When wave height is ranged from 1.0m-2.5m, berm was formed on low area of beach face. And when wave height exceed 3m berm was located on the top of original beach face. The results also showed that wave direction plays an importance role in term of berm location, and berm size.

From topographic change and shoreline change it can be said that under the incoming waves with wave height less than 1.3m and wave period smaller than 8s, there is no significant change of beach morphology as well as shoreline position. However when wave height is larger than 2m and wave period larger than 8s, berm development has begun and shoreline position has changed significantly. From numerical simulation results it can be said the reason leading to such kind of differences is the change on characteristic of flow field under low energy condition and high energy condition. In the case of high energy waves, sediments on the lower part of beach face were be rolled up due to strong flow field caused by wave breaking near the coastal and moved to the top of the beach, then berm occurred and shoreline retreat as consequently. Moreover topographic change and shoreline change in the area behind artificial reef was smaller in compare with the area without artificial reef. Numerical simulation results showed that in case of artificial reef, wave breaking over artificial reef reduced wave energy off to the coast, then reduced cross-shore and long-shore velocity, so reduced sediment transport in nears-shore area.

Three dimensional numerical simulation was adopted to investigate the near-shore flow field in the present of artificial reef over impermeable bed. When considering the permeability of the seabed, flow field extended to inside the permeable seabed layer,

and accordingly, the difference was found in the average flow field in the vicinity of the water surface. In addition, changing on the porosity of artificial reef material also influenced the breaking point.

Wave breaking on the artificial reef crest revealed a higher average water level on the top of artificial, and a relatively high average water level was also formed in the area behind artificial reefs. Water level on artificial lee also increased, but decreased far from artificial reef. Onshore flow occurred when wave breaking returned to the sea through lower part artificial reef crest and through the gap between two artificial reefs.

Artificial reef played an importance role on reducing wave energy and prevent coast from erosion. And most of study focused on function of artificial reef on beach erosion. However artificial reef is a long-term anti-erosion countermeasure, so preventing artificial reef itself from erosion is also important. Hence, for making a good design decision, the characteristic of flow field around artificial reef is also important. It means that the final design decision needs to be chosen based on the three dimensional flow field characteristic rather than the two dimension flow field characteristic. Moreover as mentioned in chapter 4, when distance between beach and artificial reef become shorter, the flow inside permeable layer increases, then reduces the offshore direction flow and reduces offshore sediment transport amount, and it can be expected to reduce beach erosion. On the other hand, the mean flow in the gap between artificial reefs increases when the distance become smaller, therefore also the erosion at artificial reef lee increase as well. So it is required to conduct more studies to figure out a best arrangement of artificial reef which reducing beach erosion as well as artificial reef itself erosion simultaneously.

Although the author obtained the aforementioned conclusions, there are some unsolved problems, which need to do more researches in future as shown followings:

About image processing method: As mentioned above, shoreline extracted by method proposed by the author was the highest run up position. Hence in order to remove the effects of tide level as well as run–up length, in this study only the data which have same tide level and less effect of wave run up (e.g. wave high less than 1m and wave period less than 7s) was used. Hence, a method which can help to remove

such kind of effect is required to gain more continuous data set.

About numerical simulation for flow field in swash zone: in this study the effect of sea bed permeability on behavior of flow field in swash zone was confirmed. In the future, more study should be conducted to investigate the relationship between artificial reef arrangement and three-dimensional flow fields in swash zone. Moreover, this study have discussed about mechanism of flow field in swash zone under different wave heights and wave periods. However, as shown in Chapter 2 and Chapter 3, wave direction also plays an importance role on berm formation and shoreline change, hence more studies which consider the effect of wave direction on flow field in swash zone should be conducted.

References

A. D. Matthias, A. Fimbres, E. E. Sano, D. F. Post, L. Accioly, A. K. Batchily, and L. G. Ferreira, Surface roughness effects on soil albedo, Soil Sci. Soc. *Am. J. 64* (2000) 1035-1041.

Aarninkhof, S., Turner, I., Dronkers, T., Caljouw, M. and Nipius, L. (2003). A video-based technique for mapping intertidal beach bathymetry. *Coastal Engineering*, 49(4), pp.275-289.

Akbari, H. and Namin, M. (2013). Moving particle method for modeling wave interaction with porous structures. *Coastal Engineering*, 74, pp.59-73.

Allen, J. (1988). Nearshore Sediment Transport. *Geographical Review*, 78(2), p.148.

Austin, M. and Masselink, G. (2006). Observations of morphological change and sediment transport on a steep gravel beach. *Marine Geology*, 229(1-2), pp.59-77.

B. Parker, Where is the shoreline? The answer is not as simple as one might expect. *Hydro International*, 5(5) (2001) 6–9.

Bakhtyar, R., Barry, D., Li, L., Jeng, D. and Yeganeh-Bakhtiary, A. (2009). Modeling sediment transport in the swash zone: A review. *Ocean Engineering*, 36(9-10), pp.767-783.

Boak, E. and Turner, I. (2005). Shoreline Definition and Detection: A Review. *Journal of Coastal Research*, 214, pp.688-703.

Buscombe, D. and Masselink, G. (2006). Concepts in gravel beach dynamics. *Earth-Science Reviews*, 79(1-2), pp.33-52.

Callaghan, D., Nielsen, P., Short, A. and Ranasinghe, R. (2008). Statistical simulation of wave climate and extreme beach erosion. *Coastal Engineering*, 55(5), pp.375-390.

Chan, H., Huang, W., Leu, J. and Lai, C. (2007). Macroscopic modeling of turbulent flow over a porous medium. *International Journal of Heat and Fluid Flow*, 28(5), pp.1157-1166.

Chang, K., Hsu, T. and Liu, P. (2005). Vortex generation and evolution in water waves propagating over a submerged rectangular obstacle. *Coastal Engineering*, 52(3), pp.257-283.

Corvaro, S., Mancinelli, A., Brocchini, M., Seta, E. and Lorenzoni, C. (2010). On the wave damping due to a permeable seabed. *Coastal Engineering*, 57(11-12), pp.1029-1041.

D. Barber, J. Mills, and S. S.-Voysey, Geometric validation of a ground-based mobile laser scanning system Original Research Article, *ISPRS J. Photogramm. 63* (1) (2008) 128-141.

D. C. Mason, C. Gurney, and M. Kennett, Beach topography mapping – a comparison of techniques, *Journal of Coastal Conservation 6* (2000) 113-124.

D. Lague, N. Brodu, and J. Leroux, Accurate 3D comparison of complex topography with terrestrial laser scanner: Application to the Rangitikei canyon (N-Z) Original Research Article, *I ISPRS J. Photogramm. 82* (2013) 10-26.

D. M. Cobby, D. C. Mason, and I. J. Davenport, Image processing of airborne scanning laser altimetry data for improved river flood modelling Original Research Article, *ISPRS J. Photogramm. 56 (2)* (2001) 121-138.

D. Theler, E. Reynard, C. Lambiel, and E. Bardou, The contribution of geomorphological mapping to sediment transfer evaluation in small alpine catchments Original Research Article, *Geomorphology 124* (2010) 113-123.

Manuel del Jesus, M., Lara, J. and Losada, I. (2012). Three-dimensional interaction of waves and porous coastal structures. *Coastal Engineering*, 64, pp.57-72.

Dong-O Kim, and Rae-Hong Park, (2009). New Image Quality Metric Using the

Harris Response. *IEEE Signal Process. Lett.*, 16(7), pp.616-619.

E. P. Baltsavias, A comparison between photogrammetry and laser scanning, *ISPRS J. Photogramm. 54* (1999) 83–94.

E. S. Oude, and G. Vosselman, Quality analysis on 3D building models reconstructed from airborne laser scanning data, *ISPRS J. Photogramm. 66* (2011) 157–165.

E. Schiefer, and R. Gilbert, Reconstructing morphometric change in a proglacial landscape using historical aerial photography and automated DEM generation Original Research Article, *Geomorphology 88* (2007) 167-178.

El Kadi Abderrezzak, K., Paquier, A. and Gay, B. (2008). One-dimensional numerical modelling of dam-break waves over movable beds: application to experimental and field cases. *Environmental Fluid Mechanics*, 8(2), pp.169-198.

F. H. McBeth, A method of shoreline delineation, Photogramm. Eng. 22 (2) (1956) 400–405.

Friedlander, S. and Serre, D. (2007). *Handbook of mathematical fluid dynamics*. Amsterdam: Elsevier.

Funt, B. (2004). Retinex in MATLABâ„¢. *J. Electron. Imaging*, 13(1), p.48.

Galgano, F. and Douglas, B. (2000). Shoreline Position Prediction: Methods and Errors. *Environ Geosci*, 7(1), pp.23-31.

Gonzalez, R., Woods, R. and Eddins, S. (2004). *Digital Image processing using MATLAB*. Upper Saddle River, N.J.: Pearson Prentice Hall.

Hervouet, J. (2007). *Hydrodynamics of free surface flows*. Chichester: Wiley.

Holthuijsen, L. (2007). *Waves in oceanic and coastal waters*. Cambridge: Cambridge University Press.

Honjo, Y. and Kashiwagi, N. (1999). Matching objective and subjective information in groundwater inverse analysis by Akaike's Bayesian information

criterion. *Water Resour. Res.*, 35(2), pp.435-447.

Horn, D. (2002). Beach groundwater dynamics. *Geomorphology*, 48(1-3), pp.121-146.

Hsu, T., Sakakiyama, T. and Liu, P. (2002). A numerical model for wave motions and turbulence flows in front of a composite breakwater. *Coastal Engineering*, 46(1), pp.25-50.

Hu, K., Hsiao, S., Hwung, H. and Wu, T. (2012). Three-dimensional numerical modeling of the interaction of dam-break waves and porous media. *Advances in Water Resources*, 47, pp.14-30.

Hu, K., Hsiao, S., Hwung, H. and Wu, T. (2012). Three-dimensional numerical modeling of the interaction of dam-break waves and porous media. *Advances in Water Resources*, 47, pp.14-30.

Huang, C. and Dong, C. (1999). Wave deformation and vortex generation in water waves propagating over a submerged dike. *Coastal Engineering*, 37(2), pp.123-148.

Hyun-Ho Ma, N. Mizitani, S.Eguchi (2005). Study on velocity field above gravel beach and sediment movements. *Journal of JSCE*, 789, pp.73-82 (In Japanese).

I. Puente, H. G.-Jorge, P. Arias, and J. Armesto, Land-based mobile laser scanning systems: A review, Spain International Archives of the Photogrammetry, Remote Sensing and Spatial Information Sciences, Volume XXXVIII-5/W12, 2011 ISPRS Calgary 2011 Workshop, 29-31 August 2011, Calgary, Canada.

J. C. Adams, and J. H. Chandler, Evaluation of Lidar and medium scale photogrammetry for detecting soft-cliff coastal change, *Photogramm. Rec. 17* (2002) 405–418.

J. H. List, and A. S. Farris, Large-scale shoreline response to storms and fair weather. *Proceedings of the Coastal Sediments '99*, ed., Long Island, New York, 1999,

pp. 1324–1337.

J. W. Woolard, and J. D. Colby, Spatial characterization, resolution, and volumetric change of coastal dunes using airborne LIDAR: Cape Hatteras, North Carolina, *Geomorphology 48* (2002) 269–287.

Jensen, B., Jacobsen, N. and Christensen, E. (2014). Investigations on the porous media equations and resistance coefficients for coastal structures. *Coastal Engineering*, 84, pp.56-72.

Jiachun, L. and Mian, L. (1995). On the interaction of water waves and seabed by the porous medium model. *Acta Mech Sinica*, 11(2), pp.129-136.

K. Kraus, and N. Pfeifer, Determination of terrain models in wooded areas with airborne laser scanning data, *ISPRS J. Photogramm. 53* (1998) 193 – 203.

Karunarathna, S. and Lin, P. (2006). Numerical simulation of wave damping over porous seabeds. *Coastal Engineering*, 53(10), pp.845-855.

Kawashima, K., Okamoto, M., Kioka, W., Sato K., (1992). About flow pattern around submerged breakwaters. *Annual Journal of Coastal Engineering*, JSCE, (39), pp. 216-220 (In Japanese)

Kumar, A., Narayana, A. and Jayappa, K. (2010). Shoreline changes and morphology of spits along southern Karnataka, west coast of India: A remote sensing and statistics-based approach. *Geomorphology*, 120(3-4), pp.133-152.

Kuriyama, Y. and Nakatsukasa, T. (2000). A one-dimensional model for undertow and longshore current on a barred beach. *Coastal Engineering*, 40(1), pp.39-58.

Kuriyama, Y., Ito, Y. and Yanagishima, S. (2008). Cross-shore variation of long-term average longshore current velocity in the nearshore zone. *Continental Shelf Research*, 28(3), pp.491-502.

L. Gorman, A. Morang, and R. Larson, Monitoring the coastal environment. Part

IV. Mapping, shoreline changes, and bathymetric analysis, J. Coastal Res. 14 (1) (1998) 61–92.

L. Gorman, A. Morang, and R. Larson, Monitoring the Coastal Environment; Part IV: Mapping, Shoreline Changes, and Bathymetric Analysis, J. Coastal. Res. 14 (1) (1998) 61-92.

Lara, J., del Jesus, M. and Losada, I. (2012). Three-dimensional interaction of waves and porous coastal structures. *Coastal Engineering*, 64, pp.26-46.

Lara, J., Losada, I., Maza, M. and Guanche, R. (2011). Breaking solitary wave evolution over a porous underwater step. *Coastal Engineering*, 58(9), pp.837-850.

Lee, K., Mizutani, N., Hur, D. and Kamiya, A. (2007). The effect of groundwater on topographic changes in a gravel beach. *Ocean Engineering*, 34(3-4), pp.605-615.

Lin, M. and Huang, L. (2012). Numerical simulation of waveâ€“structure interaction using a Lagrangian vortex method. *Ocean Engineering*, 44, pp.11-22.

Liu, P., Xu, J., Liu, J. and Tang, X. (2009). Pixel Based Temporal Analysis Using Chromatic Property for Removing Rain from Videos. *Computer and Information Science*, 2(1).

Liu, T. and Su, D. (2013). Numerical analysis of the influence of reef arrangements on artificial reef flow fields. *Ocean Engineering*, 74, pp.81-89.

Longuet-Higgins, M. (1983). Wave Set-Up, Percolation and Undertow in the Surf Zone. *Proceedings of the Royal Society A: Mathematical, Physical and Engineering Sciences*, 390(1799), pp.283-291.

Longuet-Higgins, M. (1983). Wave Set-Up, Percolation and Undertow in the Surf Zone. *Proceedings of the Royal Society A: Mathematical, Physical and Engineering Sciences*, 390(1799), pp.283-291.

M. Larson, and N. C. Kraus, Temporal and spatial scales of beach profile change, Duck, North Carolina, Mar. Geol., 117 (1994) 75–94.

Ma, G., Shi, F., Hsiao, S. and Wu, Y. (2014). Non-hydrostatic modeling of wave interactions with porous structures. *Coastal Engineering*, 91, pp.84-98.

Maiti, S. and Bhattacharya, A. (2009). Shoreline change analysis and its application to prediction: A remote sensing and statistics based approach. *Marine Geology*, 257(1-4), pp.11-23.

Martinez, W. and Martinez, A. (2010). *Exploratory data analysis with MATLAB*. London: Chapman & Hall.

Masselink, G. and Puleo, J. (2006). Swash-zone morphodynamics. *Continental Shelf Research*, 26(5), pp.661-680.

Masselink, G., Russell, P., Blenkinsopp, C. and Turner, I. (2010). Swash zone sediment transport, step dynamics and morphological response on a gravel beach. *Marine Geology*, 274(1-4), pp.50-68.

Matthias, A., Fimbres, A., Sano, E., Post, D., Accioly, L., Batchily, A. and Ferreira, L. (2000). Surface Roughness Effects on Soil Albedo. *Soil Science Society of America Journal*, 64(3), pp.1035.

Medina, R., Losada, M., Losada, I. and Vidal, C. (1994). Temporal and spatial relationship between sediment grain size and beach profile. *Marine Geology*, 118(3-4), pp.195-206.

Nakamura, T. and Mizutani, N. (2012). Three-dimensional coupled fluid-sediment interaction numerical model for suspended sediment analysis, *International Journal of Offshore and Polar Engineering*, 22 (4), pp. 314–322

Nolan, T., Kirk, R. and Shulmeister, J. (1999). Beach cusp morphology on sand and mixed sand and gravel beaches, South Island, New Zealand. *Marine Geology*, 157(3-4), pp.185-198.

Pérez-Romero, D., Ortega-Sánchez, M., Antonio Moñino, A. and Losada, M. (2009). Characteristic friction coefficient and scale effects in oscillatory porous flow.

Coastal Engineering, 56(9), pp.931-939.

R. A. Morton, M. P. Leach, J. G. Paine, and M.A. Cardoza, Monitoring beach changes using GPS surveying techniques, J. Coastal Res. 9 (1993) 702-720.

R. Dolan, B. P. Hayden, P. May, and S. May, The reliability of shoreline change measurements from aerial photographs, *Shore and Beach*, 48 (1980) 22–29.

R. Jennings, and J. Shulmeister, A field based classification scheme for gravel beaches, *Mar. Geol. 186* (2002) 211–228.

R. Ranasinghe, I. L. Turner, and G. Symonds, Shoreline response to multi-functional artificial surfing reefs: A numerical and physical modelling study, *Coast Eng. 53* (2006) 589–611.

R. W. G. Carter, and J. D. Orford, Coarse clastic barrier beaches: a discussion of the distinctive dynamic and morpho-sedimentary characteristics, *Mar. Geol. 60* (1984) 377–389.

Ren, B., Wen, H., Dong, P. and Wang, Y. (2014). Numerical simulation of wave interaction with porous structures using an improved smoothed particle hydrodynamic method. *Coastal Engineering*, 88, pp.88-100.

Ruggiero, P. (2004). Wave run-up on a high-energy dissipative beach. *J. Geophys. Res.*, 109(C6).

S. Pu, G. Vosselman, Knowledge based reconstruction of building models from terrestrial laser scanning data Original Research Article, *ISPRS J. Photogramm. 64* (6) (2009) 575-584.

Sato, T., Ooe, M., Nawa, K., Shibuya, K., Tamura, Y. and Kaminuma, K. (1997). Long-period tides observed with a superconducting gravimeter at Syowa Station, Antarctica, and their implication to global ocean tide modeling. *Physics of the Earth and Planetary Interiors*, 103(1-2), pp.39-53.

Shankar, N. and Jayaratne, M. (2003). Wave run-up and overtopping on

smooth and rough slopes of coastal structures. *Ocean Engineering*, 30(2), pp.221-238.

Shen, L. and Chan, E. (2011). Numerical simulation of nonlinear dispersive waves propagating over a submerged bar by IB-VOF model. *Ocean Engineering*, 38(2-3), pp.319-328.

Shimizu, M., Imai, S., Terada, K. (1993): Topographic change due to artificial reef construction. *Annual Journal of Coastal Engineering*, JSCE, 40, 546-550. (In Japanese)

Suga, K., Mori, M. and Kaneda, M. (2011). Vortex structure of turbulence over permeable walls. *International Journal of Heat and Fluid Flow*, 32(3), pp.586-595.

Suzuki, K., Ariji, R., Morohoshi, K., Yanagashima, S., Takahashi, S., Matsuyaki, S.,and Suzuki, N. (2008): Development of Coastal Observation System using WEB Camera, *Annual Journal of Coastal Engineering*, JSCE, 55, 446-1450. (In Japanese).

Tonnon, P., van Rijn, L. and Walstra, D. (2007). The morphodynamic modelling of tidal sand waves on the shoreface. *Coastal Engineering*, 54(4), pp.279-296.

Tsai, R. (1987). A versatile camera calibration technique for high-accuracy 3D machine vision metrology using off-the-shelf TV cameras and lenses. *IEEE J. Robot. Automat.*, 3(4), pp.323-344.

Turner, I. and Masselink, G. (2012). Coastal gravel barrier hydrology â€" Observations from a prototype-scale laboratory experiment (BARDEX). *Coastal Engineering*, 63, pp.13-22.

Van Rijn, L. (2014). A simple general expression for longshore transport of sand, gravel and shingle. *Coastal Engineering*, 90, pp.23-39.

Van Wellen, E., Chadwick, A. and Mason, T. (2000). A review and assessment

of longshore sediment transport equations for coarse-grained beaches. *Coastal Engineering*, 40(3), pp.243-275.

W.A. Birkemeier, Field data on seaward limit of profile change, J. Waterw. Port. C-Asce 111(3) (1985) 598-602.

Watanabe, Y., Saeki, H. and Hosking, R. (2005). Three-dimensional vortex structures under breaking waves. *Journal of Fluid Mechanics*, 545(-1), p.291.

Wu, Y. and Hsiao, S. (2013). Propagation of solitary waves over a submerged permeable breakwater. *Coastal Engineering*, 81, pp.1-18.

Wu, Y., Yeh, C. and Hsiao, S. (2014). Three-dimensional numerical simulation on the interaction of solitary waves and porous breakwaters. *Coastal Engineering*, 85, pp.12-29.

Xie, L., Wu, K., Pietrafesa, L. and Zhang, C. (2001). A numerical study of wave-current interaction through surface and bottom stresses: Wind-driven circulation in the South Atlantic Bight under uniform winds. *J. Geophys. Res.*, 106(C8), p.16841.

Zhang, Z. (2000). A flexible new technique for camera calibration. *IEEE Trans. Pattern Anal. Machine Intell.*, 22(11), pp.1330-1334.

Zhou Wang, and Bovik, A. (2002). A universal image quality index. *IEEE Signal Process. Lett.*, 9(3), pp.81-84.